High Efficiency Milling of Steam Turbine Blade

2017 年 3 月

長崎大学大学院工学研究科

YUAN XIN

Contents

Chapter 1 Introduction

1.1 Research background

Owing to exponential population growth, rapid industrialization, urbanization, modernization and improvement in the standard of living, the global electricity consumption is expected to increase significantly in coming years [1-3]. It is predicted to continue to grow at an annual rate of 2.4 percent from 2009 to 2035[4-5]. Largest power generation method in the world is coal fired power generation(see **Fig.1.1**), there is a large proportion in developing countries with a focus on China. On the other hand, the coal-fired generation, although in the state-of-the-art supercritical pressure steam turbine power generation system, carbon dioxide of 0.9kg per kWh and is discharged, when compared to other power generation methods, the more improvement of further power generation efficiency , it is required to reduce emissions of carbon dioxide[6-9].

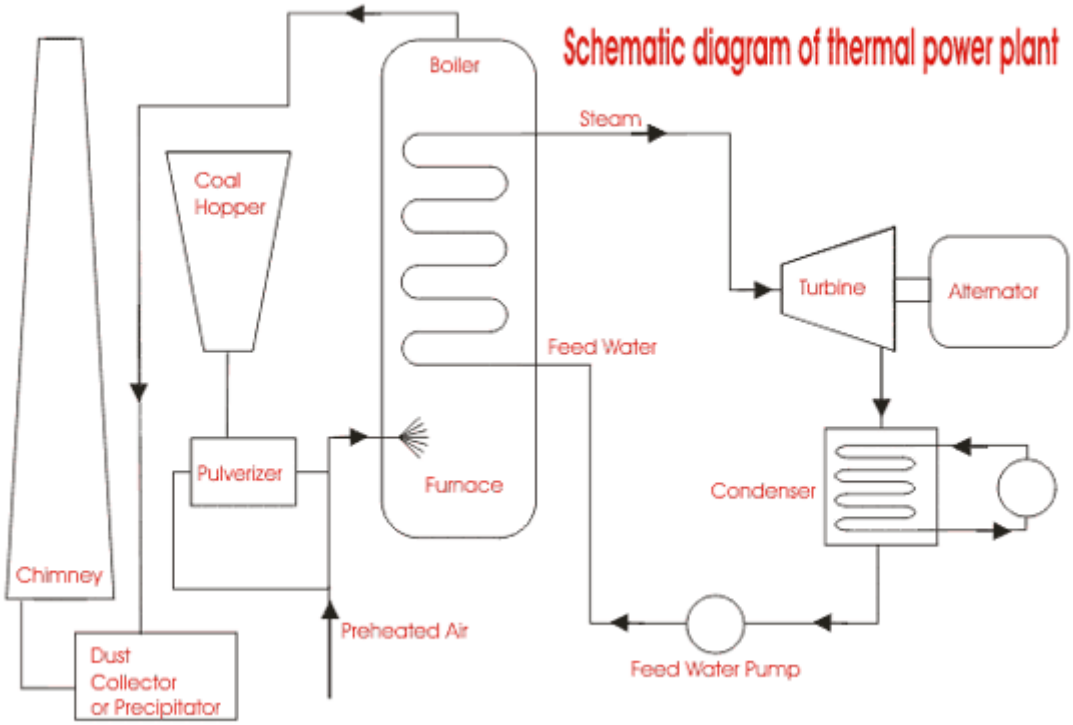

Fig. 1.1. Line diagram of thermal power plant.

The continuous adjustments of the structure of electric power generation industry during last ten years confirm the leading position of large-scale (ultra-) supercritical coal-fired power plant with extremely high steam parameters in the foreseeable future. Steam turbine has been adopted in a wide range of power generation system of the thermal power, nuclear power, geothermal, solar thermal, etc. Most of the power generating motor used in the whole world is steam turbine, therefore, it plays an important role for generating power at a high efficiency, and supplying it stable and sustainable[10-12].

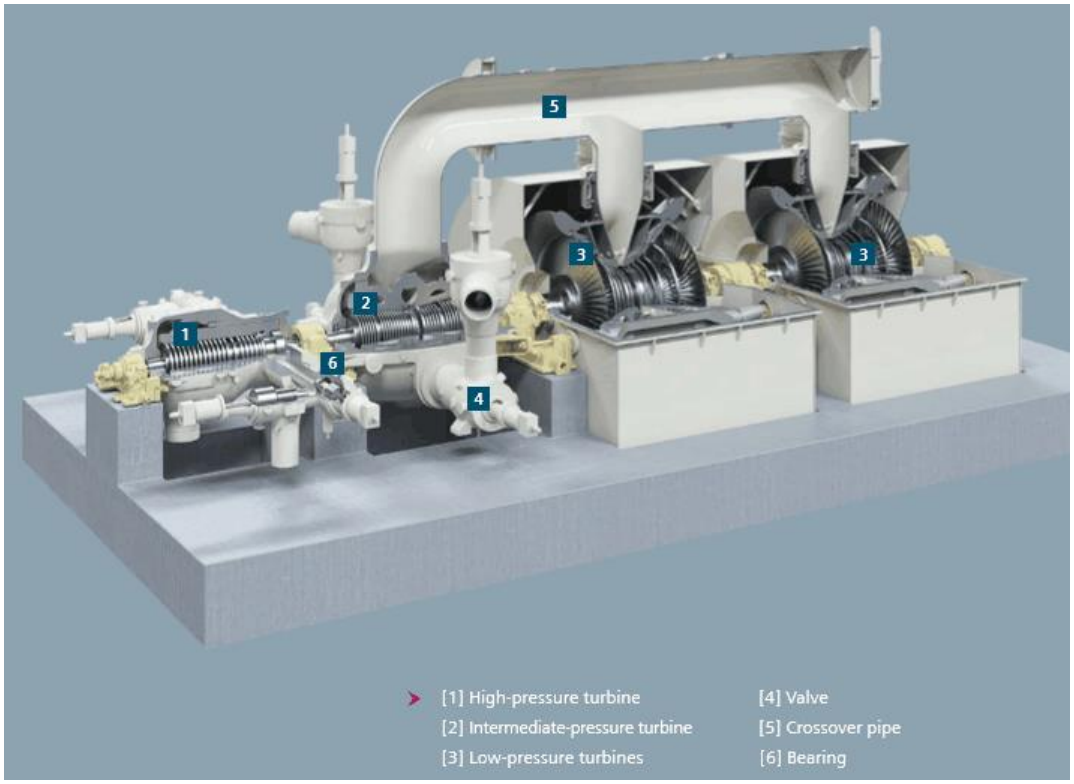

Fig.1.2. 1200MW SST-6000 series steam turbines (Siemens).

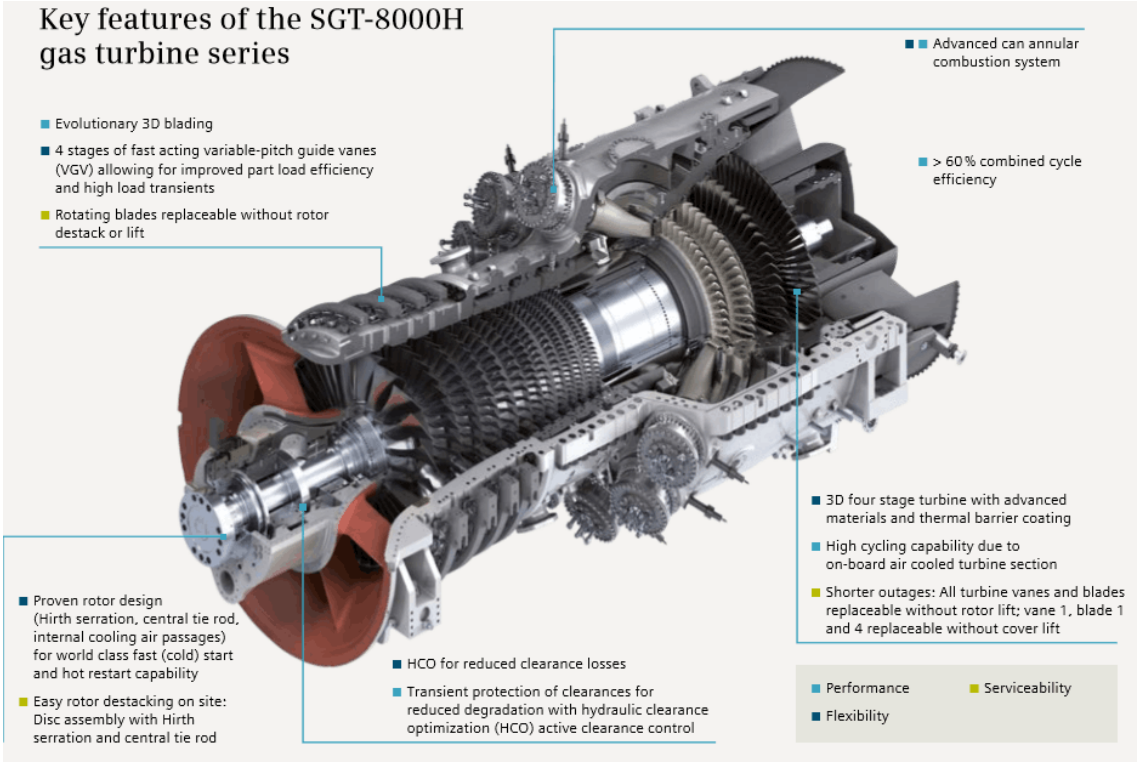

Fig.1.3. 296MW SGT6-8000H heavy-duty gas turbines (Siemens).

Fig. 1.4. 60-inch last-stage blades for steam turbines (Hitachi).

Fig.1.5. Example of 60-inch low pressure turbine blade (Toshiba).

Fig.1.6. Example of high pressure turbine blade (Toshiba).

Generally, gas and steam turbines operate in environments where the ingestion of solid particles is inevitable (**Fig.1.2** and **Fig.1.3**). Due to their high inertia, these solid particles are deviated from the flow streamlines, hitting the blade surfaces and inflicting severe wear damage. This can be characterized by pitting, micro-cutting, cracks and hot corrosion actions on the leading and trailing edges of the blades causing an increase in the blade surface roughness. The effects of this phenomenon are an increase of the pressure loss and a modification of the blade

geometry. In a steam turbine, numbers of blades are used for energy transfer. The blades are subjected to centrifugal force hence, become critical parts, which affect the satisfactory function of a turbine [13-16]. As indicated by its name, the final stage blade is the longest wing that located in the rearmost of the steam turbine. This steam energy (mainly kinetic energy) after passing through the wing cannot be used in power generation. It is effective to reduce the speed of the steam flowing out to reduce the loss of this kinetic energy. The longer wings are, the larger area that vapor can pass through so that the flow rate of the steam becomes smaller. Therefore, high-efficiency steam turbine can be designed according to this [17-19].

A number of blades are used in steam turbines ranging from a few centimeters in height in high pressure (HP) turbines to almost one meter long low pressure (LP) turbines(See **Fig.1.5** and **Fig.1.6**). The failure causes for HP and LP turbines are high cyclic fatigue caused by number of factors, centrifugal forces, steady and dynamic stresses, fracture propagation, etc. The best way of avoiding these failures is by thorough inspection of raw material and defect free manufacturing of turbine blades. In general, high alloy steels with high chromium content are used for manufacturing of turbine blades. The machinability of these materials is poor and therefore these components are invariably produced by shell-mold-investment casting route directly as net- shaped products. Achieving dimensional accuracy is one of the main challenges of investment casting, on account of shrinkage allowances. Hence, turbine blades are machined using turning, milling and finishing operation s [20]. The material is also important along with the machining process. There are basically three groups of steam turbine blade materials used by turbine manufacturers. These are various grades of 12–13% chromium (Cr) steels with addition of Mo, W, Cb, V, Cu, Al, Ta, Ti and Nb. Higher chromium precipitation hardening steels such as 17-4PH and Titanium alloys are also very popular. Following the steam path through a turbine, the environment for the converging blades varies strongly and, as a consequence, so do the mechanical requirements. These requirements have a strong influence on the choice of material and the design with respect to temperature, wetness and cleanliness of medium, acting forces as well as other factors such as hardenability and oxidation. Therefore, different blade families exist which can be categorized according to their use in the primary three turbine modules as high, intermediate and low pressure blades (HP, IP, and LP). The first two turbine modules, HP and IP, are characterized [21] by high temperatures and they contain

comparably small blades that have to sustain small centrifugal forces but large steam-induced bending forces due to relatively high static pressure differences and impulse changes at the stage. They are equipped mostly with statically determinate T-roots assembled in tangential grooves around the rotor. The blades are tightly bound to each other by integral roots and shrouds that ensure high stiffness of the blade row and also introduce frictional damping to the structure. Of course, the integral shrouds also serve to seal the blade and hence reduce the aerodynamic leakage losses. With increasing requirements on life-span and security of steam turbines, the quality of turbine blades becomes more and more important. So there is a need to improve the surface qualities, such as surface hardness and wear resistance [22-23]. Some authors like [24], studied the CO2 laser based alloying of 17-4PH material and found that the hardness of the surface is double than the substrate and the surface finish has been improved. Few authors [25] re-ported direct laser forming (DLF) of turbine blade using the metal powder. Their paper describes the fabrication of the steam turbine blade from 316L powders by DLF. The influence of laser specific energy, scanning speed and powder feeding rate on the forming characteristics of elementary units is also systematically investigated. The limitation of DLF method is that the average surface roughness obtained was much higher (10–26μm) and hence needs a finishing process to obtain a good surface finish. Others [26] studied the effect of shot-peening at fir tree roots of the blades for the residual stresses and found that the blades roughness was still high and there was no discernible effect from fatigue loading when the mean stress was set at 600 MPa. Quality and productivity improvement are most effective when they are an integral part of the product and process development cycle. The literature on Design of experiments (DOE) applied to CNC turning process can be classified based on the measured responses like tool wear in terms of a sensor (accelerometer, strain gauge, acoustic emission, temperature, ultrasonic emission, and wear area), surface roughness, tool life, cutting forces, spindle/drive, chip reflectance, and power or current.

The rotor blade, as shown in **Fig.1.4**, which is typically 60 inches in length, has a complex shape and needs to be made out by a material of low thermal conductivity to withstand temperatures above 600 degree Celsius. 12%Cr steel is a series of heat-resistant steel used as turbine blade material because of its high creep rupture properties as well as superior oxidation and corrosion resistance properties [27-28]. In order to satisfy the accuracy requirement, it is

usual to be machined on an over 4–axis machine tool using a small diameter ball end mill. To satisfy the requirements of surface roughness, it is necessary to lower the pick feed, which leads to an increase of cutting distance and time. In a material which is low thermal conductivity, as heat flow is hardly to diffuse, the tool wear easily progresses. As a result, it leads to deterioration of surface roughness in spite of long cutting time.

There are many researchers have done a lot of work for improving its accuracy and reduce the lead time. Farouki et al. optimized tool orientation control for 5-axis CNC milling with ball –end cutters for improvements in accuracy and efficiency [29]. Chiou et al. proposed a machining potential field method to generate tool path for multi-axis sculptured surface machining to achieve better surface finish with shorter machining time [30]. Beudaert et al. proposed an algorithm to smooth 5-axis tool paths to maximize the real federate and to reduce the machining time [31]. Grigoriev et al. presented a method to simultaneously increase the accuracy and decrease the calculation time for complex tool path programming in multi-axis machining centers [32].

Furthermore, poor machinability due to this causes high temperature on the tool face and strong chemical affinity with most tool material, thereby leading to premature tool failure [33]. Many investigations have been carried out on tool wear and machinability of stainless steel. Shao et al. [27] investigated the effects of tool geometry, cutting speed, and feed on surface finish as well as tool wear mechanisms when milling the 3%Co-12%Cr stainless steel, and Akasawa et al. [34] studied the effects of free-cutting additives on the machinability of austenitic stainless steel. All the work is contribute to improve the milling efficiency or accuracy, but it still has a limit due to a small pick feed value. The responses measured in most of the above mentioned literature is surface roughness, tool wear, cutting forces and tool life. There are very few reports on re- searches which studied the power consumption [35], material removal rate [36] and effect of coolant [37] during cutting operation.

Furthermore, development of the machine tools with a high speed spindle and table and the improvement of the cutting performance of tool have dramatically increased the cutting speed and material removal rate. Work to date has shown that little work has been carried on the high efficiency milling of steam turbine blade systematically.

1.2 Purpose

Conventional machining method of turbine blade, often use a small diameter, in the pick feed direction, the surface roughness definitely occurs. In general, hand finish is necessary. In order to satisfy the surface integrity, small pick feed value is selected, which caused the cutting distance to be longer. Due to this, tool wear is severe when milling stainless steel. It will shorten the tool life and affect the surface accuracy. Moreover, the removal rate is very low because it takes quite a long time to milling a piece of blade using ball end mill. For improving the milling efficiency of steam turbine blade and retarding the tool wear, we propose a new method. The surface roughness and shape error are set 6μm and 200μm respectively. The research will verify its validity both in theoretically and experimentally, and develop a special CAD/CAM for generating the toolpath of the new method, furthermore, the machining mechanism of the proposed method is explained though cutting force and cutting temperature.

1.3 Composition

In order to set forth the research, the flowchart of each chapter as shown in **Fig.1.7.**

1) Chapter 2: This chapter will introduce the proposed tilt taper end mill method. Considering the shortcoming using ball end mill, a new method using ball end mill is proposed, and its validity in both feed direction and pick feed direction is discussed in theoretically, simulation of waviness error is performed.

2) Chapter 3: This part will introduce the validity of taper end mill by tool wear experiments. In order to verify the validity of tilt taper end mill, it will compare it with ball end mill and square end mill method, the optimum cutting conditions are selected according to experiments, surface integrity and tool wear will evaluated to examine the validity of proposed method.

3) Chapter 4: this chapter will clean up the mechanism of tilt taper end mill. Cutting force and cutting temperature are measured of ball end mill, square end mill and tilt taper end mill respectively. Influences on tool wear are examined, and the mechanism of validity using tilt taper end mill will be elucidated.

4) Chapter 5: Commercial CAD/CAM cannot be used for tilt taper end mill. For that reason a special CAD/CAM is developed for generating the tool path of proposed method, and its validity is examined by experiments.

5) Chapter 6 will summary the research until now, and what will do from now on.

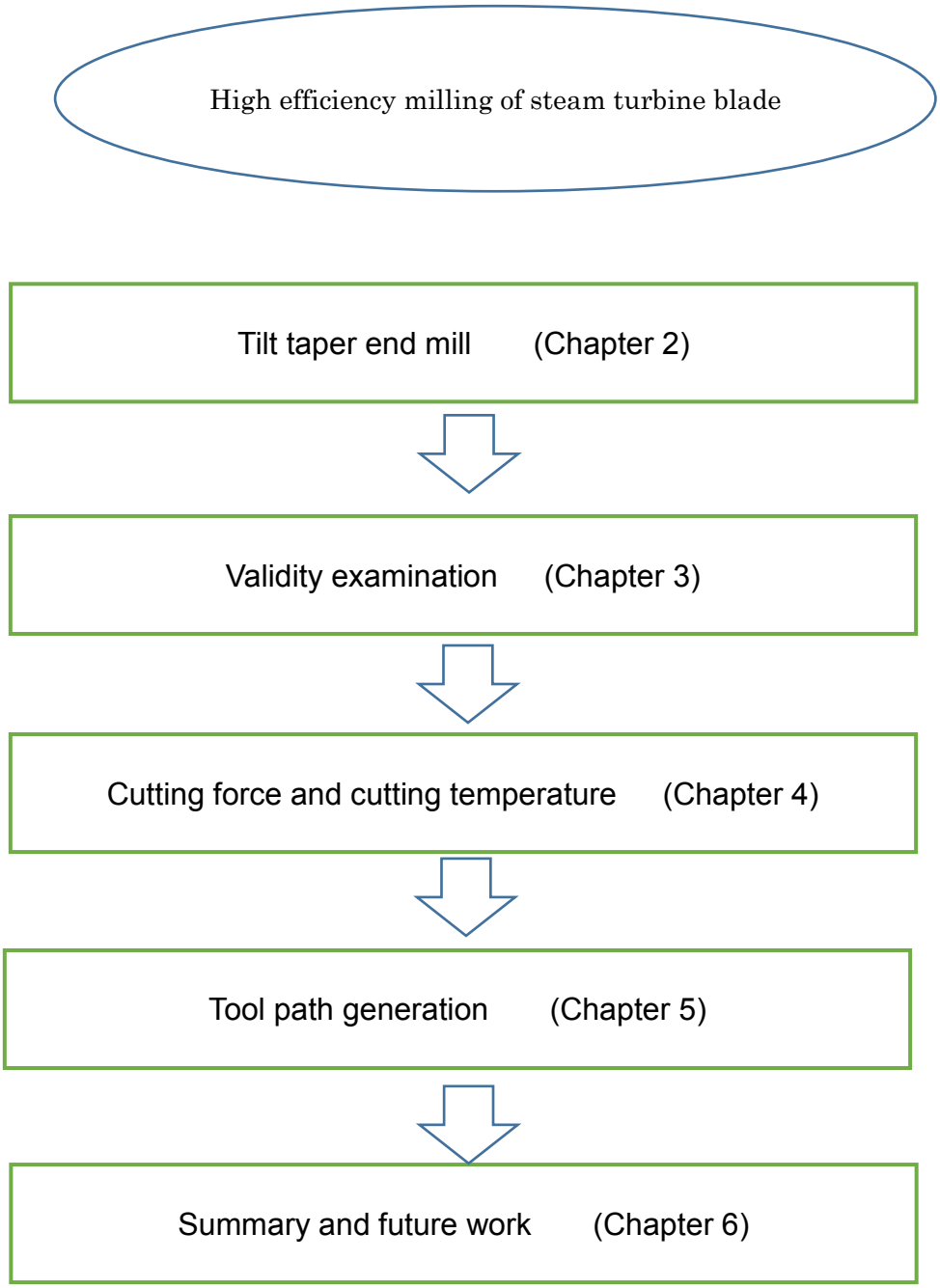

Fig.1.7. Flowchart of each chapter.

1.4 Reference

[1] Pazheri FR, Othman MF, Malik NH. A review on global renewable electricity scenario. Renewable Sustainable Energy Rev 2015; 31:835–45.
[2] Eshita Gupta. Global warming and electricity demand in the rapidly growing city of Delhi: A semi-parametric variable coefficient approach. Energy Economics2012; 34:1407-1421.
[3] Guido Pleßmann, Matthias Erdmann, Markus Hlusiak, Christian Breyer. Global energy storage demand for a 100% renewable electricity Supply. Energy Procedia2014; 46: 22 – 31.
[4] OECD/IEA, World Energy Outlook 2011, November (2011)
[5] Evangelos Panos, Martin Densing, Kathrin Volkart. Access to electricity in the World Energy Council's global energy scenarios: An outlook for developing regions until 2030. Energy Strategy Reviews2016; 9:28-49.
[6] Turbo Machinery Association, Steam Turbine New Revised Edition, 2013. (In Japanese)
[7] M.K. Gupta, S.C.Kaushik, K.R.Ranjan, N.L.Panwar, V.SivaReddy, S.K.Tyagi. Thermodynamic performance evaluation of solar and other thermal power generation systems: A review. RenewableandSustainableEnergyReviews2015; 50:567–582.
[8] Shengwei Huang, Gang Xu, Yongping Yang, Chenxu Zhang, Ligang Wang, Ningling Wang, Zhiping Yang. System Integration and Flowsheet Optimization of 1000 MWCoal-fired Supercritical Power Generation Units. Energy Procedia2014; 61:1816 – 1819.
[9] Dawid P. Hanak, Vasilije Manovic. Calcium looping with supercritical CO2 cycle for decarbonisation of coal-fired power plant. Energy2016; 102:343-353.
[10] DOE/EIA, International Energy Outlook 2011, September (2011)
[11] Gang Xu, Cheng Xu, Yongping Yang, Yaxiong Fang, Yuanyuan Li, Xiaona Song. A novel flue gas waste heat recovery system for coal-fired ultra-supercritical power plants. Applied Thermal Engineering2014; 67: 240-249.
[12] Shengwei Huang, Gang Xu, Yongping Yang, Chenxu Zhang, Ligang Wang, Ningling Wang, Zhiping Yang. System Integration and Flowsheet Optimization of 1000 MW Coal-fired Supercritical Power Generation Units. Energy Procedia 2014; 61:1816 – 1819.
[13] M. Shankar, K. Kumar, S.L. Ajit Prasad. T-root baldes in a steam turbine rotror: A case study. Engineering Failure Analysis 2010; 17: 1205-1212.

[14] Bernd M. Schonbauer, Stefanie E. Stanzl-Tschegg, Andrea Perlega, Ronald N. Salzman, Neville F. Rieger, Shengqi Zhou, Alan Turnbull, David Gandy. Fatigue life estimation of pitted 12% Cr steam turbine blade steel in different environments and at different stress ratios. International Journal of Fatigue2014; 65:33–43.
[15] J. Kubiak Sz., G. Urquiza B., J. Garcı´a C., F. Sierra E. Failure analysis of steam turbine last stage blade tenon and shroud. Engineering Failure Analysis2007; 14:1476–1487.
[16] Loveleen Kumar Bhagi, Pardeep Gupta, Vikas Rastogi. Fractographic investigations of the failure of L-1 low pressure steam turbine blade. Case Studies in Engineering Failure Analysis 2013; 1:72–78.
[17] H. Nomoto. High-performance technology of steam turbine blades. TOSHIBA REVIEW 2010; 65 No.12:66- 67. (In Japanese)
[18] Gotoh Jinichiro, Kuba Shunichi, Teranishi Mitsuo, Kamino Kenji, Hirose Fumiyuki. Hitachi's Gas Turbine Product Range and Development Background. Hitachi Review2012; Vol.94 No.11:762-763.
[19] Senoo Shigeki, Asai Kunio, Kurosawa Atsuhiro, Lee Goingwon. Titanium 50-inch and 60-inch Last-stage Blades for Steam Turbines. Hitachi Review2012; Vol.94 No.11:764-765.
[20] C. Phaneendra Kiran, Shibu Clement. Surface quality investigation of turbine blade steels for turning process. Measurement2013; 46:1875–1895.
[21] C.-H. Richter. Structural design of modern steam turbine blades using ADINA™, Computers & Structures2003; 81:919–927.
[22] K.H. Lo, E.T. Cheng, C.T. Kwok, H.C. Man. Improvement of cavitation erosion resistance of AISI 316 stainless steel by laser surface alloying using fine WC powder. Surface & Coatings Technology2003; 258:165–167.
[23] J. Wang,H.Zou. The microstructure evolution of type 17-4PH stainless steel during long-term aging at 350℃. Nuclear Engineering and Design2006; 236:2531–2536.
[24]J. Yao, L. Wang, Q. Zhang, F. Kong, C. Lou, Z. Chen, Surface laser alloying of 17-4PH stainless steel steam turbine blades, Optics & Laser Technology 40 (6) (2008) 838–843.
[25] Z.L. Lu, D.C. Li, Z.Q. Tong, Q.P. Lu, M.M. Traore, A.F. Zhang, B.H. Lu. Investigation into the direct laser forming process of steam turbine blade, Optics and Lasers in Engineering2011; 49:1101–1110.
[26] M.N. James, M. Newby, D.G. Hattingh, A. Steuwer. Shot-peening of steam

turbine blades: residual stresses and their modification by fatigue cycling, Procedia Engineering2010; 2:441–451.
[27] H. Shao, L. Liu, H.L. Qu, Machinability study on 3%Co-12%Cr stainless steel in milling, Wear2007; 263:736-744.
[28] N.R. Dhar, M. Kamruzzaman, Cutting temperature, tool wear, surface roughness and dimensional deviation in turning AISI-4037 steel under cryogenic condition, International Journal of Machine Tools & Manufacture 2007; 47:754-759.
[29] Rida T. Farouki, Shiqiao Li. Optimal tool orientation control for 5-axis CNC milling with ball-end cutters. Computer Aided Geometric Design 2013; 30:226-239.
[30] Chuang-Jang Chiou, Yuan-Shin Lee. A machining potential field approach to tool path generation for multi-axis sculptured surface machining. Computer – Aided Design 2002; 34:357-371.
[31] Xavier Beudaert, Pierre-Yves Pechard, Christophe Tournier. 5-Axis tool path smoothing based on drive constraints. International Journal of Machine Tools & Manufacture 2011; 51:958-965.
[32] Sergej N. Grigoriev, A. A. Kutin, V. V. Pirogov. Advanced method of NC programming for 5-axis machining. Procedia CIRP2012; 1:102-107.
[33] Balkrishna Rao, Chinmaya R. Dandekar, Yung C. Shin. An experimental and numerical study on the face milling of Ti-6Al-4V alloy: Tool performance and surface integrity. Journal of Materials Processing Technology 2011; 211:294-304.
[34] T. Akasawa, H. Sakurai, M. Nakamura, T. Tanaka, K. Takano. Effects of free-cutting additives on the machinability of austenitic stainless steels. Journal of Materials Processing Technology 2003; 143-144: 66-71.
[35] A. Aman, S. Hari, K. Pradeep, S. Manmohan. Optimizing power consumption for CNC turned parts using response surface methodology and Taguchi technique – a comparative analysis. Journal of Material Processing Technology2008; 200:373–384.
[36] L. Tian-Syung, W. Ming-Yung. Competitive parameter optimization of multi-quality CNC turning. International Journal of Advanced Manufacturing Technology2009; 41:820–826.
[37] M. Joseph Davidson, K. Balasubramanian, G.R.N. Tagore. Surface roughness prediction of flow-formed AA6061 alloy by design of experiments. Journal of Materials Processing Technology2008; 202:41–46.

1.5 Nomenclature

p_f pick feed of the end mill
R radius of ball end mill
R_{th} theoretical surface cusp height of machined surface using a ball end mill
R'_{th} theoretical surface cusp height of machined surface using tilt taper end mill
ρ_p curvature radius in pick feed direction of turbine blade
W_z waviness error in pick feed direction
f_z feed per tooth
R' the distance from tool rotation axis to cutting edge
ρ_f curvature radius in feed direction of turbine blade
ρ_{in} curvature radius of concave surface in feed direction
ρ_{out} curvature radius of convex surface in feed direction
R_f theoretical surface cusp height of machined surface in feed direction
Z milling efficiency
V cutting speed
a_a axial depth of cut
n number of tooth
D outside diameter of cutting tool
k_r cutting edge angle
γ rake angle
α clearance angle
d shank diameter
R_z height of profile
N rotational speed
VB_{max} maximum width of flank wear
Fx cutting force in X direction
Fy cutting force in Y direction
Fz cutting force in Z direction
Temp cutting temperature
$\boldsymbol{t_r}$ the edge point of top end
$\boldsymbol{t_\theta}$ angle of the taper edge
$\boldsymbol{t_p}$ a point at the cutting edge
$\boldsymbol{v}$ the length from $\mathbf{t_r}$ to $\mathbf{t_p}$
$\boldsymbol{\omega}$ the angle in rotating direction relative to Z axis of tool coordinate.
$\boldsymbol{u_s}$ the start angle in rotating direction of part surface

u_e the end angle in rotating direction of part surface

v_s the start angle in height direction of part surface

v_e the end angle in height direction of part surface

n normal vector of part surface

Pn the number of tool path

i the ordinal number of the tool path

Ps the start tool path angle in height direction

Pd the angle of two adjacent tool paths

b spatial parameter of the tool path

cp tool path formula

*D***cp** tangent vector of tool path

l the distance from pivot point of B axis to the bottom surface of tool

dd depth of cut in normal vector direction

cf the unit tangent vector of the cutter contact points in feed direction

cn surface normal at the point

cb cross product **cf** and **cn**

ccp the local coordinate of the starting point

Chapter 2 Tilt taper end mill

2.1 Conventional methods

Development of the machine tool with a high speed spindle and table and the improvement of the cutting performance of tool materials have dramatically increased the cutting speed and material removal rate [1]. Furthermore, the widespread multi-axis machine tools permit the high efficiency and high precision machining free surface of a product by controlling the trajectory and the posture of a ball end mill [2]. Conventional machining method of turbine blade, often use a small diameter on an over 4 control axes machining tool, **Fig.2.1** show the raw material after rough machining. Give it a feed direction and a pick feed direction, tool and the table keep an inclination angle which can be adjusted so as to obtain the required shape. On this occasion, in the pick feed direction, height of cusps generated on the machined surface.

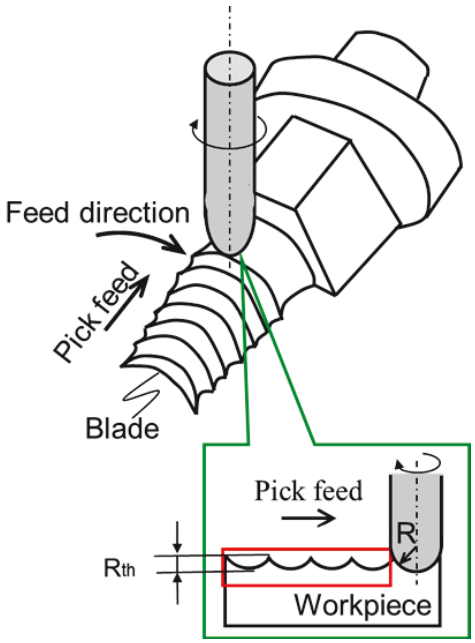

Fig.2.1. Conventional method.

The cusp height R_{th} of the surface machined by a ball end mill with the radius of R is theoretically expressed as the following equation:

$$R_{th} = \frac{P_f^2}{8R} \tag{2.1}$$

where p_f is the pick feed of the ball end mill.

Therefore, the pick feed value affects the cusp height greatly. In addition, thermal conductivity of the blade material should be low due to the temperature of working environment is more than 600 degree Celsius. Such as chromium kind SUS403, its low thermal conductivity causes the tool wear to be accelerated. In order to satisfy surface roughness requirement, it should use a small pick feed. When the pick feed is small, the cutting length becomes longer so that the tool wear becomes serious. Although the number of tool change increases, this also increase the machining cost. Another, cutting speed at the tip in zero so that it cannot removal the material completely, the larger change range of cutting speed at cutting edge also affect the stability of cutting process.

Obviously, conventional method that use small diameter ball end mill can obtain a high accuracy surface, but milling efficiency is low. Generally, hand finish is also needed. Based on the problems of conventional method, instead of the ball end mill, a new method that can shorten the cutting length and adopt a large pick feed to lower the surface roughness value and the cost as much as possible is needed.

2.2 Tilt taper end mill

Turning with an end mill so called turn-milling is proposed instead of turning with a single point cutting tool [3-6]. This method prevents troubles often caused by a long continuous chips produced in turning process and permits the automation of machining process. However, height of cusps generated on the curved surface machined with a ball end mill or a corner radius end mill if often larger than the height of feed marks in turning with a single point tool.

Based on the preceding paragraph, tilt taper end mill method is proposed, it can use a large pick feed and the surface roughness value is small.

The schema is shown as **Fig.2.2**. It is given a feed direction and a same pick feed direction as conventional ball end mill method. The diameter is larger, and cutting speed not only can be higher but also can keep the cutting speed changing in a small range, the holder and the table also keep an inclination angle that can be adjusted to ensure the cutting edge is parallel to the pick feed direction. The surface roughness value of this method is close to zero in pick feed direction,

so it can adopt a large pick feed to shorten the cutting distance.

When it is used to machining a curved surface, as shown in **Fig.2.3**, instead of curves, it combined by short straight lines, therefore, when real machining the steam turbine blade, tool wear can be retarded due to short cutting length, the pick feed is large so that the cutting time becomes shorter, moreover, the surface roughness value is very small so that can eliminate the hand finish.

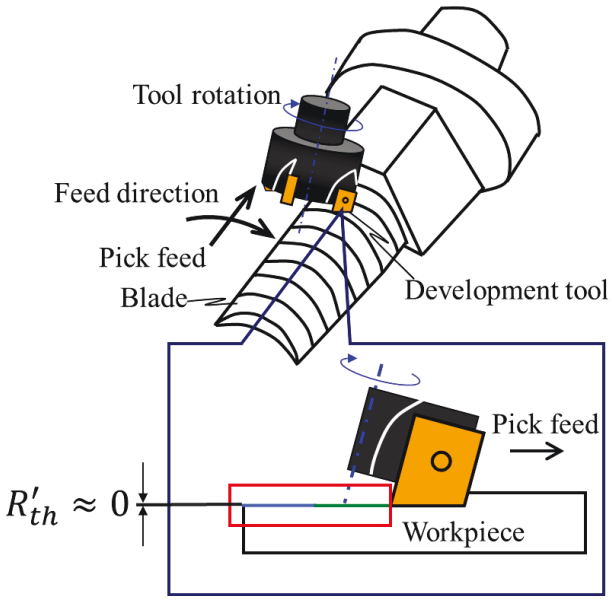

Fig.2.2. Schema view of tilt taper end mill.

2.3 Waviness error

Pick feed is an important factor that influencing the milling efficiency, additionally, its value also influences the surface integrity. To the 60 inches last stage blade, pick feed and feed direction are given as shown in **Fig.2.3.** In the pick feed direction, arc and short straight line deviate occurs, the waviness error formula is given as **Eq. (2.2)**.

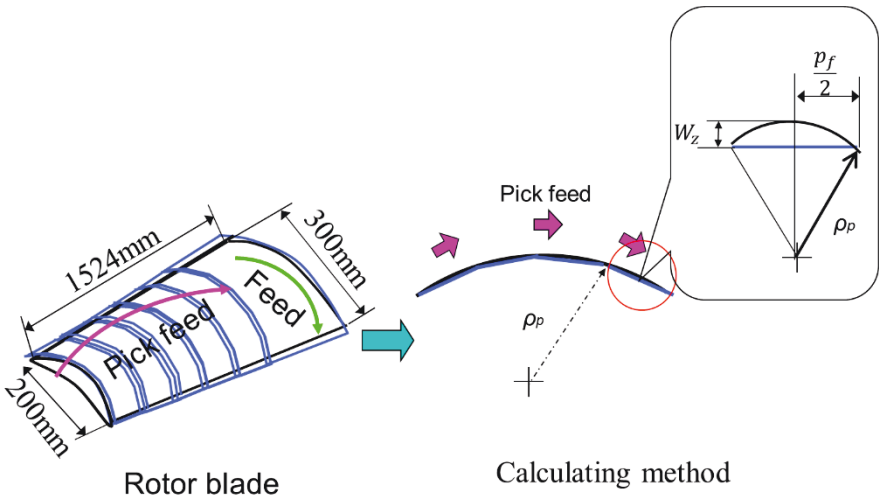

Fig.2.3. Waviness error.

$$W_z = \rho_p - \sqrt{{\rho_p}^2 - \left(\frac{p_f}{2}\right)^2} \tag{2.2}$$

where ρ_p represent the curvature radius in pick feed direction, the p_f denotes the pick feed value.

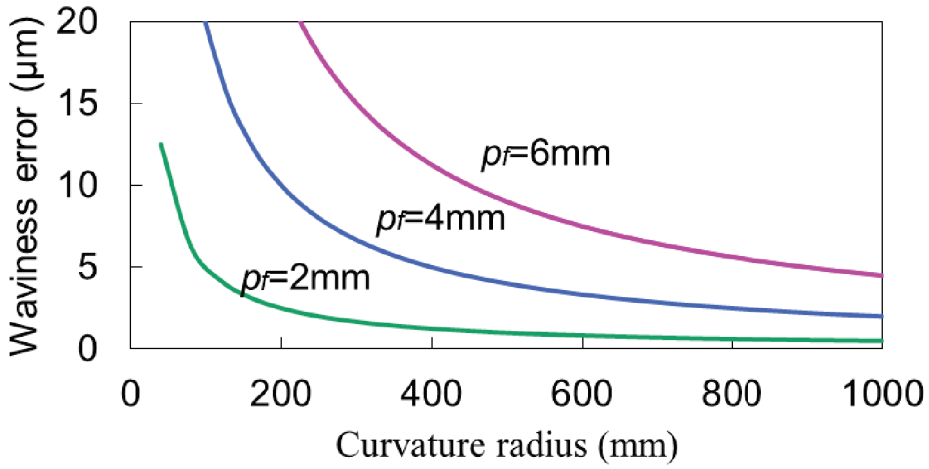

Fig.2.4. Waviness error at different pick feed values.

A simulation was carried out when pick feed values were 2mm, 4mm and 6mm (see **Fig.2.4**). Waviness error grows down with curvature radius. For 60-inch rotor blade, the curvature radius ρ_p of steam turbine blade in pick feed direction discussed is more than 400mm, so only *pf*=2mm and *pf*=4mm can satisfy the

surface roughness requirement, when pick feed value is larger, the cutting time become shorter, moreover, cutting length also can be shorter so that the tool wear slightly. Therefore, p_f=4mm can be selected for following tool wear experiments.

2.4 Theoretical surface roughness in feed direction

Processing the blade when p_f = 4mm, the accuracy has been discussed smaller enough than the target accuracy (6μm). In contrast, if the shape is curved in feed direction, as shown in **Fig.2.5**, the feed amount per tooth f_z, the radius of curvature ρ_{in} (concave surface)and ρ_{out} (convex surface), the maximum cusps height R_f is given by **Eq. (2.3)** and **Eq. (2.4)**. R' is the distance from tool rotation axis to cutting edge (**Fig.2.6**). Here, if the tool and cutting conditions are constant, the first half in parentheses is a constant. R' selects as maximum value16mm, the effect of f_z and ρ_f on R_f is shown in **Fig.2.7**. From this result, it can see that the height of cusps increases with feed per tooth, and decreases with curvature radius grows. Concave impact the cusps height is greater than the that of the convex surface, moreover, the influence of the per tooth is small when radius of curvature over 100mm, both concave and convex surface can also be a $R_f \leqq$ 6μm when feed per tool within 1.4mm/tooth.

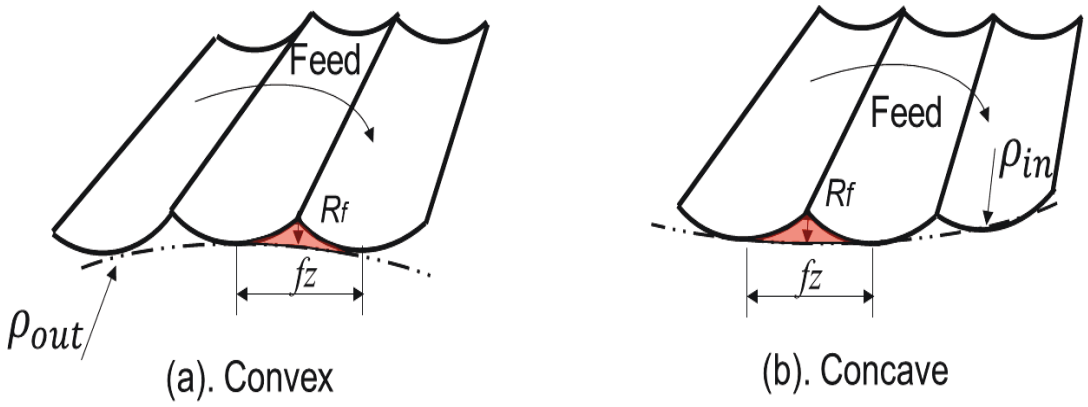

Fig.2.5. Cusps when milling curved surface

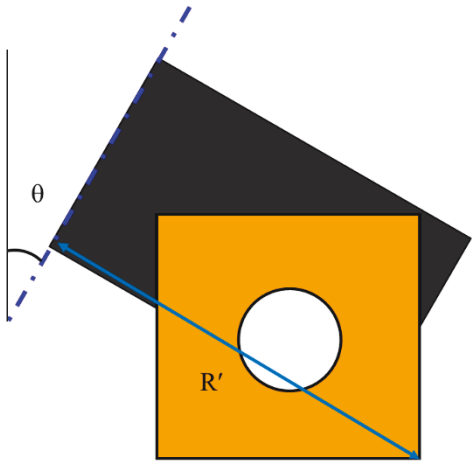

Fig.2.6. Sectional view of tilt taper end mill.

$$\boldsymbol{R_f} = \left[R' - \sqrt{R'^{\,2} - \left(\frac{f_z}{2}\right)^2}\ \right] \sin\theta - \left[\rho_{out} - \sqrt{\rho_{out}{}^2 - \left(\frac{f_z}{2}\right)^2}\ \right] \tag{2.3}$$

$$\boldsymbol{R_f} = \left[R' - \sqrt{R'^{\,2} - \left(\frac{f_z}{2}\right)^2}\ \right] \sin\theta + \left[\rho_{in} - \sqrt{\rho_{in}{}^2 - \left(\frac{f_z}{2}\right)^2}\ \right] \tag{2.4}$$

where R' is the distance from tool rotation axis to cutting edge, f_z is the peed per tooth, ρ is curvature radius in feed direction, θ is the inclination angle.

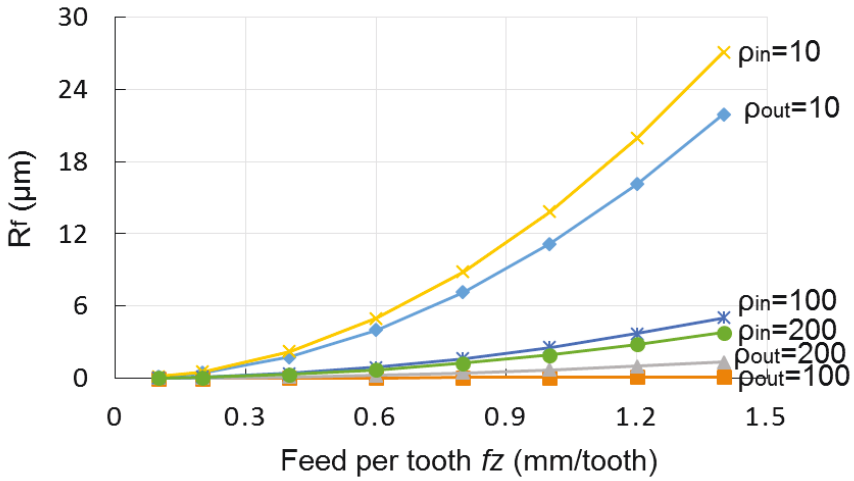

Fig.2.7. Relationships between feed per tooth and surface roughness R_f.

2.5 Conclusions

Considering the problems of conventional method using ball end mill, a new method using tilt taper end mill was proposed, conclusions can be drawn as following:

1. In pick feed direction, waviness error occurs, in case of curvature radius over 400mm, it is under 6μm when pick feed less than 4mm.
2. In the feed direction, cusps occurs, the height increases with the feed per tooth and decreases with curvature radius grows, the value is less than 6μm when curvature radius over 100mm. When milling concave, the value is larger than milling convex.

References

[1] H. Onozuka, K. Utsumi, I. Kono, J. Hirai, Y. Numata, T. Obikawa. High speed milling processes with long oblique cutting edges, Journal of Manufacturing Processes 2015; 19: 95-101.
[2] T. Muraki, H. Yamamoto. Current state and outlook of the multi-tasking machine. Journal of the Japan Society for Precision Engineering 2012; 78(9):740-743 (in Japanese).
[3] Seimitsu Kogaku Kaishi. Mill-turning by using multi-tasking machine (lathe with milling spindle)-The method of high speed dry turning. Journal of the Japan Society for Precision Engineering 2003; 69(7): 965-969 (in japanese).
[4] H. Savas, C. Ozay. Analysis of the surface roughness of tangential turn-milling for machining with end milling cutter. Journal of Materials Processing Technology 2007; 186:279-283.
[5] H. Schulz, T. Kneisel. Turn- Milling of Hardened Steel – an Alternative to Turning. CIRP Annals- Manufacturing Technology 1994; 43(1): 93-96.
[6]Joel Martins Crichigno Filho. Prediction of cutting forces in mill turning through process simulation using five-axis machining center. The International Journal of Advanced Manufacturing Technology 2012; 58(1): 71-80.

Chapter 3 Validity examination

3.1 Introduction

In chapter 2, a new method was proposed for milling steam turbine blade, and the validity had been discussed in theoretically. The validity in real milling is also need to be examined. However, when we use freeform surface, it is difficult to ensure the same conditions and evaluate the accuracy. Considering the differences of conventional method and proposed method, model experiment is needed. In order to measure the surface integrity, the surface is plane. An important merit of taper end mill is that can retard the tool wear, therefore, tool wear experiments is necessary. When doing the experiments, surface integrity such as surface roughness and surface profiles are be evaluated, using these factors to examine the validity. Tilt taper end mill owns the characteristics of ball end mill and square end mill, in order to prove the advantage of tilt taper end mill method, tool wear experiments of the three methods are carried out, the results will be discussed.

3.2 Experimental conditions

Removal rate is the removal amount in per unit time. Here, we use removal rate to represent the milling efficiency. Its formula is given as the following:

$$\textbf{Milling efficiency } Z = \frac{p_f \times f_z \times V \times a_a \times n}{\pi D} (\mathrm{mm^3/min}) \qquad (3.1)$$

where, p_f: pick feed (mm), f_z: feed per tooth (mm/tooth), V: cutting speed (m/min), a_a: axial depth of cut (mm), **D**: the diameter of the tool, n: number of tooth.

The tool diameter and number of tooth are constant, so only pick feed, feed per tooth, cutting speed and axial depth of cut influence on the milling efficiency.

Pick feed is an important factor that influence the milling efficiency, additionally, its value also influences the surface integrity. For the 60 inches last stage blade, when using tilt taper end mill ,as discussed in chapter 2, the pick feed value can be selected 4mm. The commercial tool was selected in these experiments. Therefore, the left three parameters can be selected in the recommended range. Experimental diagram of tilt taper end mill as shown in **Fig.3.1**. Cutting angle is 10 degree, in order to keep the cutting edge is parallel to the pick feed direction, the table was rotated 10 degree relative to Y axis. The feed direction and pick

feed direction see **Fig.3.1**.

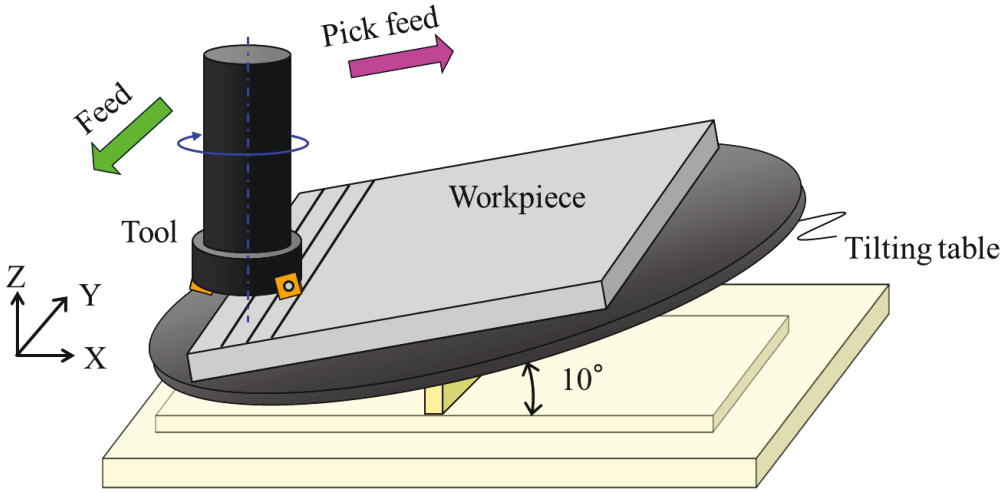

Fig.3.1. Experimental diagram.

The holder used a throw away end mill which the inserts could be changed conveniently, the holder (SANDVIK R210-032A25-09M) as shown in **Fig.3.2**. It has two cutting edges, the cutting edge angle k_r is 10 degree, its setting up error is less than 0.2 degree, rake angel γ and clearance angle α are 0° and 7°respectively. The important sizes is shown in **Table 3.1.** Deflections of cutting tools are ignored. Cutting tool wear is the result of load, friction, and high temperature between the cutting edge and the workpiece. Several wear mechanisms can occur during metal cutting: adhesive wear, abrasive wear, diffusion wear, oxidation wear, and fatigue wear [1]. The tribological properties of a single tool material never satisfy all performance requirements. Coated tools can produce high wear resistance on the surface with high toughness in the substrate material. Properly applied coatings increase the hardness of cutting tools at high cutting temperatures, thus minimizing abrasive wear. The coating provides a chemical barrier to decrease diffusion or reaction between the tools and the workpiece, thus reducing tool wear. Most of the heat generated during machining goes into the chips, and the tool substrate stays cooler than with uncoated tools. The high lubricity of most coatings reduces the coefficient of friction between the cutting tool and the workpiece, which also reduces cutting temperature. Lubricity and the chemical–thermal barriers provided by coatings reduce adhesion and welding of chips to the tools. The formation of built-up edge

(BUE) and cratering of the workpiece are also minimized. While coating increases initial cost, the benefits of coatings are often more than their cost. Coated tools generally have longer tool life, fewer tool changes, with improved workpiece surface finish, etc. The cost per part is lowered [2-7]. In these experiments, the inserts (SANDVIK R210-090412M-MM 1040) is M kind cemented carbide coated by TiAlN multilayer which is fit the holder. One insert milling operations were used to evaluate the machinability. The schema and important sizes as shown in **Fig. 3.3.**

The experiments were carried out on the 3-axis control milling machine (Osakakiko rakuraku-mill 3V), as shown in **Fig.3.4**. In order to keep the cutting edge is parallel to the pick feed direction, the workpiece needs to be inclined, here, tilt table (Tudacoma TT-200) was used, as shown in **Fig.3.5**.

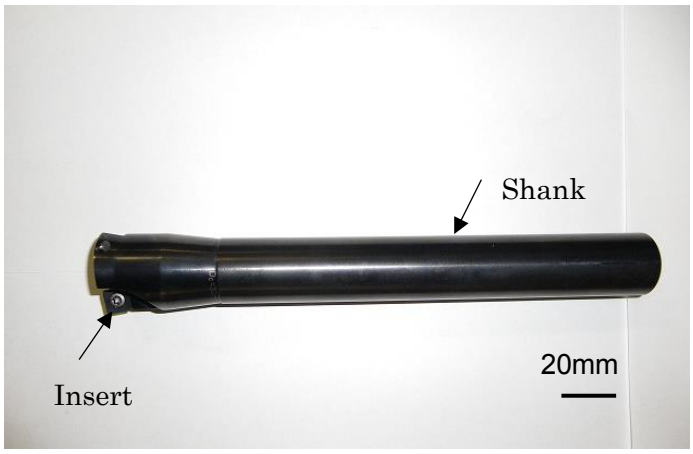

(a) Holder for tilt taper end mill

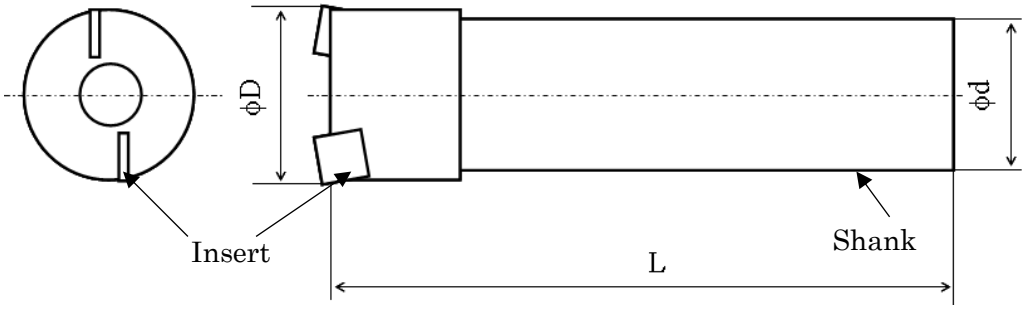

(b) Schema of the holder.

Fig.3.2. Throw away cutter holder for tilt taper end mill.

Table 3.1 Tool specification.

Maximum diameter D	32 [mm]
Shank diameter d	25[mm]
Overall length L	210 [mm]
Rake angle	0 [℃]
Clearance angle	7 [℃]

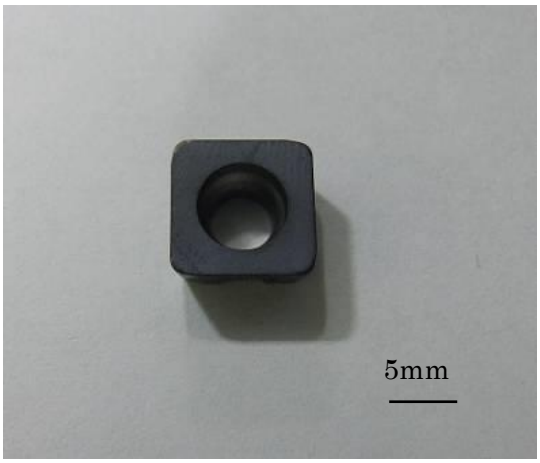

(a) Images of insert

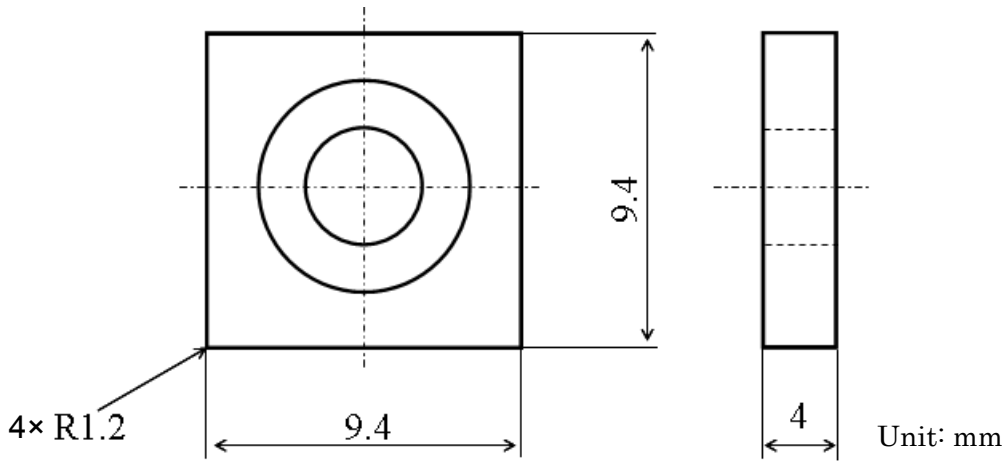

(b) Schema of cutting insert.

Fig.3.3. Cutting insert.

Fig.3.4. Photograph of machine tool (Osakakiko rakuraku-mill 3V).

Fig.3.5. Photograph of tilt table (Tudacoma TT-200).

Before performing the tool wear experiments, it needs to determine the left three parameters. Cutting conditions are given in **Table 3.2**. Pick feed is 4mm, the feed length is 80mm. When two parameters are constant, the left one is variable, the surface roughness value are used to evaluate the influence on surface integrity, the smaller the value, the better surface quality can be obtained. As it need many times to justify each cutting factors influence on surface roughness, here, the workpiece width is taken 100mm as shown in **Fig.3.6**. Surface roughness was measure by the digital microscope ACCRETECH SURFCOM 130A as shown in **Fig.3.7**. The down-milling method was chosen in the experiments to reduce the tool wear and produce better quality of workpiece surface finish [8].

The relationships between feed per tooth and surface roughness R_z is presented in **Fig.3.8**. When cutting speed and axial depth of cut are constant, surface roughness increases with feed per tooth except fz=0.1 mm/tooth, besides, when fz=0.38mm/tooth, surface roughness value is minimum. At feed per tooth 0.1mm/tooth, surface profile keeps steady, but in some places, peculiarity occurred, it probably caused by remained chips.

The relationships between cutting speed and surface roughness is shown in **Fig.3.9**. When axial depth of cut is constant and fz=0.38mm/tooth, surface roughness decreases with cutting speed, when V=160m/min, surface roughness value is the smallest. From the result, it also can see that high cutting speed can improve the surface integrity, this may be due to the reduction of work hardening when the high cutting speed cause the temperature at the tip.

The relationships between axial depth of cut and surface roughness is denoted in **Fig.3.10.**When selected feed per tooth and cutting speed are constant, the surface roughness values have a slight up and down. Although the surface roughness value is minimum when a_a =0.05mm, a_a=0.05mm is the base condition, when a_a =0.15mm, the surface roughness is very little as well and the efficiency is higher than that of a_a=0.05mm, therefore, here, select a_a as the optimum factor value.

According to the former three experiments, the base conditions of removal amount in per unit time are selected as following:

- Feed per tooth fz=0.38 [mm/tooth]
- Cutting speed V=160 [m/min]
- Axial depth of cut a_a=0.15 [mm]

For the selected cutting condition, the milling efficiency is 365 mm^3, and then

when the efficiency and a factor were constant, the influences the other two factors on surface roughness were examined.

Table 3.2 Cutting conditions.

Machine tool	Osakakiko rakuraku-mill 3V Tudacoma TT-200
Tool holder	Φ32 (Sandvik R210-032A25-09M)
Insert	Coated cemented carbide (Sandvik R210-0904 12M-MM 1040)
Workpiece	SUS403 (100×80)
Cutting speed V [m/min]	30~160
Tool revolution N [rev/min]	300~1600
Feed per tooth f_z [mm/tooth]	0.1~1.54
Pick feed p_f [mm]	4
Axial depth of cut a_a [mm]	0.05~0.4

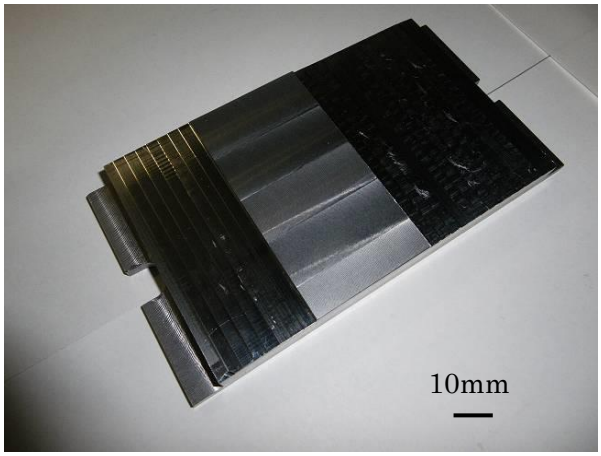

Fig.3.6. Image of workpiece used for parameter selection.

(a) Detector

(b) Operator

Fig.3.7. Photographs of surface roughness tester (ACCRETECH SURFCOM 130A).

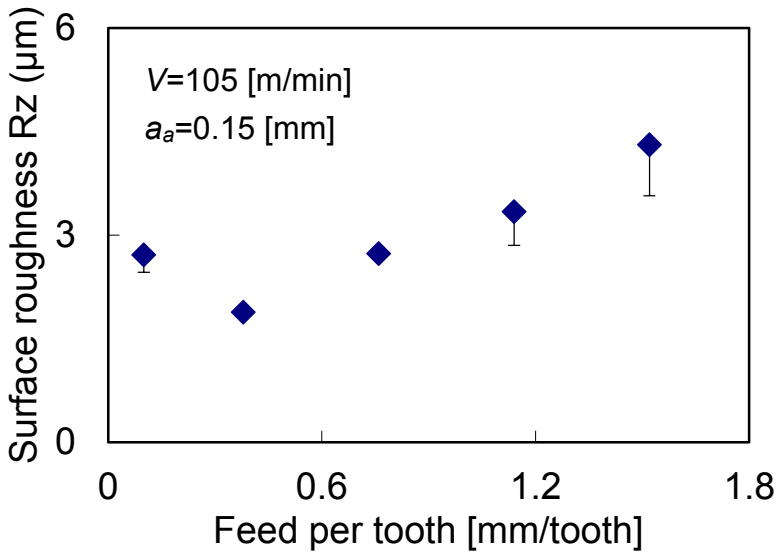

Fig.3.8. Relationships between feed per tooth and surface roughness.

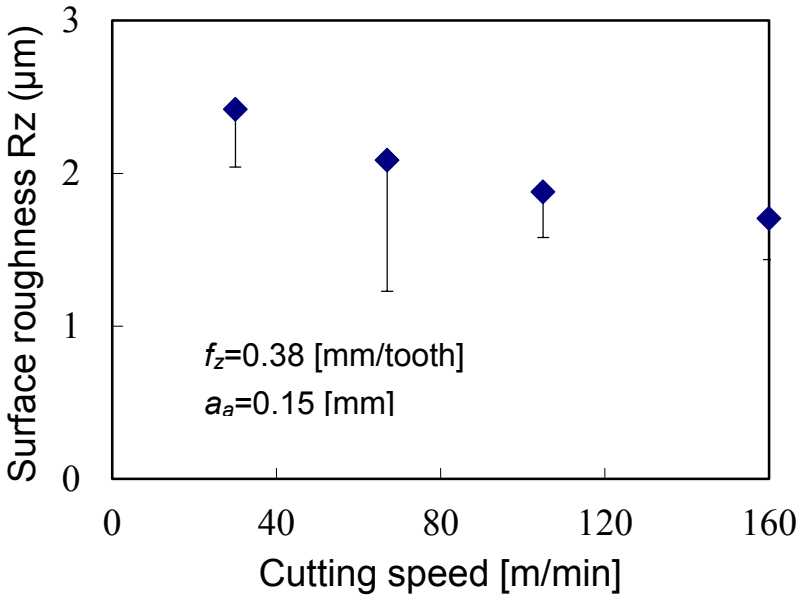

Fig.3.9. Relationships between cutting speed and surface roughness.

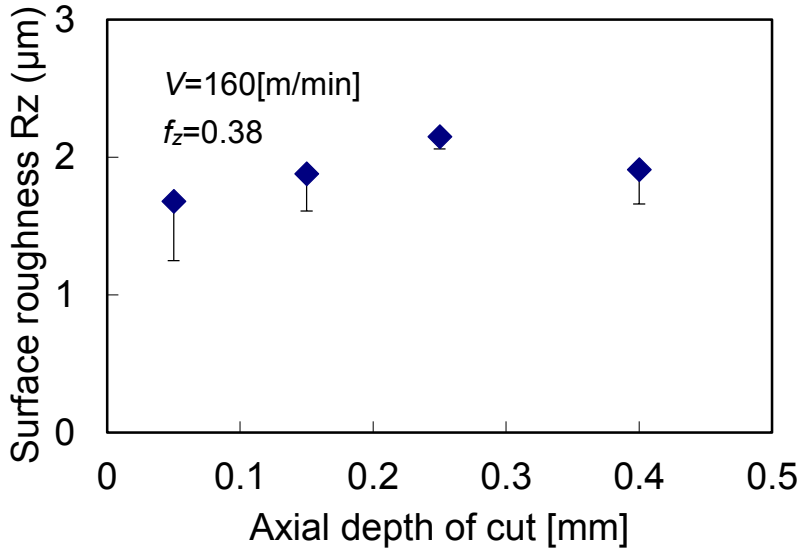

Fig.3.10. Relationships between axial depth of cut and surface roughness.

When cutting speed was constant, the influences of feed per tooth and axial depth of cut on surface roughness is presented in **Fig.3.11**. The results show when milling efficiency and cutting speed are constant, the surface roughness value nearly keep constant.

Fig.3.12 show the influence of cutting speed and axial depth on surface roughness. When cutting speed and milling efficiency are constant, surface roughness values increases with the cutting speed, while the values all around 1 micron, the former results presented that surface roughness decreases with the cutting speed, so within the experimental range of axial depth of cut, surface roughness decreases with axial depth of cut.

Fig.3.13 shows influences of feed per tooth and cutting speed on surface roughness. The results shows that when milling efficiency and axial depth of cut are constant, the surface roughness values increase with feed per tooth, as high cutting speed can lower the surface roughness value, so it can see that large feed per tooth will lower surface integrity.

It also can be seen that when the milling efficiency is constant, surface roughness changes within 1.5 μm. For verify the validity of taper end mill, we select the maximum surface roughness value, thus, the selected cutting conditions are:

• Feed per tooth ***fz***=0.91 [mm/tooth]

• Cutting speed ***V***=67 [m/min]
• Axial depth of cut a_a =0.15 [mm].

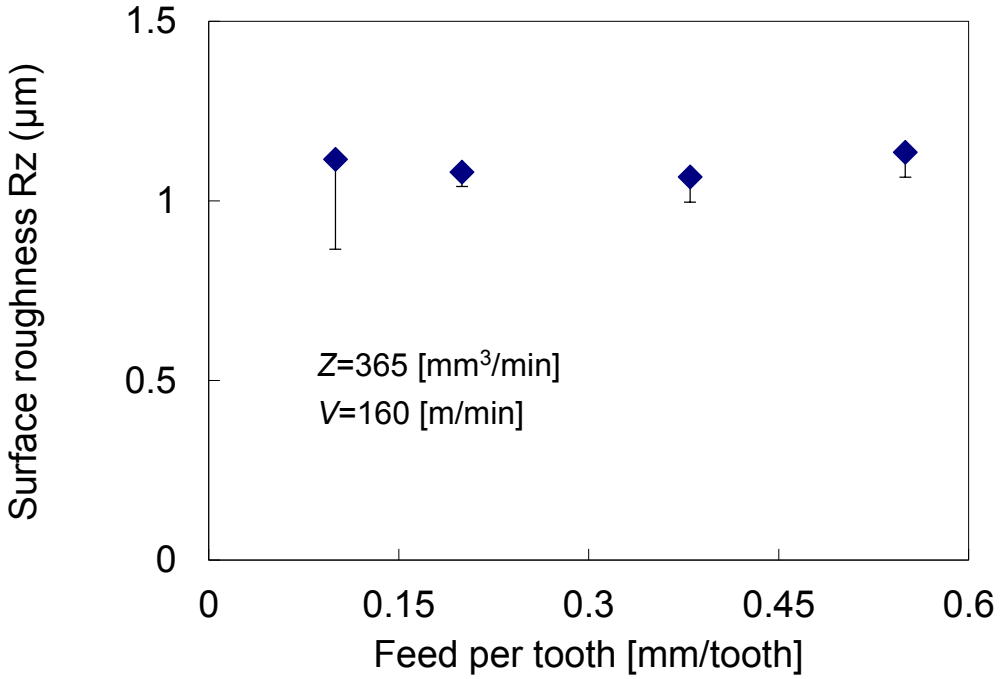

Fig.3.11. Influences of feed per tooth and depth of cut on surface roughness.

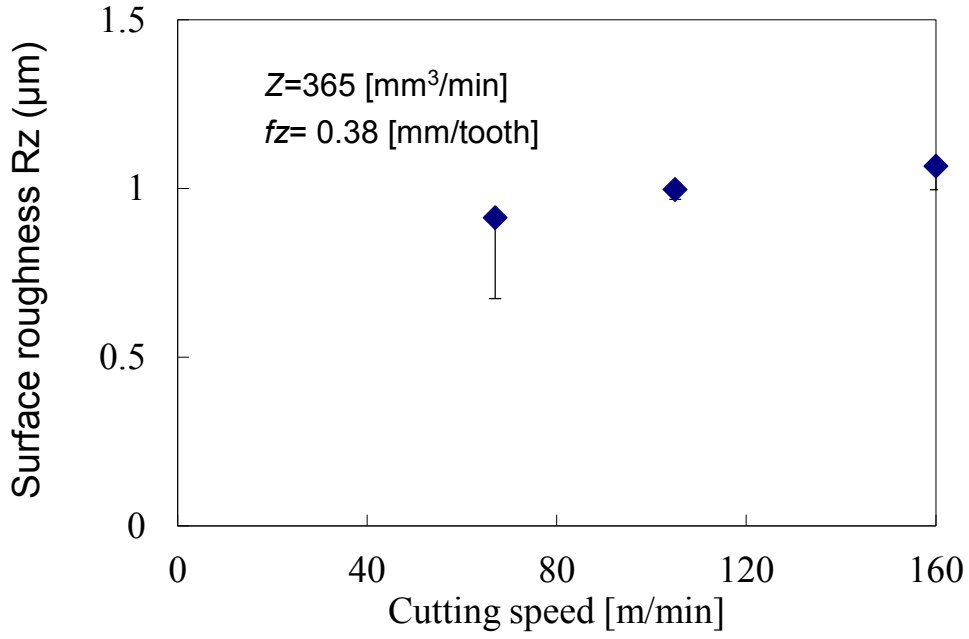

Fig.3.12. Influences of cutting speed and axial depth of cut on surface roughness.

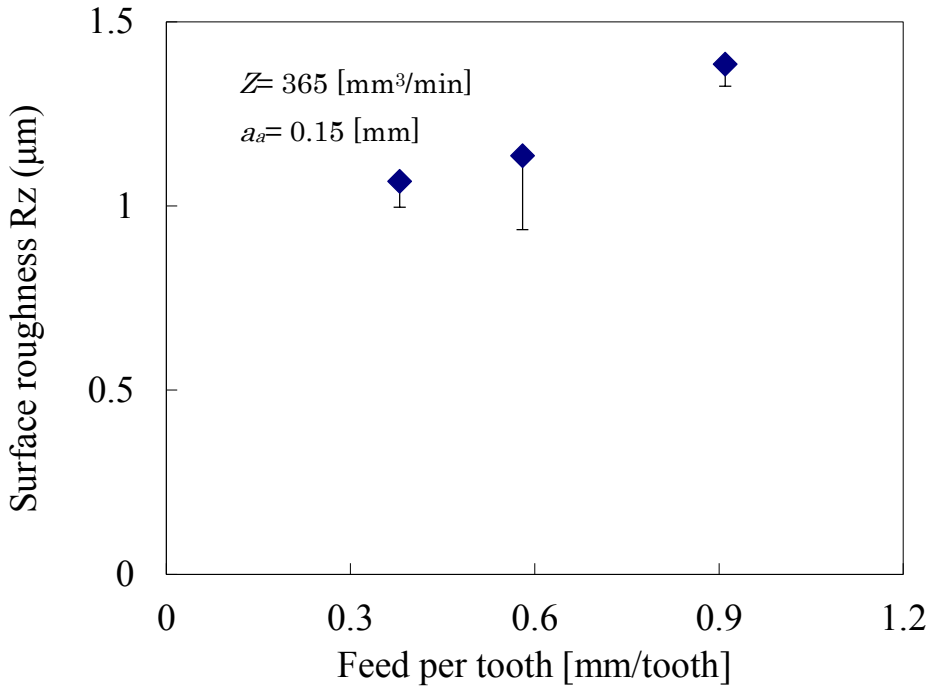

Fig.3.13. Influences of feed per tooth and cutting speed on surface roughness.

Tilt taper end mill owns some characteristics of ball end mill and square end mill, in order to confirm the validity of the proposed milling method, tool wear experiments of tilt taper end mill, ball end mill and square end mill were performed. The theoretical surface roughness of ball end mill which radius is 3mm is set 1.2μm so that the pick feed is 0.17mm, feed speed is set maximum of machine tool. For the square end mill, its diameter is 12mm, pick feed is set 4mm and tool revolution is set 1600 min^{-1} in order to ensure the cutting speed is approach the cutting speed of tilt taper end mill. Therefore, the cutting conditions is decided in **Table 3.3.** Ball end mill (Sandvik R216.42-06030-AC10P 1620) and square end mill (Sandvik1P230-1200-XA 1630) were selected, diameter are 6mm and 12mm respectively, have two-flute and the material was cemented carbide coated by TiNAl multilayer. All the experiments were carried out with coolant on.

Table 3.3. Cutting conditions.

		Tilt taper end mill	Ball end mill	Square end mill
Work material		SUS403 (HRC45)		
Tool	Material	TiAlN coated cemented carbide		
	Diameter [mm]	32	6	12
	Number of flutes	2	2	2
Pick feed p_f [mm]		4	0.17	4
Cutting speed V [m/min]		67	188	60
Feed per tooth f_z [mm/min]		0.91	0.1	0.455
Axial depth of cut a_a [mm]		0.15	0.15	0.15
Cutting fluid		Water –insoluble cutting oil N4 kind		

Another cutting conditions for tool wear experiments were selected according to experiments. This time, the cutting parameters except axial depth of cut of three cutting methods were chosen based on the influences on surface roughness. Because this research just discuss the finish milling, depth of cut is 0.1mm.The diameter of the square end mill (Sandvik1P230-0600-XA 1630) is 6mm. Cutting conditions are given in **Table 3.4**, it was performed on 3 axis milling machine (Duravetical 5060) as show in **Fig.3.14.**

Table 3.4. Cutting conditions.

		Taper end mill	Ball end mill	Square end mill
Machine tool		3 axis milling machine Duravetical 5060		
Tool	Material	TiAlN coated cemented carbide		
	Diameter [mm]	32	6	6
	Number of teeth	1	2	2
Pick feed p_f [mm]		3.0~5.0	0.08~0.22	3.0~5.0
Feed per tooth ***fz*** [mm/tooth]		0.38~1.90	0.04~0.12	0.01~0.15
Tool revolution ***N*** [mm^{-1}]		300~1600	6000~1000	2000~10000
Axial depth of cut a_a [mm]		0.1		

Fig. 3.14.Machine tool (Duravetical 5060).

According to the importance for milling efficiency of each cutting parameter, pick feed value was decided first, and then feed per tooth, at last select the cutting speed. For taper end mill, we set feed per tooth and rotational speed are 1.14mm/tooth, 1050min^{-1} respectively.

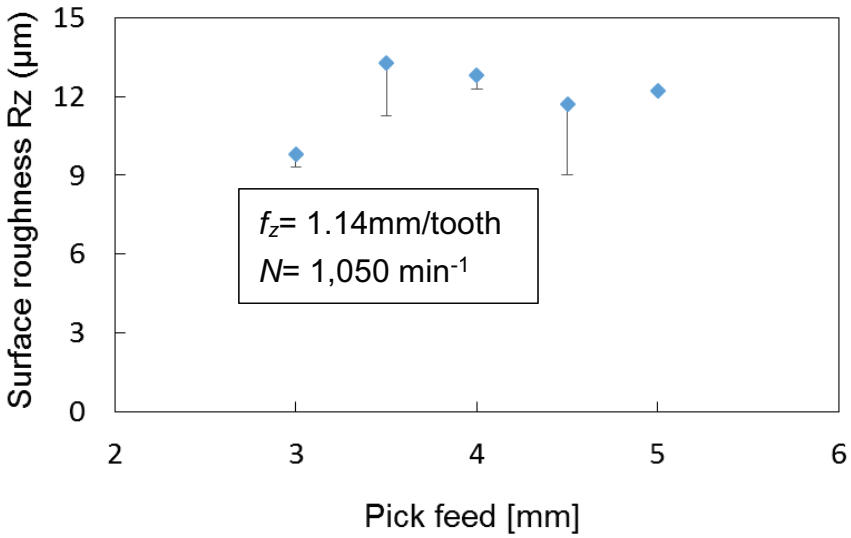

Fig.3.15. Relationships between pick feed and surface roughness using tilt taper end mill.

The results as shown in **Fig.3.15**. It was evaluated in pick feed direction. Surface roughness value grows with the pick feed and then diminishes with the pick feed, and at last becomes increasing. It can see that when pick feed value is 3mm, Rz is smallest. However, when pick feed is 4.5mm, surface roughness is extremum, and the value is approach to the value then pick feed is 3mm. Therefore, we selected pick feed value is 4.5mm.

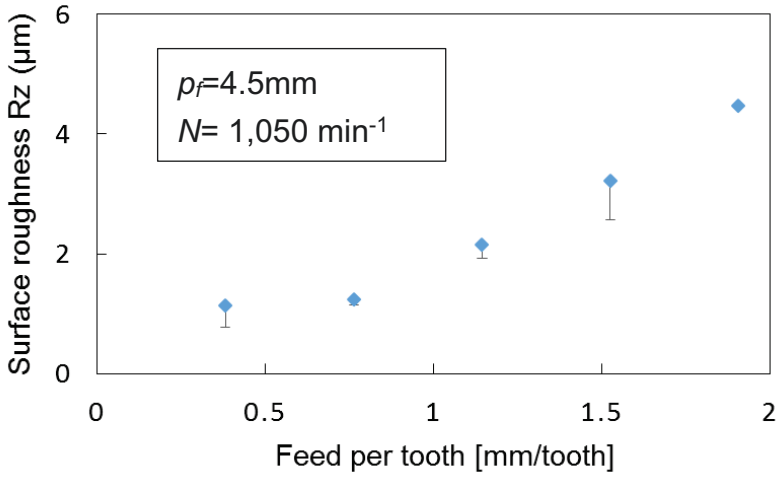

Fig.3.16. Relationships between feed per tooth and surface roughness using tilt taper end mill.

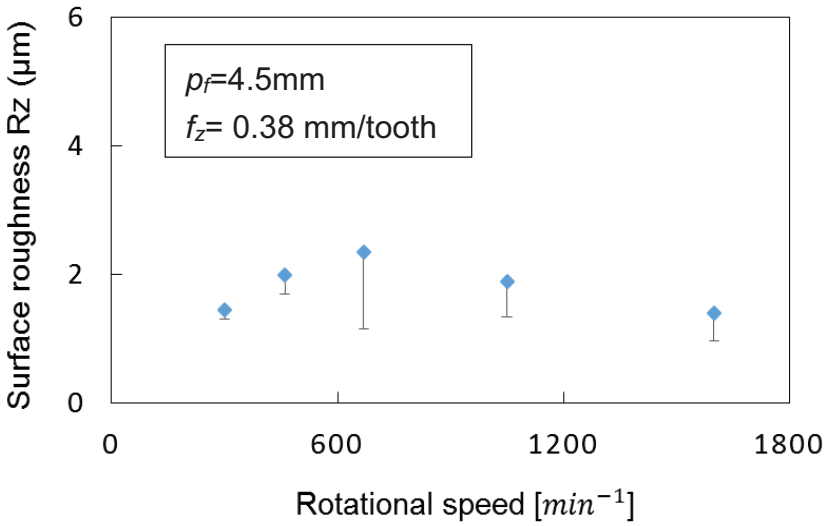

Fig.3.17. Relationships between rotational speed and surface roughness using tilt

taper end mill.

Surface roughness values in **Fig.3.16** and **Fig.3.17** are measured in feed direction**,** it can be seen that the surface roughness is minimum when feed per tooth is 0.38mm/tooth and rotational speed is 1600min^{-1} respectively. Surface roughness increases with feed per tooth, and grows quickly when feed per tooth over 0.76 mm/tooth. R_z reaches the peak at 670 min^{-1} and then becomes small gradually with the rotational speed. Thus, cutting parameters of taper end mill are as following:

- Pick feed p_f= 4.5mm
- Feed per tooth f_z=0.38 mm/tooth
- Rotational speed N= 1600min^{-1}.

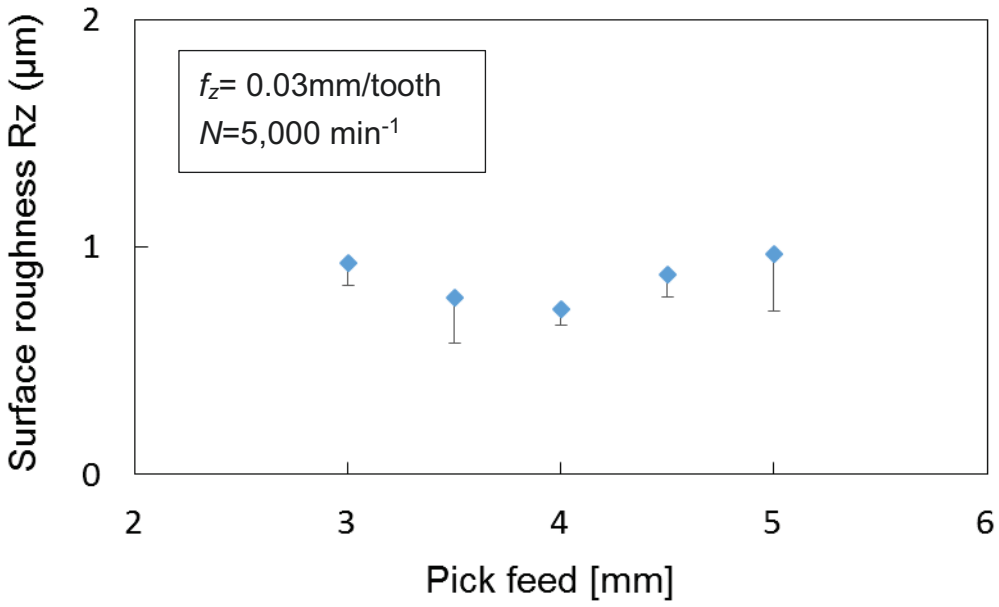

Fig.3.18. Relationships between pick feed and surface roughness using square end mill.

For square end mill, the initial conditions are feed per tooth *fz*=0.03mm/tooth and rotational speed N=5000min^{-1}, the results as shown in **Fig.3.18**. When pick feed value is 4mm, surface roughness value is lowest, so this pick feed value is decided. Relationships between feed per tooth and rotational speed with surface roughness are shown in **Fig.3.19** and **Fig.3.20** respectively. When feed per tooth is 0.03mm/tooth and rotational speed is 6000 min^{-1}, Rz is minimum. Therefore, the cutting conditions of square end mill are selected as:

- Pick feed p_f= 4mm
- Feed per tooth f_z=0.03 mm/tooth

- Rotational speed N= 6000min^{-1}.

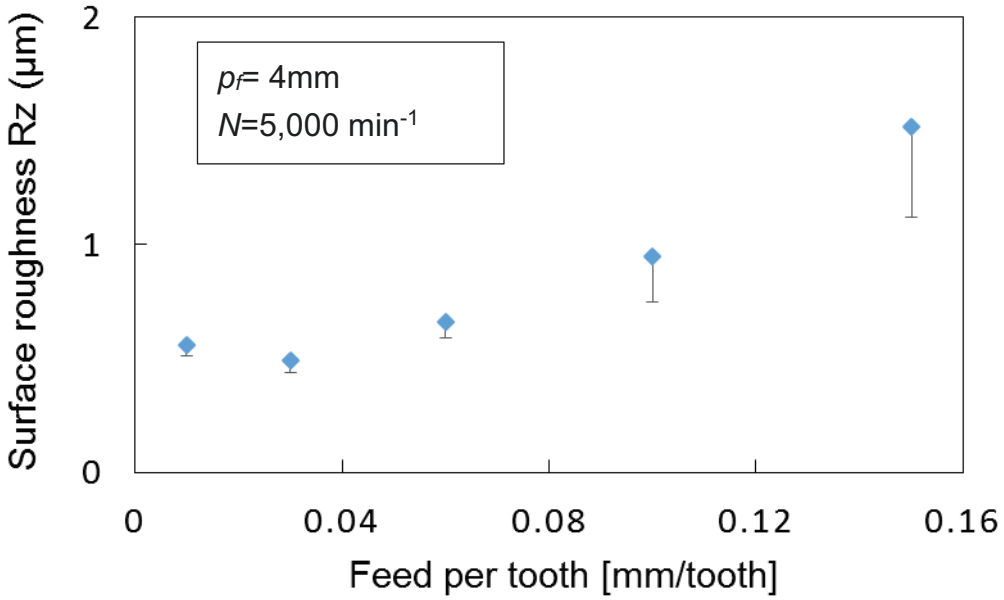

Fig.3.19. Relationships between feed per tooth and surface roughness using square end mill.

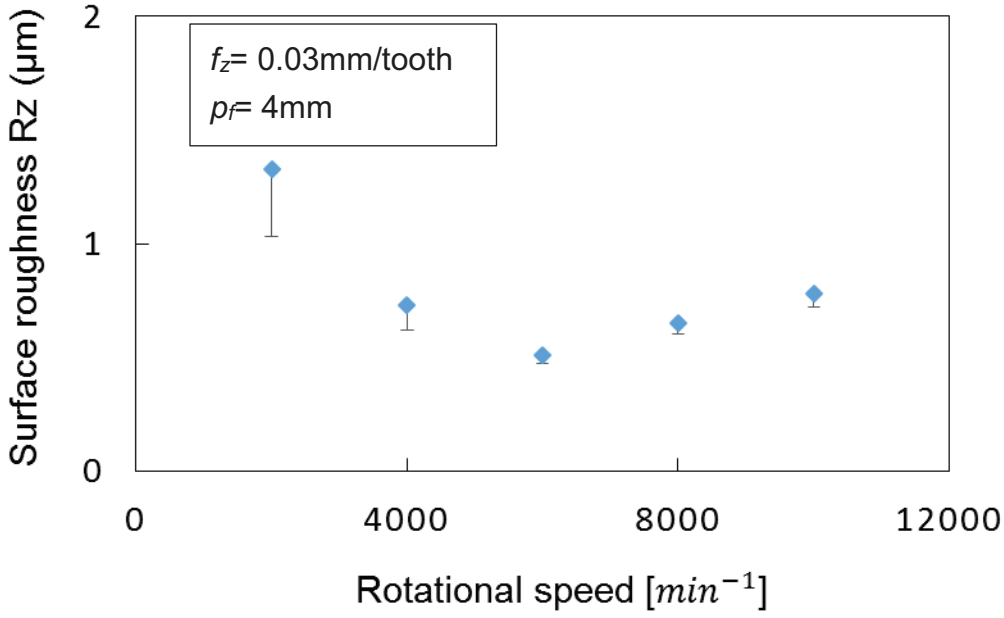

Fig.3.20. Relationships between rotational speed and surface roughness using square end mill.

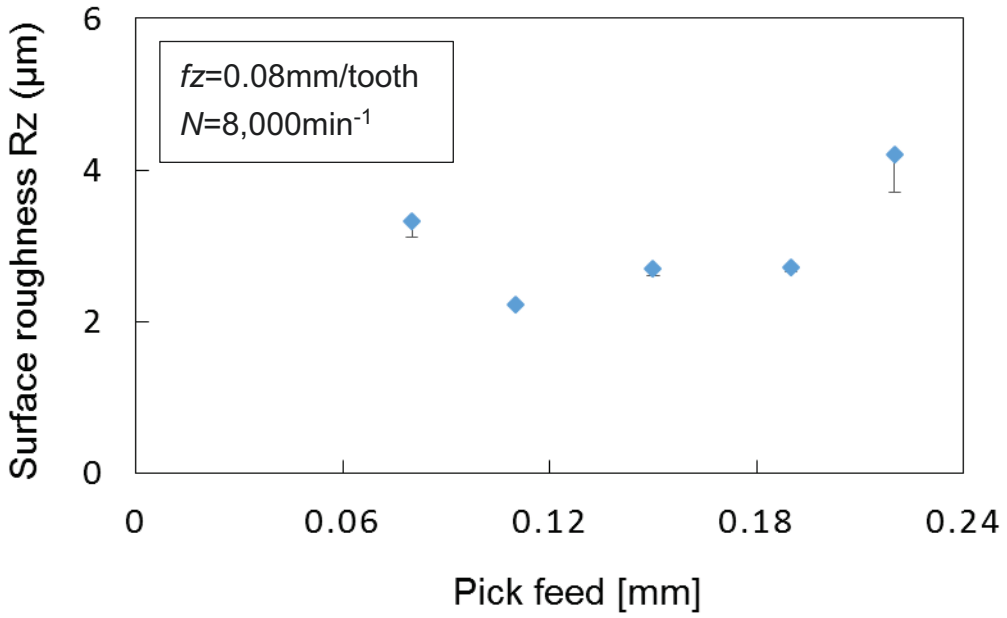

Fig.3.21. Relationships between pick feed and surface roughness using ball end mill.

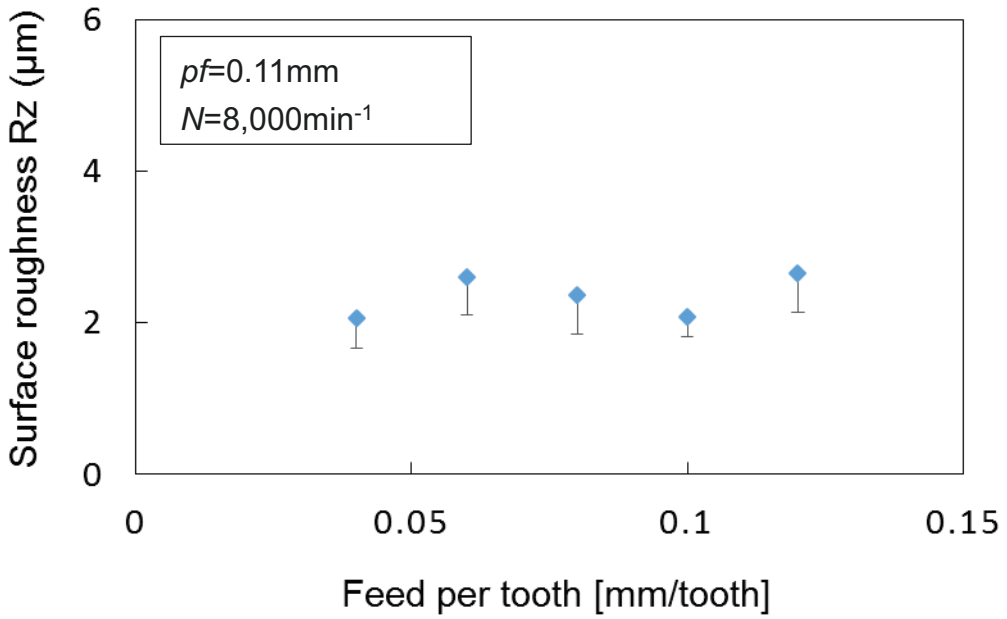

Fig.3.22. Relationships between feed per tooth and surface roughness using ball end mill.

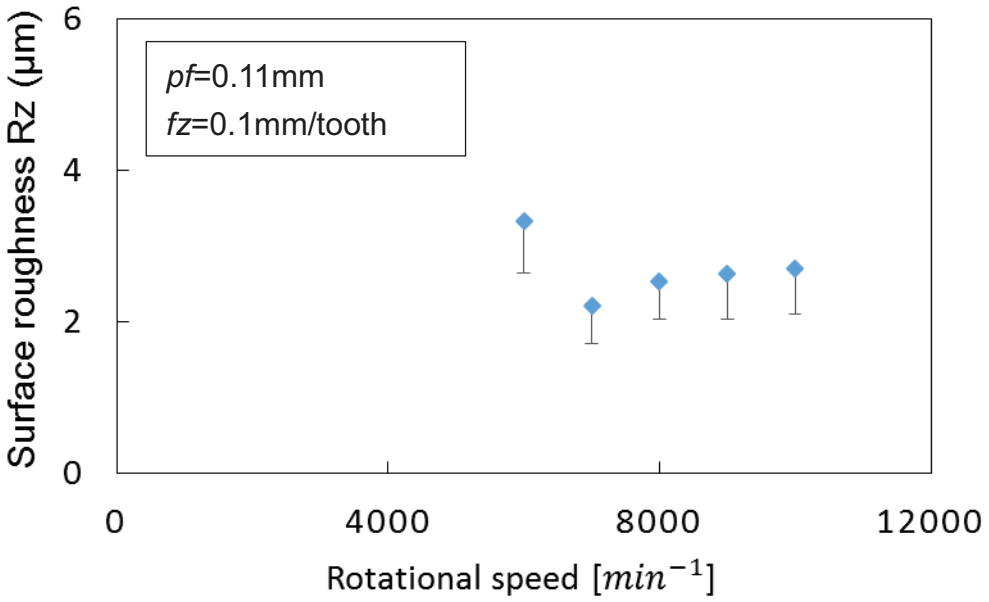

Fig.3.23. Relationships between rotational speed and surface roughness using ball end mill.

For ball end mill, the initial conditions are feed per tooth *fz*=0.08mm/tooth and rotational speed *N*=8000min^{-1}, the results as shown in **Fig.3.21**. When pick feed value is 0.11mm, surface roughness value is smallest, so this pick feed value is chosen. When feed per tooth is variable, surface roughness value is undulate, the value at fz=0.1mm/tooth is nearly same as the value at fz=0.03mm/tooth, and it is an extremum, therefore, we select feed per tooth as 0.1mm/tooth. Rotational speed is chosen as 7000min^{-1} when Rz is minimum. Thus, cutting conditions of ball end mill is decided as following:

- Pick feed p_f= 0.11mm
- Feed per tooth f_z=0.1 mm/tooth
- Rotational speed *N*= 7000min^{-1}.

According to the above experiments, the cutting conditions for tool wear experiments can be given in **Table 3.5**. We will examine the validity of taper end mill though evaluating tool wear and surface integrity.

Table 3.5. Cutting conditions.

		Tilt taper end mill	Ball end mill	Square end mill
Work material		SUS403 (HRC45)		
Tool	Material	TiAlN coated cemented carbide		
	Diameter [mm]	32	6	6
	Number of teeth	1	2	2
Pick feed p_f [mm]		4.5	0.11	4
Cutting speed V [m/min]		161	34	113
Feed per tooth f_z [mm/min]		0.38	0.1	0..03
Axial depth of cut a_a [mm]		0.1	0.1	0.1
Cutting fluid		Water –insoluble cutting oil N4 kind		

3.3 Tool wear experiments

In order to confirm the validity of the proposed milling method, tool wear experiments of tilt taper end mill, ball end mill and square end mill were performed. Because the basic examination is still in its infancy, model experiments were designed (see **Fig.3.24**). The experimental method of tilt taper end mill is similar as former section (**Fig.3.24 (a)**), ball end mill and square end mill use the same method (**Fig.3.24 (b)**). All the experiments were carried out using down milling method and kept coolant on. The material that used was SUS403 stainless steel, test workpieces

were cuboid, of dimensions 100×100×80mm. At first, we using cutting conditions that given in **Table 3.3**.For finish milling of 60 inches rotor blade, the total removal amount was set 11.43×10^3 mm^3, each milling method needed about 80 times to complete the total work. The milling efficiencies of tilt taper end mill, square end mill and ball end mill were 363.6 mm^3/min, 363.6 mm^3/min, and 51 mm^3/min respectively. Therefore, the total cutting time as shown in **Fig.3.25.** It can be seen that square end mill can finish a piece of blade taking the same time as taper end mill, and ball end mill takes about 17 times of that of taper end mill in theoretically.

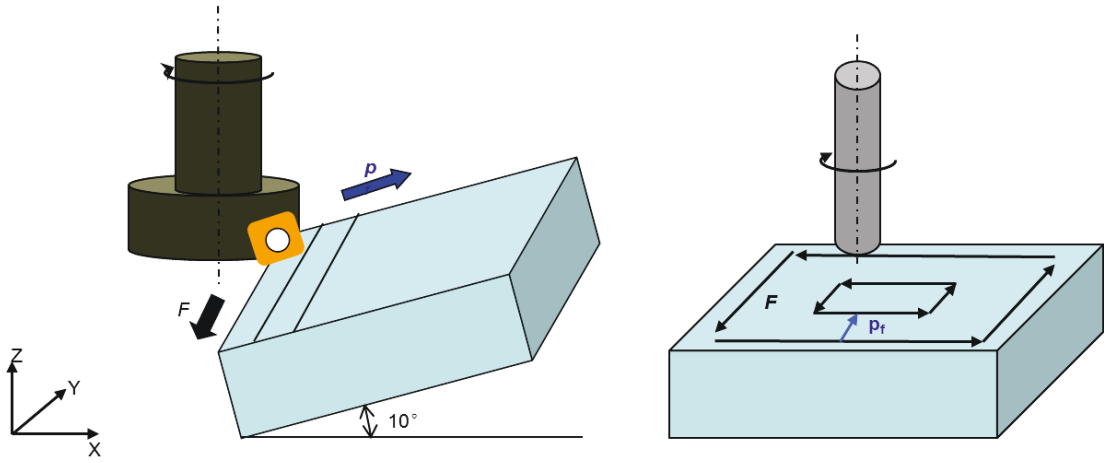

(a) Tilt taper end mill method (b) Conventional milling method

Fig.3.24. Experimental diagram.

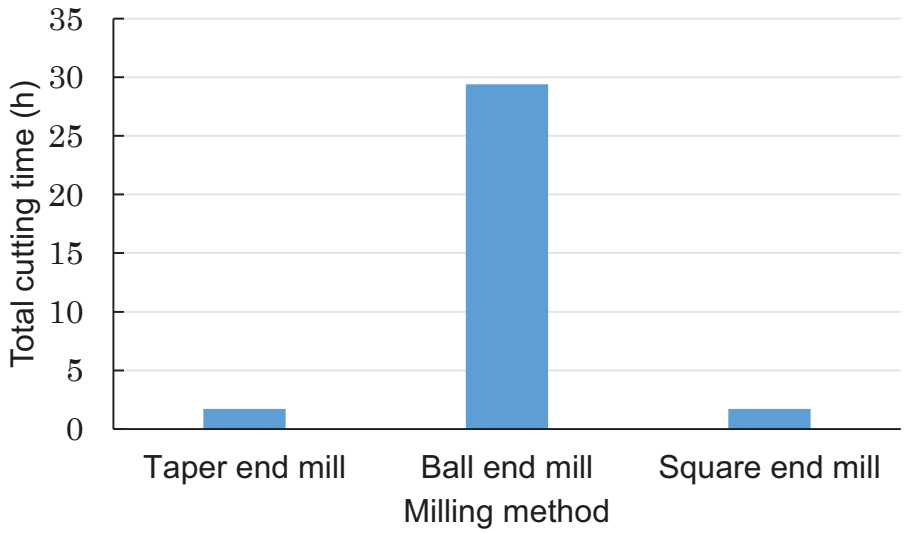

Fig.3.25. Total cutting time of each milling method.

In this experiment, tool life was determined not only by tool wear, but also take the surface quality into account. The validity of the proposed method is examined though the comparisons of surface roughness, surface profile, machined surface and tool wear. The experiments were carried out on the 3-axis control milling machine (Osakakiko rakuraku-mill 3V Tudacoma TT-200), surface roughness Rz and surface profile were measured with a surface roughness measuring device (ACCRETECH SURFCOM 130A). Tool wear and machined surfaces were evaluated with digital microscope (KEYENCE VHX-1000) and scanning electron microscopy (SEM) (JSM-5300).

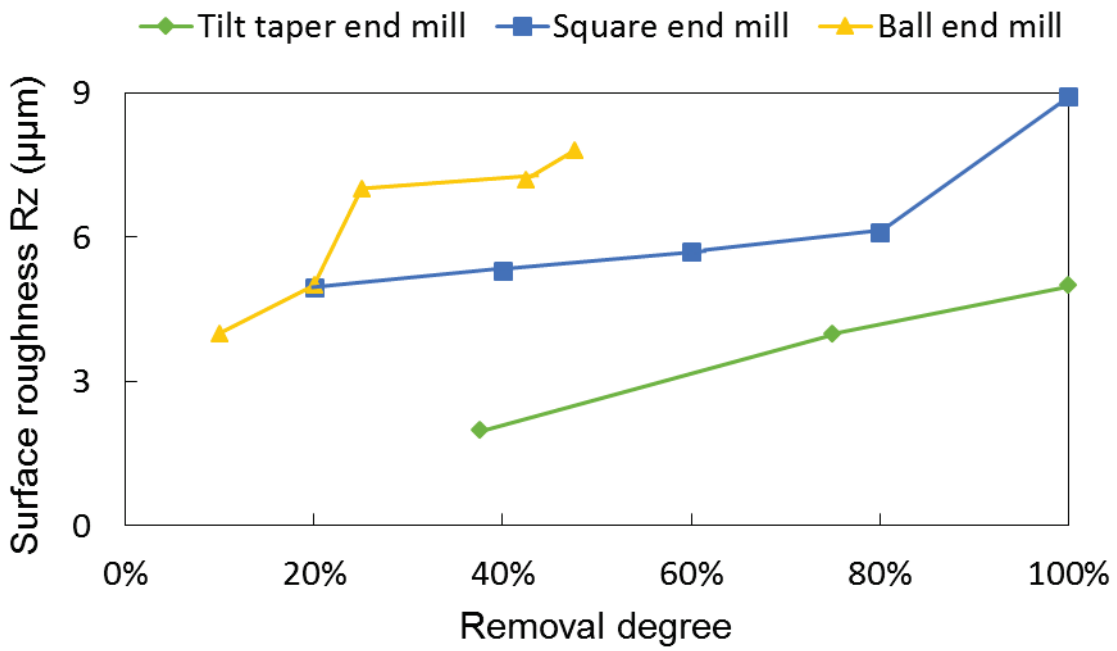

Fig.3.26. Removal degree vs. surface roughness of tilt taper end mill, square end mill and ball end mill

In this experiments, surface roughness Rz of ball end mill was measured in pick feed direction, and those of the other two method were measured in feed direction. Removal degree is the percentage of removal amount. Surface roughness R_z increases with the machining process (see **Fig.3.26**), it seems to correlate quite closely with tool wear VB_{max} variation **(Fig.3.27**). It can be found that the progression of flank wears of ball end mill and square end mill follow a three-stage pattern: rapid initial wear, gradual uniform wear and accelerating wear[9-14]. Removing the same amount, ball end mill should take a long cutting length, which probably results in reaching accelerating wear stage before completing 50 % work.

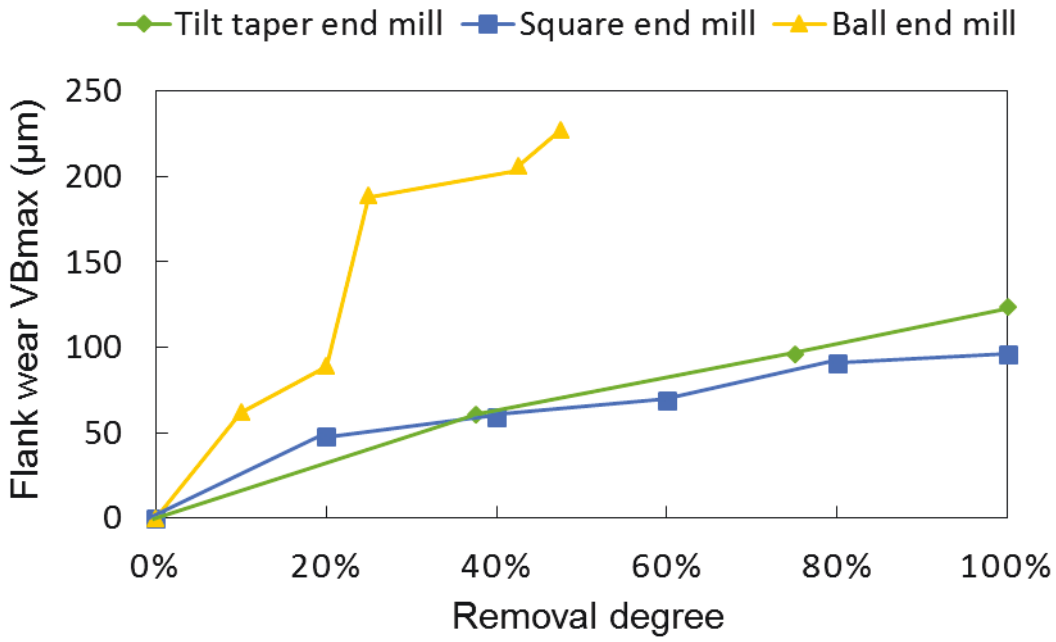

Fig.3.27. Removal degree vs. flank wear of tilt taper end mill, square end mill and ball end mill.

Machined surfaced images as shown in **Fig.3.28-30**. The materimal can not be removed completely with the tool wear. Apparent abrasion wear occurs on the rake face and flank face of ball end mill at removal degree of 47.5% (see **Fig.3.31 and Fig.3.32**), whereas no crater wear can be seen. Since the tool center is in contact with the machined surface, wear takes place on this part of the tool will have adverse effect on the surface finish (see **Fig.3.28**). When finish the total work, square end mill takes the same cutting length as using tilt taper end mill. There are no obvious abrasion wear like that of ball end mill can be seen, especially on the rake face (see **Fig.3.33-36**). Although the value of flank wear of square end mill is less than that of tilt taper end mill, it effects the surface roughness more adversely (see **Fig.3.26-27**). Another, the machined surfaced appears rubbing marks, and the marks become serious with the tool wear progress (see **Fig.3.29**). However, even at removal degree of 100%，surface profile of square end mill has not yet become disorder, which may be attribute to its smooth worn surface. For tilt taper end mill, rake face and flank face conditions are presented in **Fig.3.35** and **Fig.3.36**. Tool wears on both rake face and flank face are very slight when finishing the work about 37.5% (**Fig.3.35 (a)** and **Fig.3.36 (a)**), in spite of the width of tool wear increases with cutting length, the wear just occurs at the coating film layer, there no visible substrate wear, even removal degree at of 100%, the coating film layer has not yet removed completely.

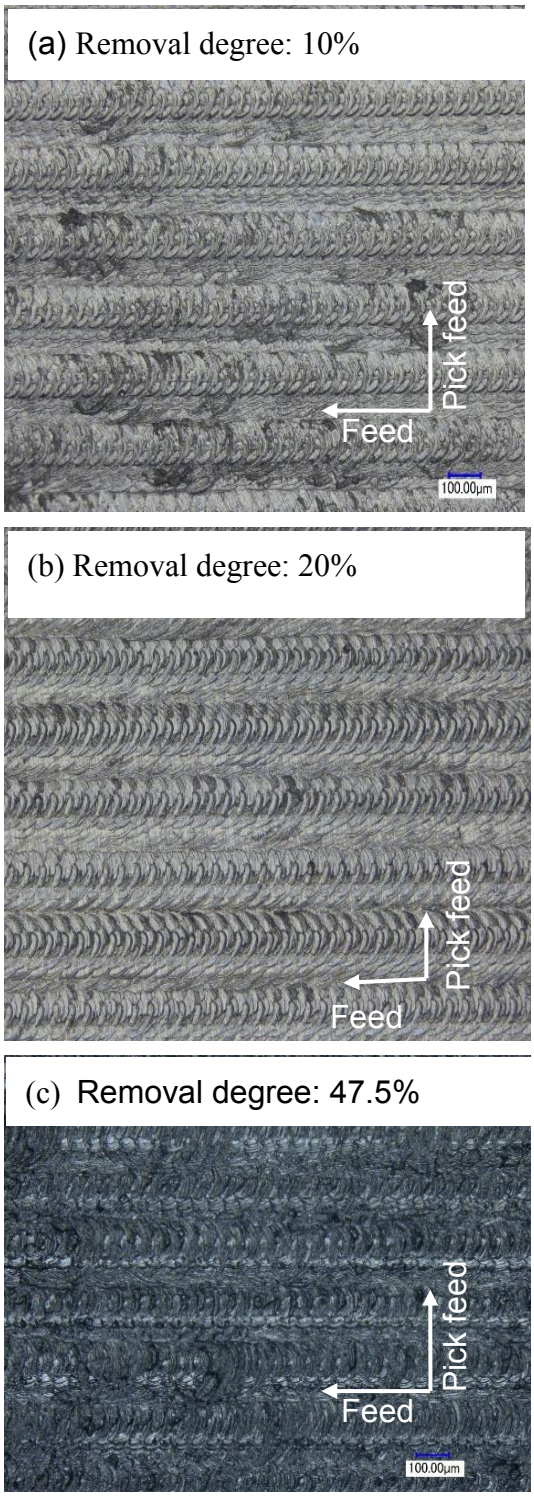

Fig.3.28. Images of machined surfaces at different removal degree using ball end mill.

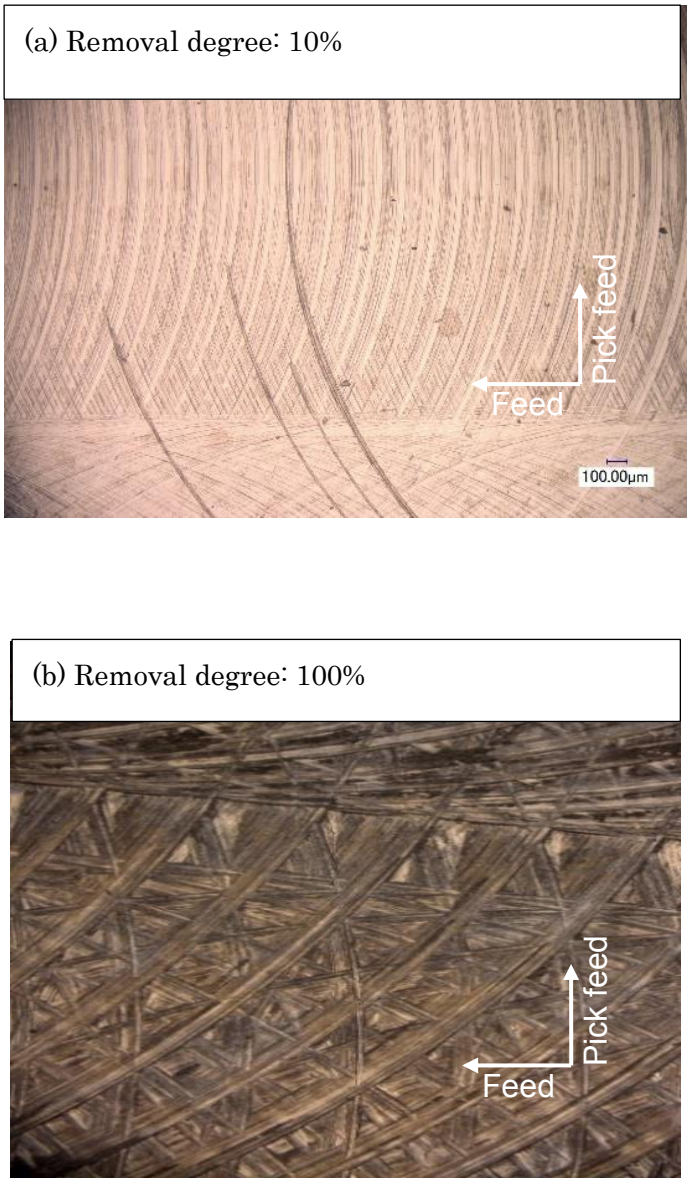

Fig.3.29. Images of machined surface using square end mill (100×) at removal degree of 10% and 100%.

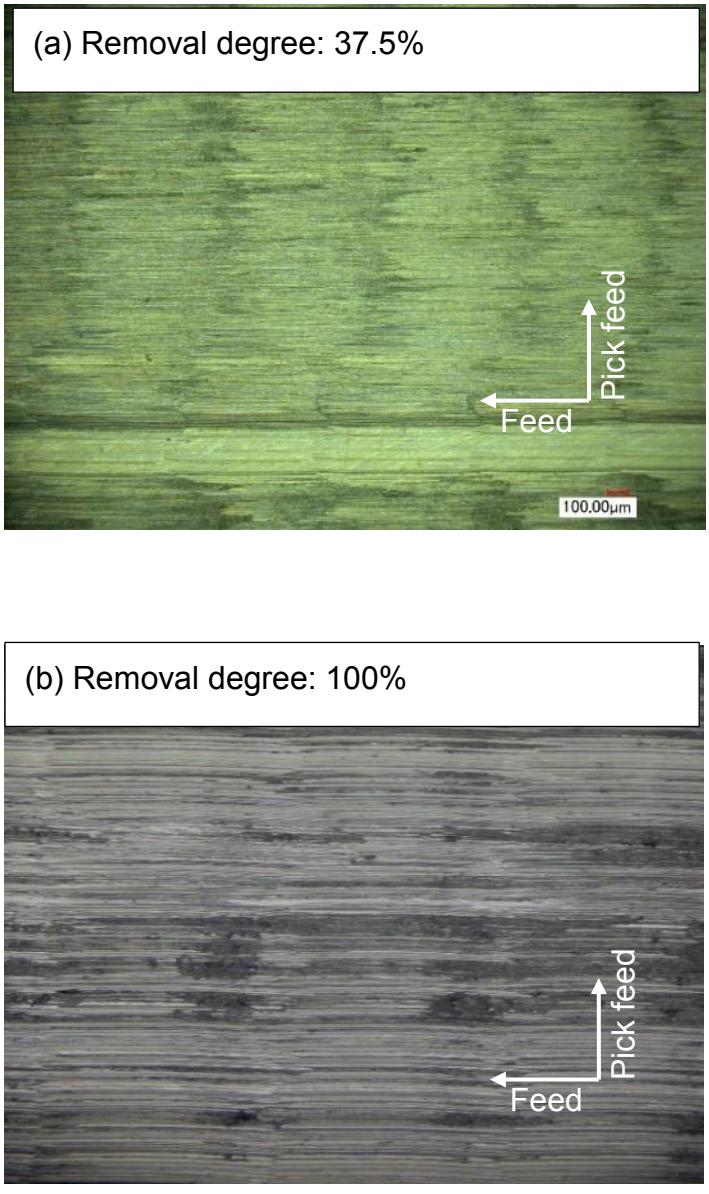

ig.3.30. Images of machined surface using tilt taper end mill (100×) at removal degree of 37.5% and 100%.

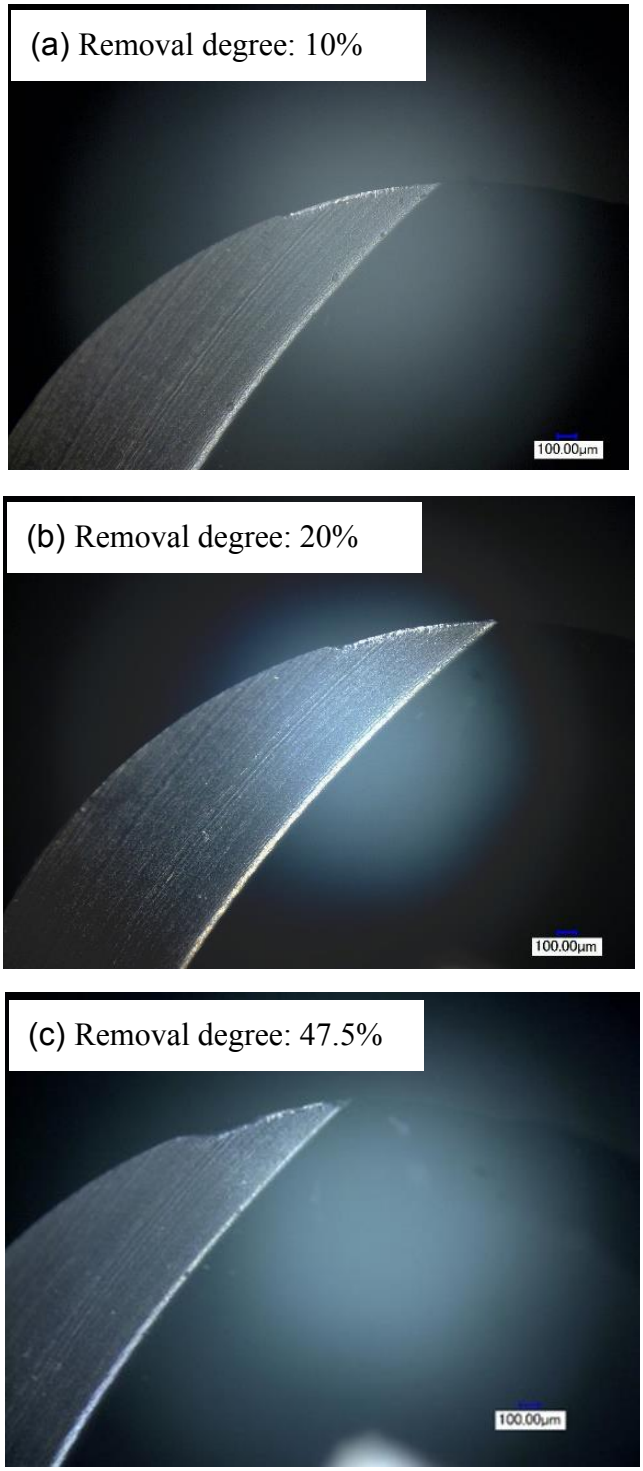

Fig.3.31. Images of rake face of ball end mill at different removal degree.

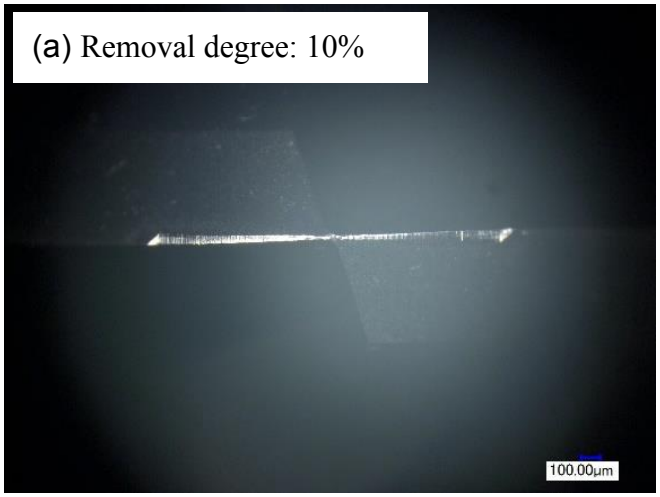
(a) Removal degree: 10%
100.00μm

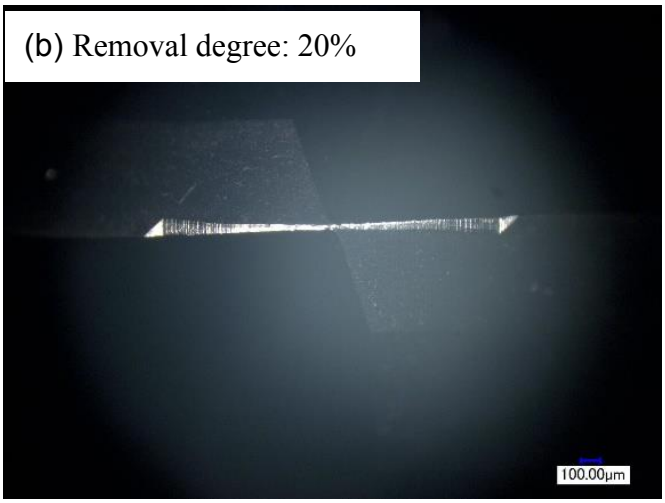
(b) Removal degree: 20%
100.00μm

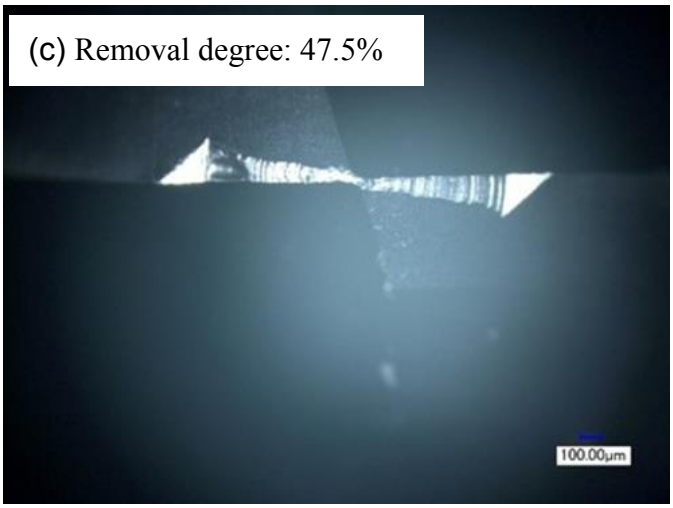
(c) Removal degree: 47.5%
100.00μm

Fig.3.32. Images of flank face of ball end mill at different removal degree.

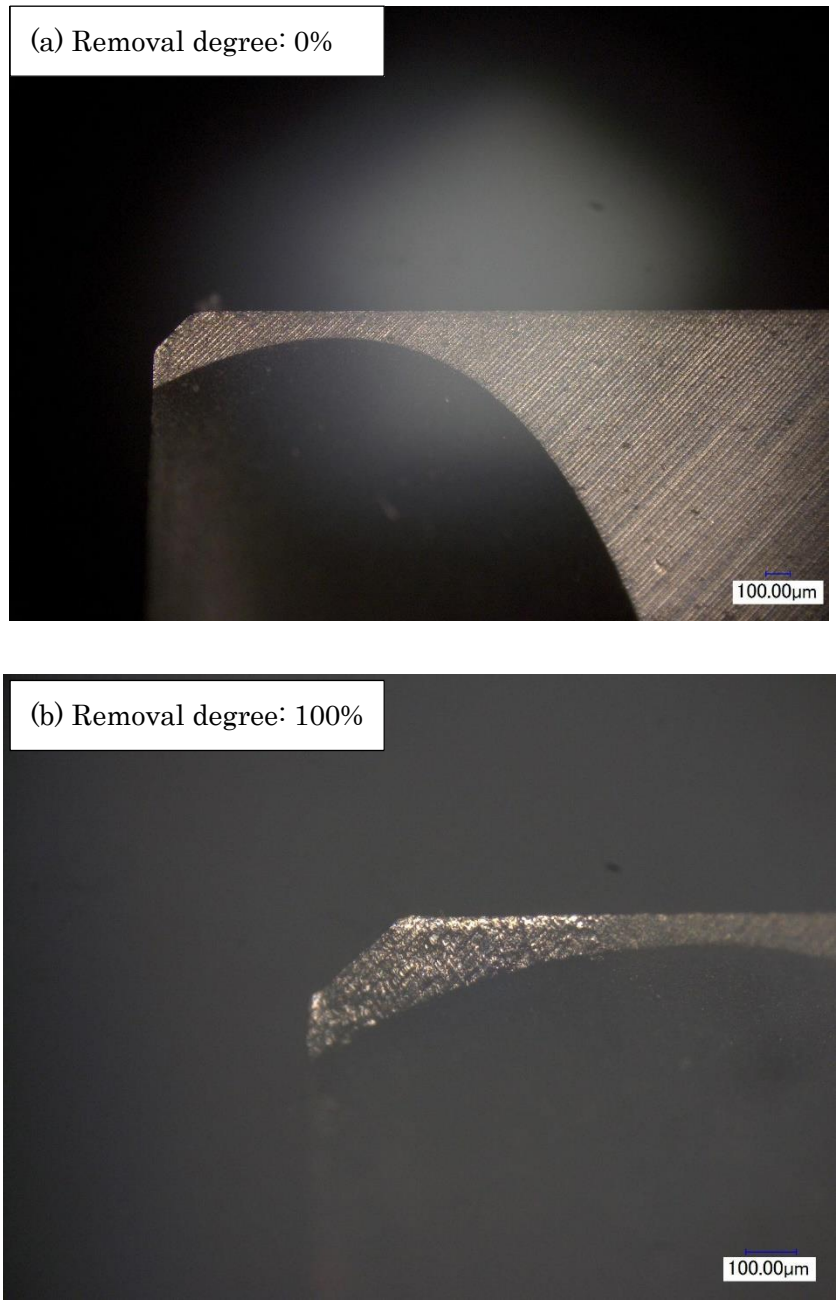

Fig.3.33. Images of rake face of square end mill at different removal degree.

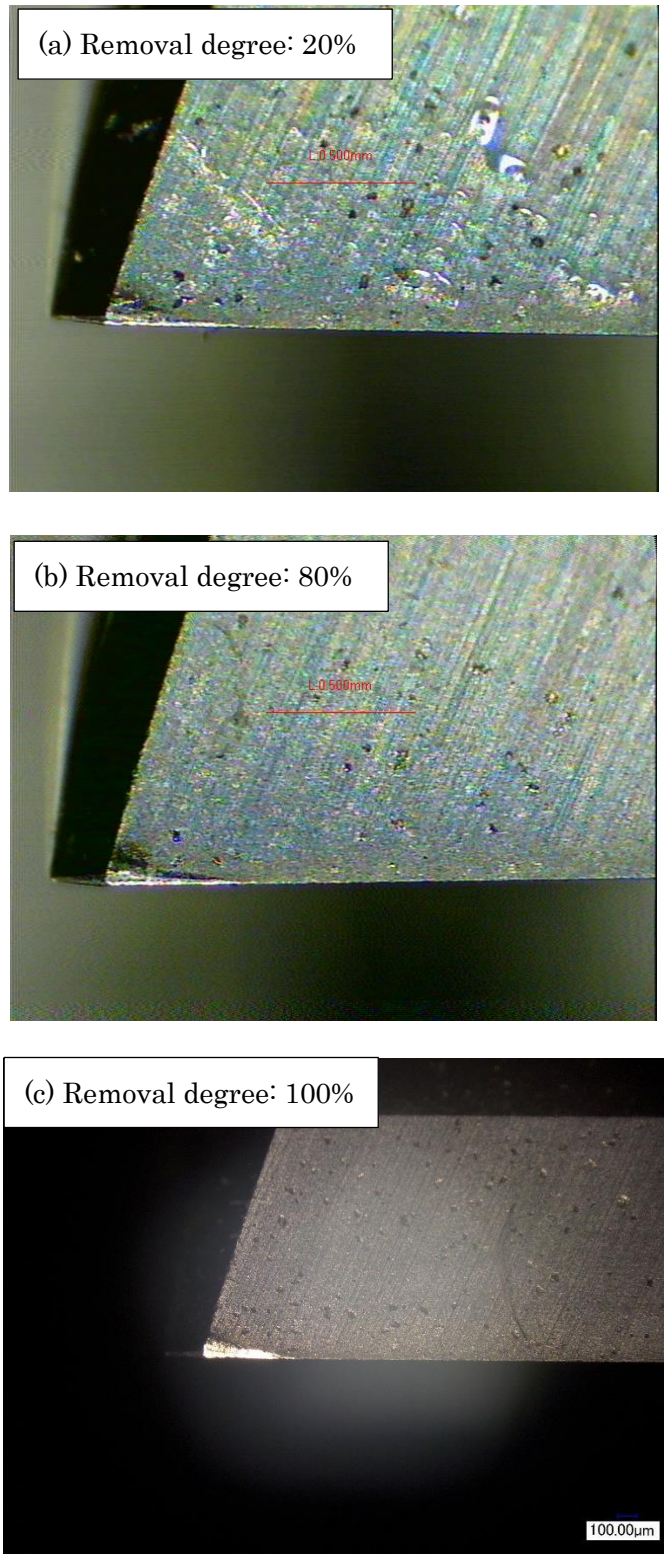

Fig.3.34. Images of flank face of square end mill at different removal degree.

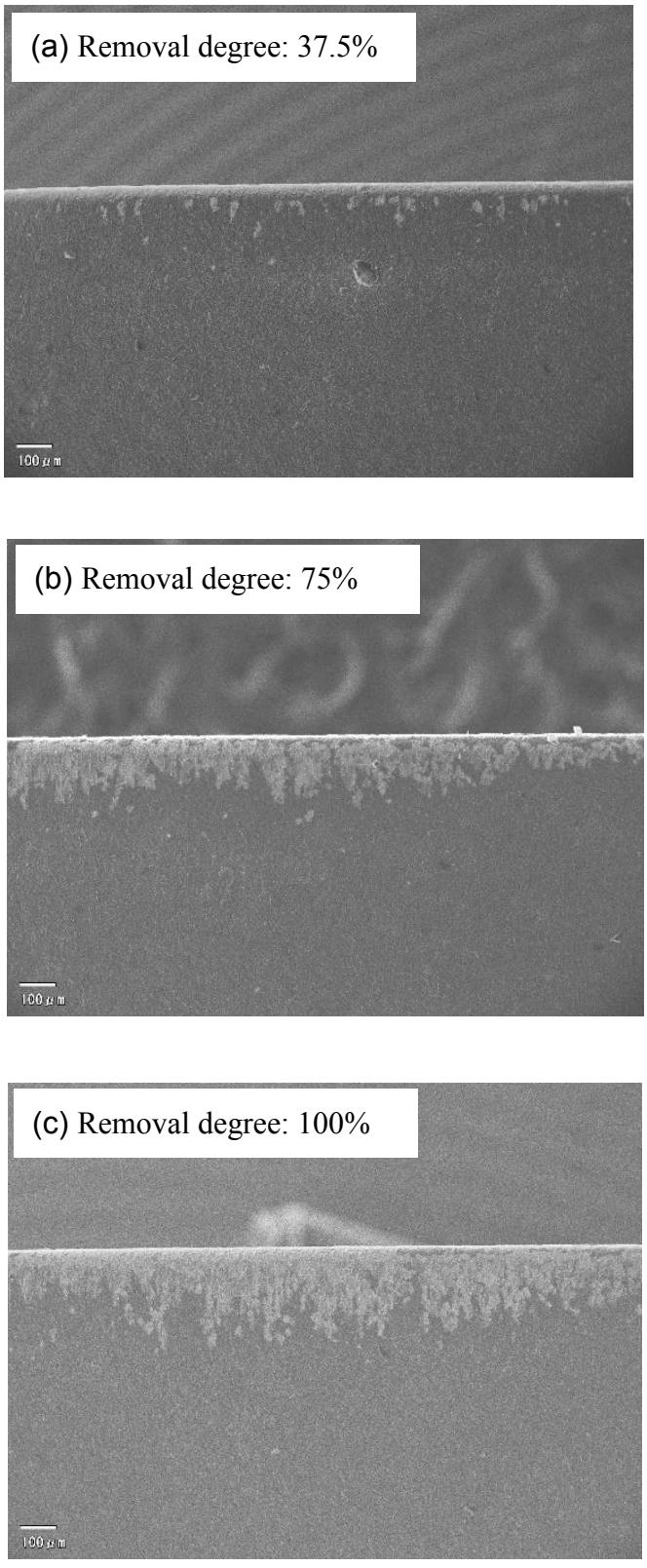

Fig.3.35. Images of rake face of taper end mill at different removal degree.

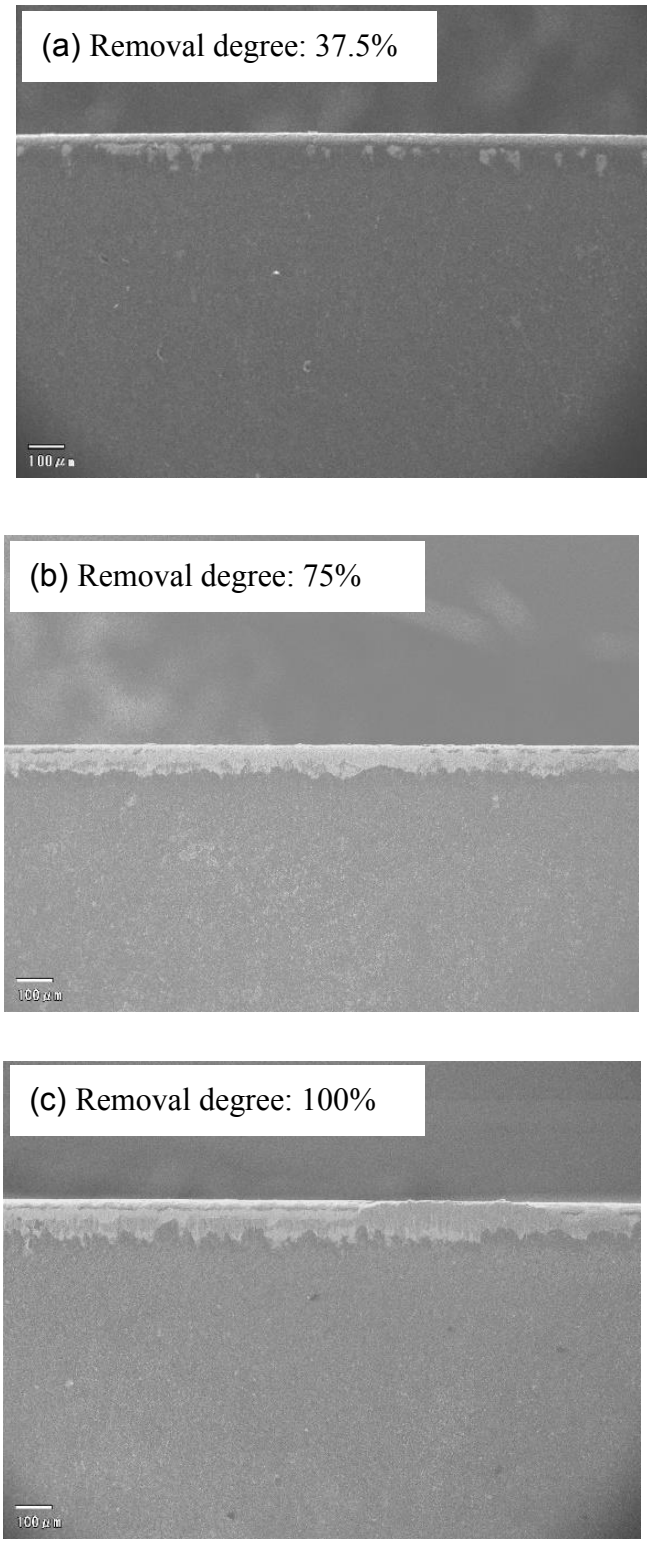

Fig.3.36. Images of flank face of taper end mill at different removal degree.

Owing to little variation of cutting speed on minor cutting edge of insert, the machined surface keeps uniform until completed the total work (**Fig.3.30**), and in somewhere the parent metal cannot be removed completely, it probably caused by tool wear at the minor cutting edge. From the surface profiles, tilt taper end mill can keep machined surface uniform until the end of milling process. In this study, the required surface roughness R_z is 6μm. Therefore, using ball end mill can only complete about 23.2% of the total work. And even using the square end mill, it cannot satisfy the surface roughness requirement after finishing about total work of 72.9%.

Furthermore, tool change not only increases the lead time and cost, but also affects the accuracy of machined surface. Although the milling efficiency of square end mill is larger than that of taper end mill, only a single insert was used in the tool wear experiments of tilt taper end mill. Compared with other two methods, the proposed method can use a high milling efficiency and the same time retard tool wear to obtain a high surface quality.

When using **Table 3.5** to examine the validity, the milling efficiency of taper end mill, ball end mill and square end mill are 273.6mm^3, 15.4mm^3 and 144mm^3 respectively. Cutting time of each milling method as shown in **Fig.3.37.** When finishing a piece of blade, using ball end mill takes about 18 times of using taper end mill in theoretically, and using square end mill takes about 2 times of using taper end mill.

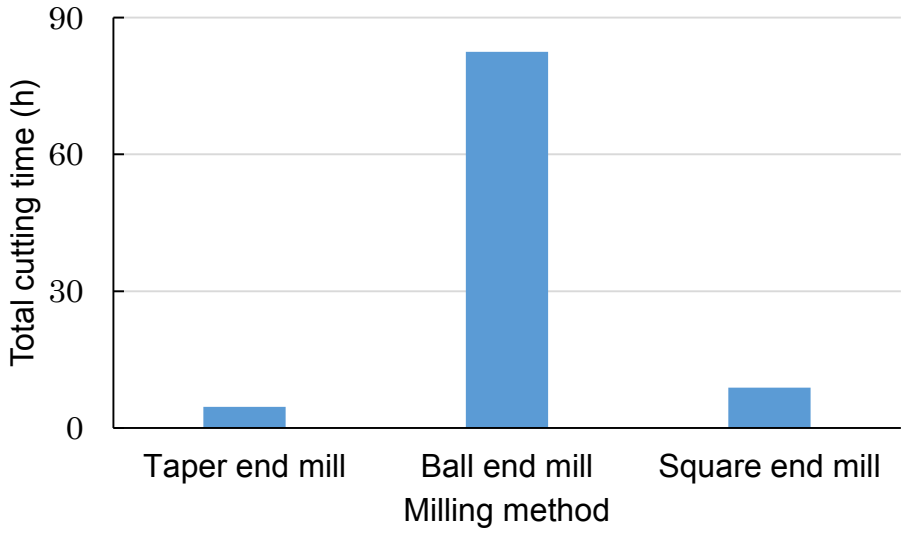

Fig.3.37. Total cutting time of each milling method.

Surface roughness Rz nearly keeps the same trend as flank wear, it can only complete about 10% of total removal amount, even square end mill, not yet 40%.

For taper end mill, flank wear increases with the removal degree, and the surface roughness can keep steady until complete the total work. The three methods owns a similar tool wear trend, at initial stage, it increases quickly and then keeps steady, at last changes rapidly.

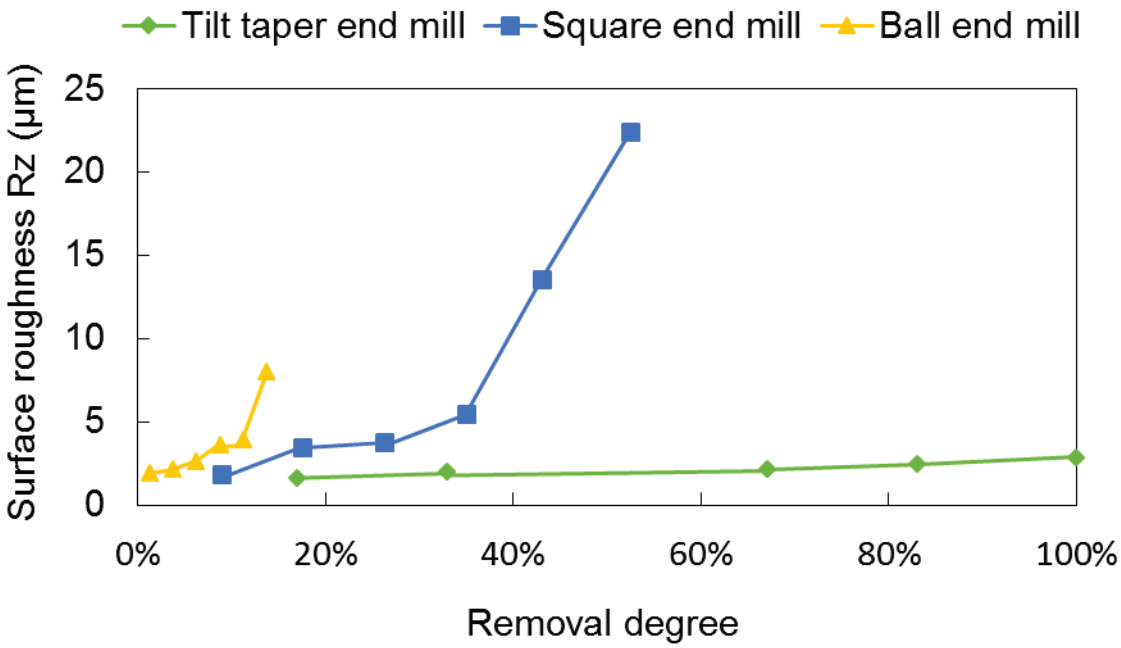

Fig.3.38. Removal degree vs. surface roughness of each milling method.

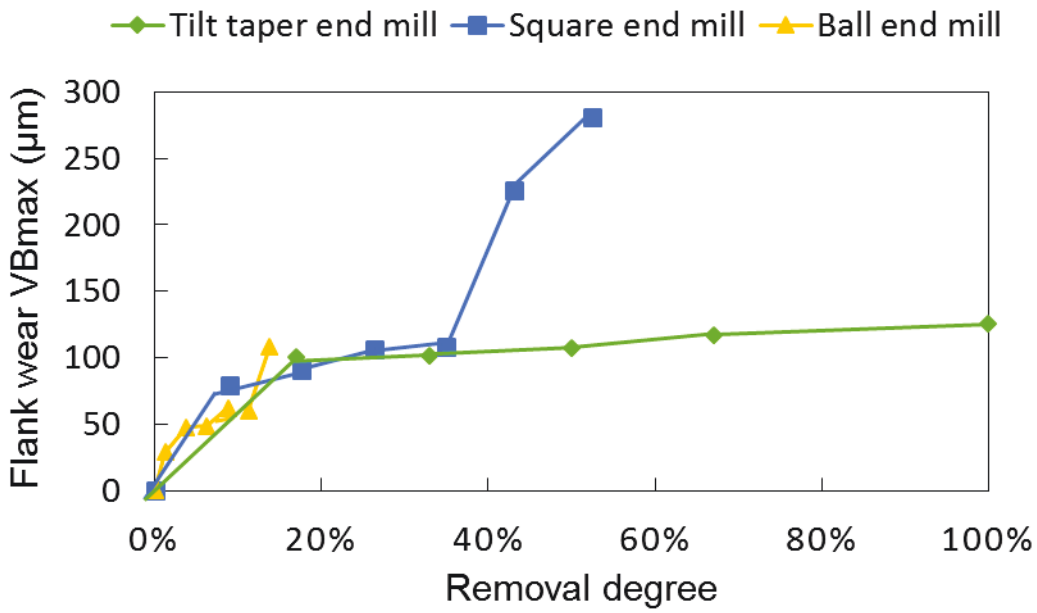

Fig.3.39. Removal degree vs. flank wear of each milling method.

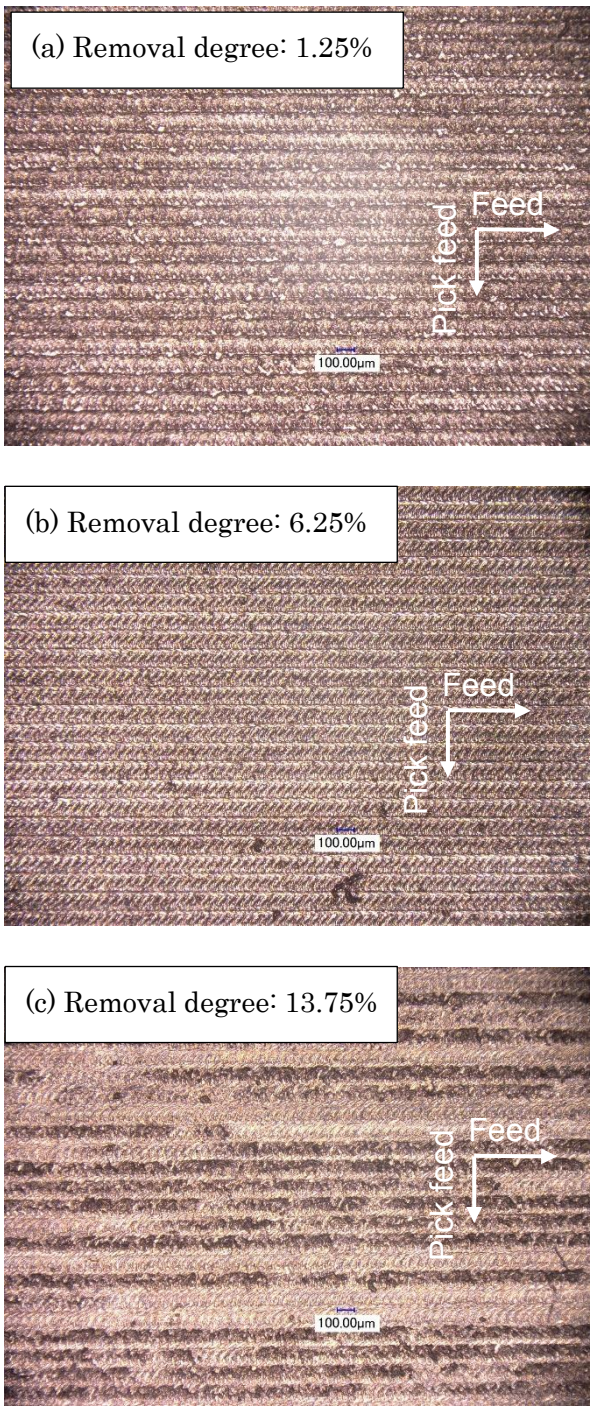

Fig.3.40. Images of machined surface using ball end mill at different removal degree.

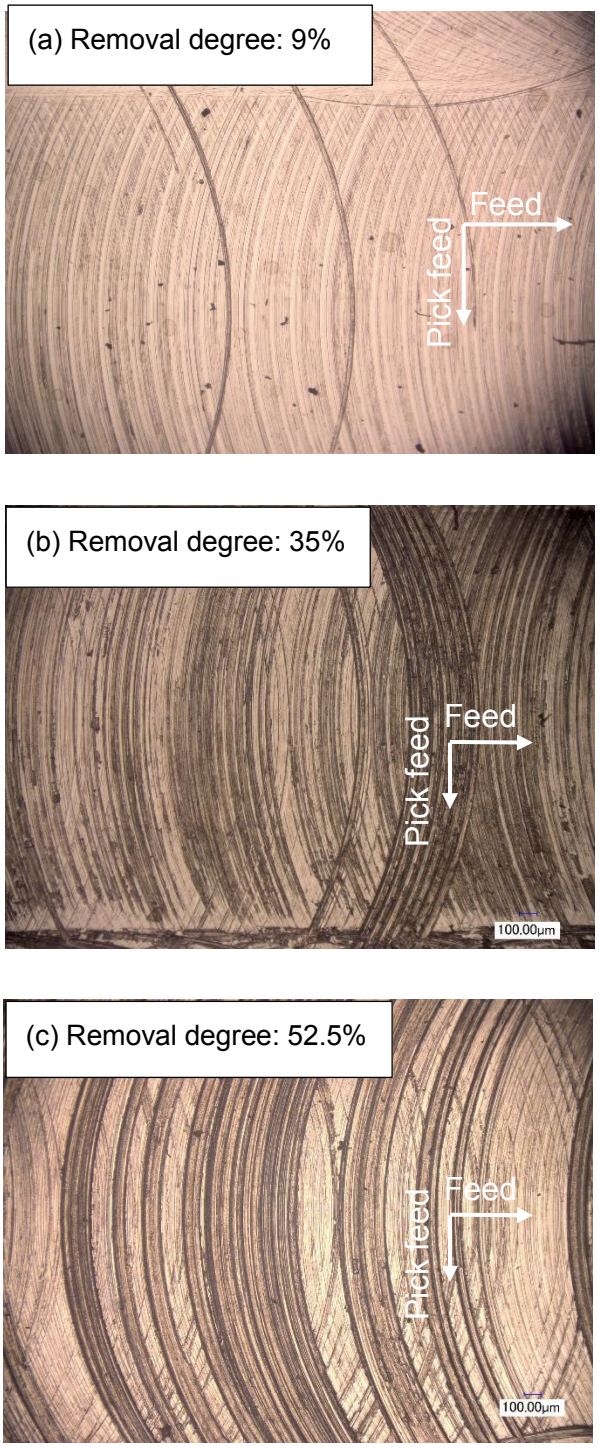

Fig.3.41. Images of machined surface using square end mill at different removal degree.

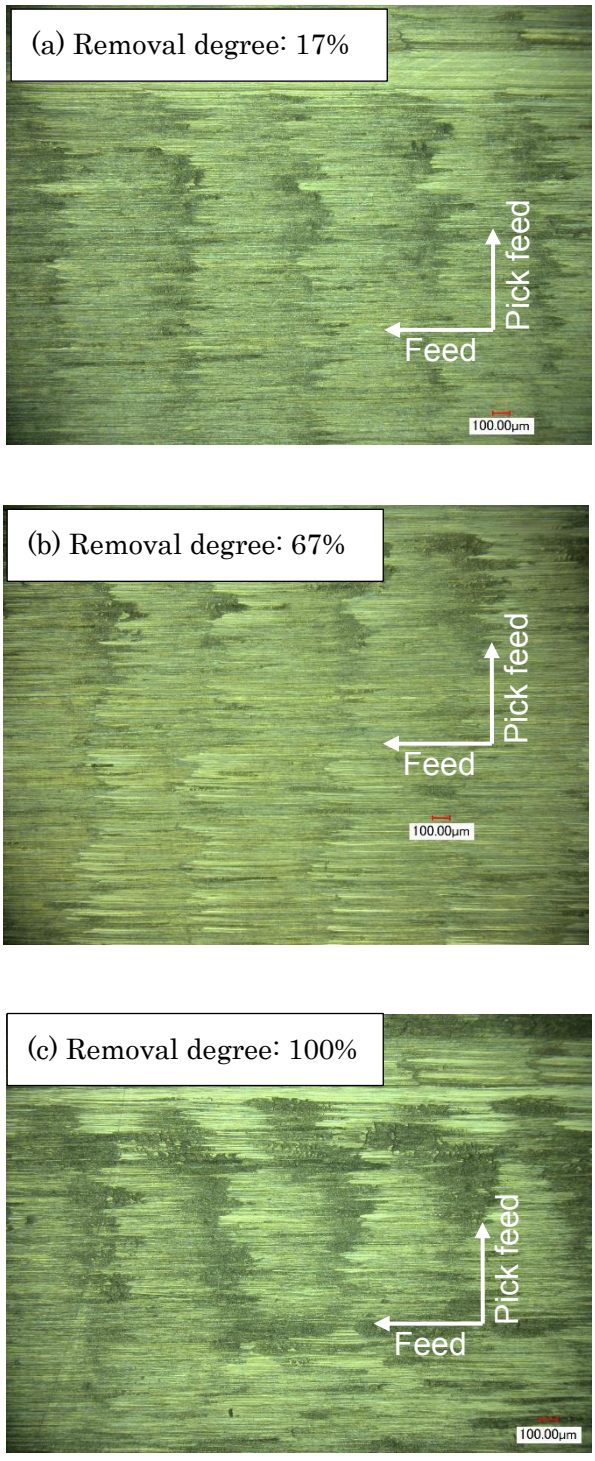

Fig.3.42. Machined surface using taper end mill at different removal degree.

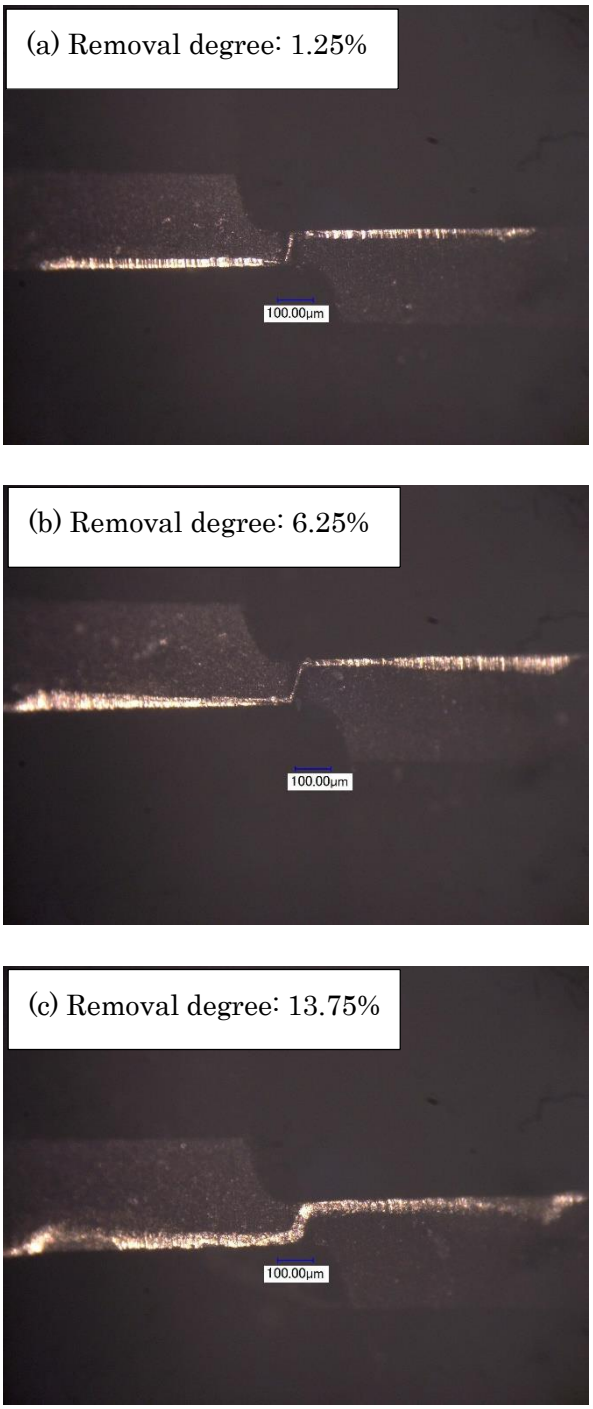

Fig.3.43. Images of flank wear of ball end mill at different removal degree.

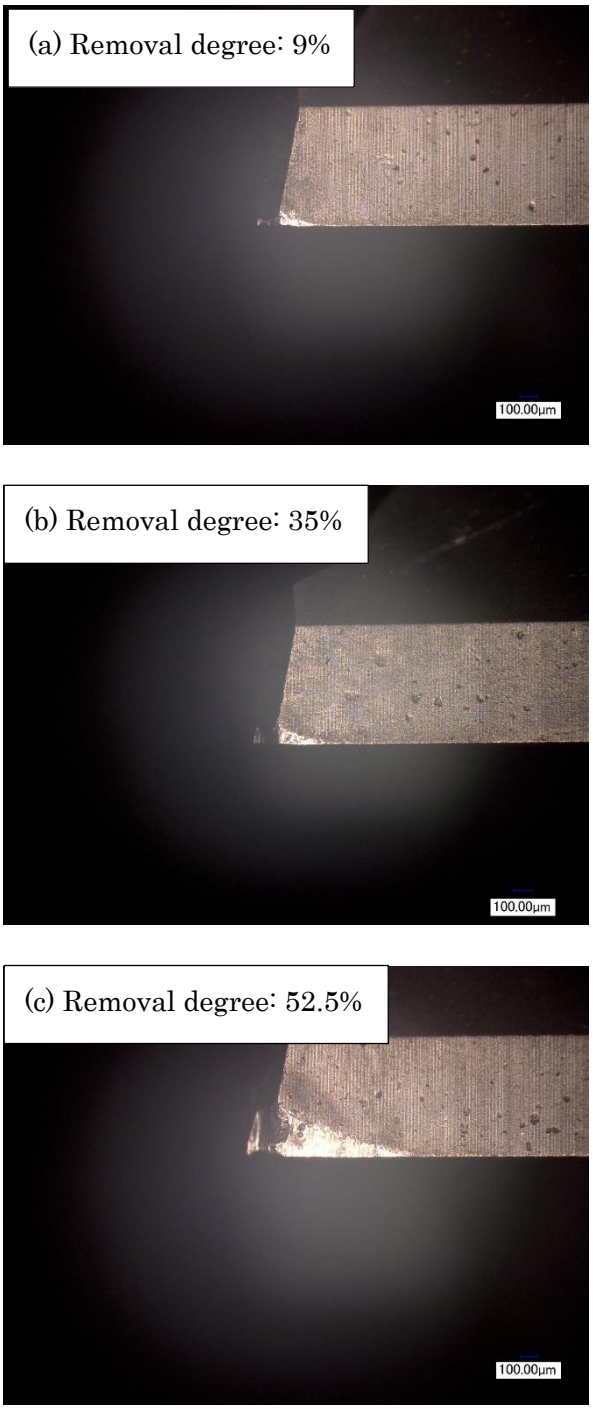

Fig.3.44. Flank wear of square end mill at different removal degree.

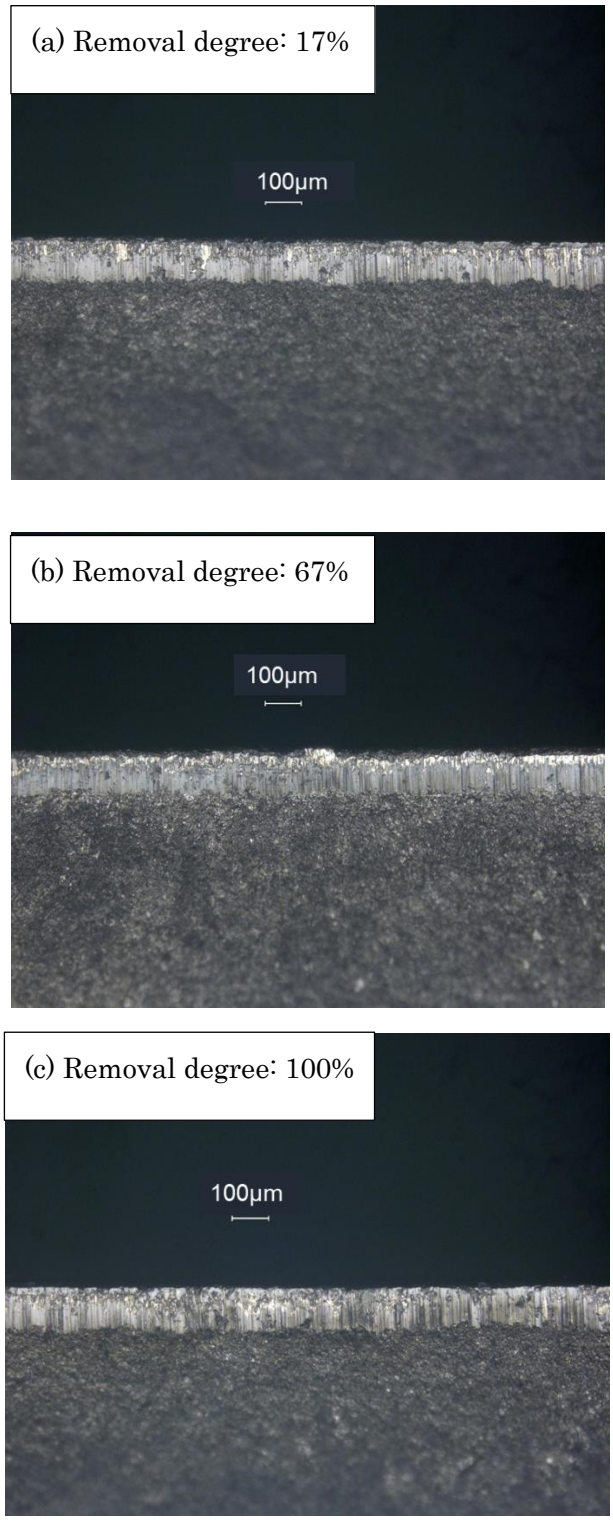

Fig.3.45. Images of flank wear of tilt taper end mill at different removal degree.

(a) Removal degree: 1.25%

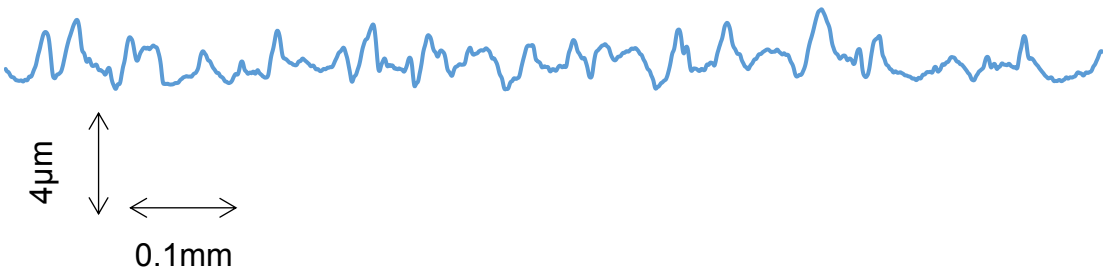

(b) Removal degree: 6.25%

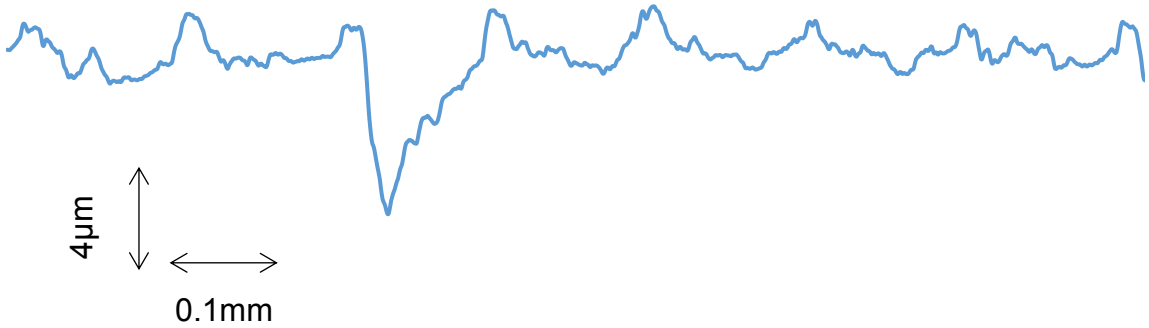

(c) Removal degree: 13.75%

Fig.3.46. Machined surface profiles using ball end mill at different removal degree.

(a) Removal degree :9%

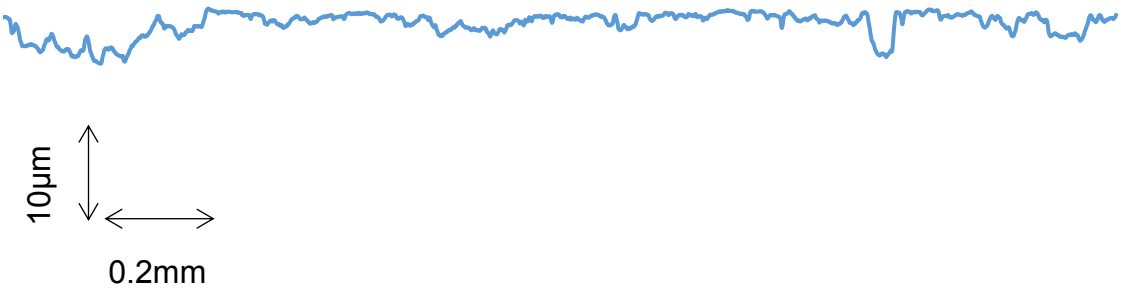

(b) Removal degree: 35%

(c) Removal degree: 52.5%

Fig.3.47. Machined surface profiles using square end mill at different removal degree.

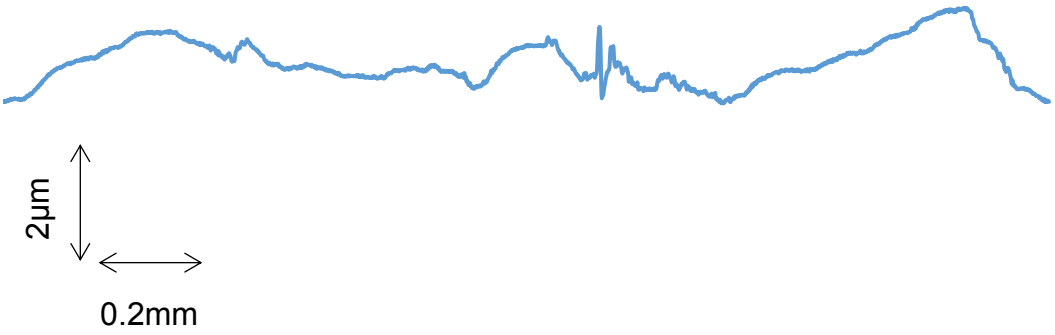

(a) Removal degree: 17%

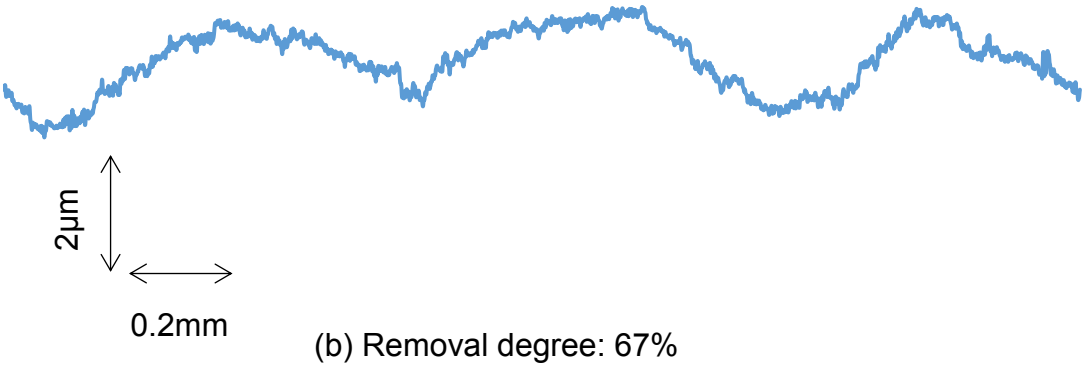

(b) Removal degree: 67%

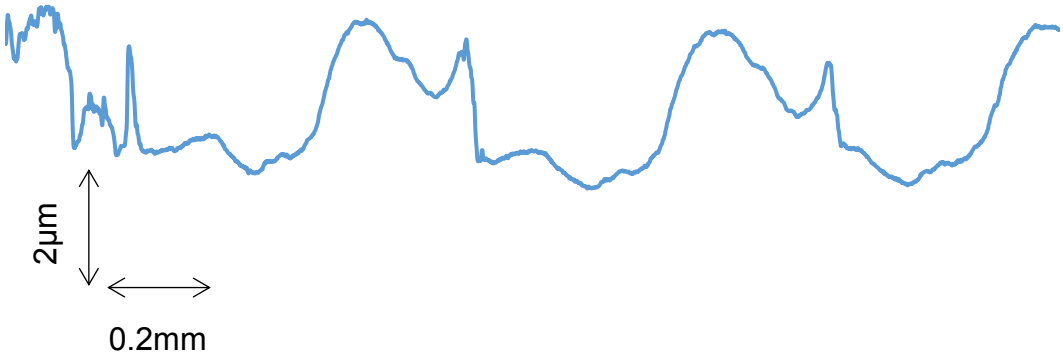

(c) Removal degree: 100%

Fig.3.48. Machined surfaced profiles using taper end mill at different removal degree.

Moreover, for ball end mill and square end mill, surface roughness value is changes similar with flank wear. Due to flank face is contact with the machined surface directly, it effected by flank wear easily. Images of machined surfaces at different removal as shown in **Fig.3.40-42**. Flank faces at different degree are presented in **Fig.3.43-45**, and machined surface profiles at different degree are shown in **Fig.3.46-48**. It can be seen materials cannot be removed from the parent material at removal degree 8.75% when using ball end mill, but the machined surface still keep regular, and with the tool wear, scratch height becomes larger(see **Fig.3.43** and **Fig.3.46**), so that lower the surface integrity. For square end mill, scratch can be seen at initial stage, and with the tool wear, scratch of machined surface becomes serious, width and height both increase rapidly (see **Fig.3.44** and **Fig.3.47**). For taper end mill, in some places, the material cannot be removed from the parent material completely with tool wear, there are no obvious scratches on the machined surface (see **Fig.3.42** and **Fig.3.48**), it probably caused by the cutting edge become blunt(see **Fig.3.45**). Machined surface profiles can keep steed until completing total removal amount. Although flank wear increases with removal degree, the cutting edge is still sharp and tool wear just occurs in coating film layer.

From this examination experiment, it can see that proposed taper end mill can not only keep a higher surface integrity, but also retard the tool wear. Among the three milling methods, only taper end mill can complete the total work, square end mill cannot finish 40%, and ball end mill just complete less than 15%.

3.4 Conclusions

This chapter examined the validity of taper end mill though tool wear experiments based on the selected conditions. The following conclusions can be drawn from this chapter:

1. For taper end mill, when pick feed was selected 4mm, the influence on surface roughness R_z of each parameter was examined, the optimum values were selected. And then when milling efficiency and a selected cutting parameter are constant, the influence on surface roughness of two parameters were examined, and the cutting conditions at the maximum point are selected. And then cutting conditions of ball end mill and square end mill were selected according to this conditions. Comparing with ball end mill and square end mill method, using tilt taper end mill can reduce the cutting time approximately 94% and 25 % respectively in theoretically.

2. Axial depth of cut is set 0.1mm, the influence on surface roughness R_z of pick feed, feed per tooth and revolution speed were examined respectively. Optimum parameters of each milling method were selected for tool wear experiments. Comparing with ball end mill and square end mill method, using tilt taper end mill can reduce the cutting time approximately 94% and 47 % respectively in theoretically.
3. Tool wear experiments were carried out according to the selected two cutting conditions. The results show that only taper end mill can complete the total removal amount under required surface roughness, and until completing the work, machined surface keeps regular with tool wear. Surface integrity of the other two methods were effected by tool wear easily, surface roughness value over the required value before completed the total work.

References

[1] Sandvik, Tool Wear, Optimizing tool performance through insert wear analysis, Sandvik Coromant, 1994.
[2] R. Suresh, S. Basavarajappa, V.N. Gaitonda, G.L. Samuel. Machinability investigations on hardened AISI 4340 steel using coated carbide insert, Int. Journal of Refractory Metal and Hard Materials 2012; 33: 75-86.
[3] Jie Gu, Gary Barber, Simon Tung, Ren-Jyh Gu. Tool life and wear mechanism of uncoated and coated milling inserts, Wear 1999; 225-229:273-284.
[4] M.V. Kowstubhan, P.K. Philip. On the tool life equation of TiN coated high speed steel tools, Wear 1991; 143: 267–275.
[5] M. Nordin,U, R. Sundstrom, T.I. Selinder, S. Hogmark. Wear and failure mechanisms of multilayered PVD TiNrTaNcoated tools when milling austenitic stainless steel, Surface and coatings Technology2000, 133-134: 240-246.
[6] M. Sokovic, J.Kopac, L.A. Dobrazanski, M. Adamiak. Wear of PVD-coated solid carbide end mills in dry high speed cutting, Journal of Materials Processing Technology 2004, vol 157-158: 422-426.
[7] Asier Ugarte, Rachid M'Saoubi, Ainhara Garay, P.J. Arrazola. Machining behaviour of Ti-6Al-4V and Ti-5553 alloys in interrupted cutting with PVD coated cemented carbide, Procedia CIRP2012; 1: 202 – 207.
[8] M. A. Hadi, J.A. Ghani, C.H. Che Haron, M. S. Kasim. Comparison between up-milling and down-milling operations on tool wear in milling Inconel 718, Procedia Engineering 2013; 68:647-653.
[9]H.Shao,L.Liu, and H. L. Qu, Machinability study on 3%Co–12%Cr stainless steel in milling, Wear 2007, vol. 263, pp. 736-744.
[10] K.A. Abou-El-Hossein, Z. Yahya. High-speed end- milling of AISI 304 stainless steels using new geometrically developed carbide inserts, Journal of Materials Processing Technology 2005, vol162-163:596-602.
[11] S. N.B Oliaei, Y. Karpat. Experimental Investigations on Micro Milling of Stavax Stainless Steel, Procedia CIRP 2014, vol14: 377 – 382.
[12] Swapnagandha S. Wagh, Atul P. Kulkarni, Vikas G. Sargade. Machinability studies of austenitic stainless steel (AISI 304) using PVD cathodic arc evaporation (CAE) system deposited AlCrN/ TiAlN coated carbide inserts, Procedia Engineering 2013, vol64:907 – 914.
[13] D. O'Sullivan, M. Cotterell. Machinability of austenitic stainless steel SS303, Journal of Materials Processing Technology2002, vol124:153–159.

[14] R. Suresh, S. Basavarajappa, V.N. Gaitonde, G.L. Samuel. Machinability investigations on hardened AISI 4340 steel using coated carbide insert, Int. Journal of Refractory Metals and Hard Materials 2012, vol33:75-85.

Chapter 4 Cutting force and cutting temperature

4.1 Introduction

Stainless steel is well known as a material that is difficult to machine, even though it is widely used in high-temperature-environment components that require corrosion resistance, high strength, and ability to withstand creep rupture. Machining is generally difficult because of the toughness of the material and work hardening behavior. Most problems encountered during machining are caused by heat generation. The low thermal conductivity of the material results in high cutting temperature, which is associated with deformation and friction at the tool-chip and tool-workpiece interface [1]. Excessive strain during the ensuring machining passes creates undesirable microstructural alterations of the machined sub-surfaces, causing work-hardening [2]. The combination of applied stresses and temperatures causes flank wear and chipping [3]. These thermos-mechanical phenomena affect the surface integrity of the piece. An important related to the properties alteration on workpiece surface occurring during machining is the residual stress distribution and corrosion behavior [4]. As is known, the cutting temperature is the important factor which directly affects the cutting tool wear, work surface integrity and machining precision in process. The temperature distribution on the tool–workpiece interface may be determined with the known heat flux conducting into the tool and the workpiece [5]. There are numerous techniques to pick up a temperature signal, for example, a tool–workpiece thermocouple, all embedded artificial thermocouple and infrared ray thermometry, which have been proposed in the field of metal machining [6-11]. The cutting forces significantly affect the cutting temperatures, tool wear and tool life, machining dynamics, the machined surface integrity, and so on [12]. Some researchers have developed a mechanistic approach to determine the effect of the flank wear on the cutting forces and the chip geometry in orthogonal cutting. In this work, they show that the thrust force component is more sensitive to tool flank wear. In the contrary, tool flank wear does not affect both qualitatively and quantitatively the shearing angle and the friction angle, but results in an additional rubbing or ploughing force on the wear land [13-15]. The wear can be defined as the loss of material from the cutting edge due to mechanical or chemical factors associated with the cutting process. The cutting edge wear process according to the cutting path in machined material shows three areas that characterize the

behavior of the tool edge recession, which are; running (abrupt wear), linear wear (known as stability period) and catastrophic wear increasing significantly the recession of the tool edge (tool failure) [16]. Especially rapid tool wear in machining has long been recognized as a challenging problem [17].

The former chapter has examined the validities using tool wear experiments, but it still cannot explain the reason of its validity, this chapter will introduce the phenomena of cutting force and cutting temperature, and though the results explain the influences on tool wear and surface integrity.

4.2 Experimental method

This research will measure the cutting force and cutting temperature based on the cutting conditions selected by experiments. Cutting conditions as shown in **Table 4.1.** The cutting forces were measured with a kistler 9251A three component dynamometer, a kistler 5015A charge amplifier, a computer data acquisition (Graphtec GL7000). The measurement system frequency was far more than 4 times than the frequency of cutting forces. The sampling frequency was 1kHz. The average value of cutting force measurements was taken as the experimental data. And in order to shows the changes of cutting force and cutting temperature, we will measure both them at the same time.

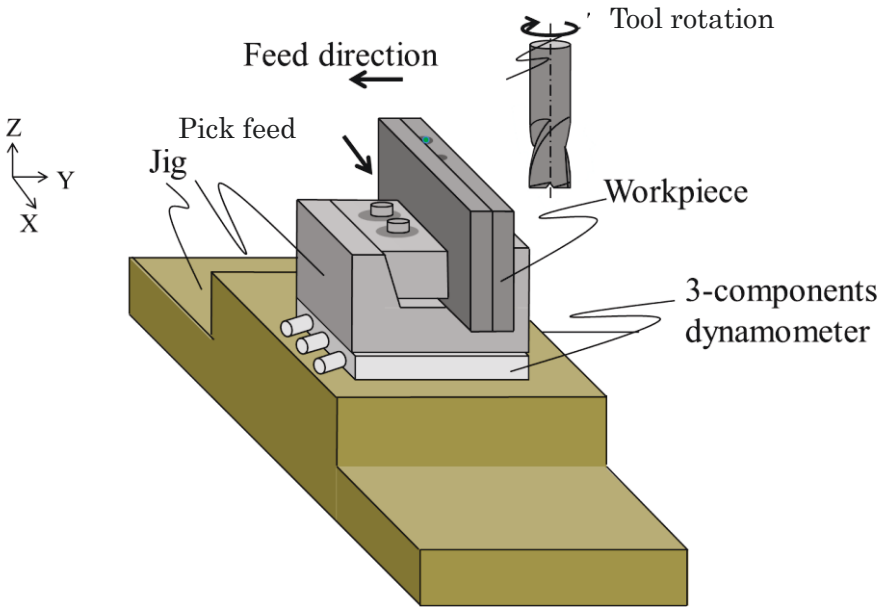

Fig.4.1. Experimental setup.

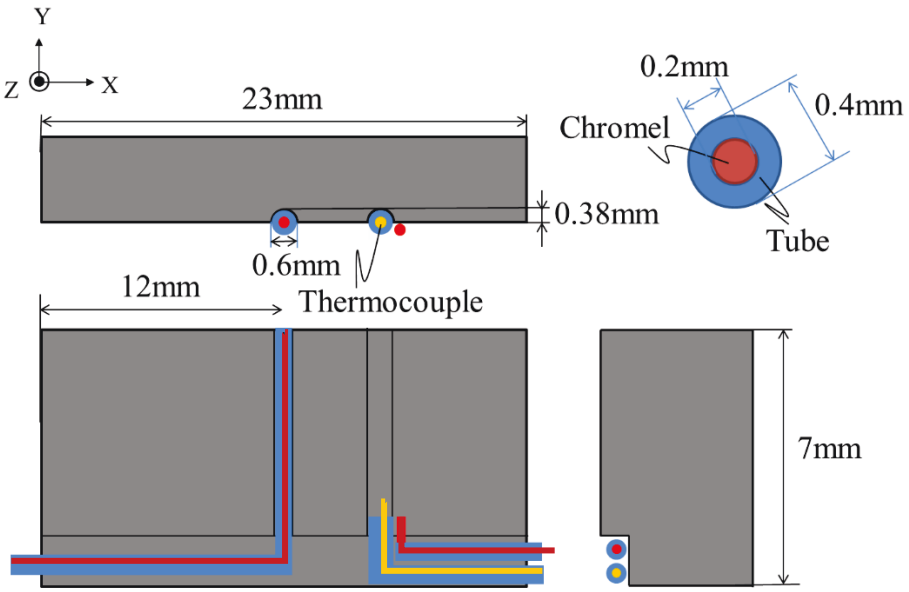

Fig.4.2. Sectional view of specimen.

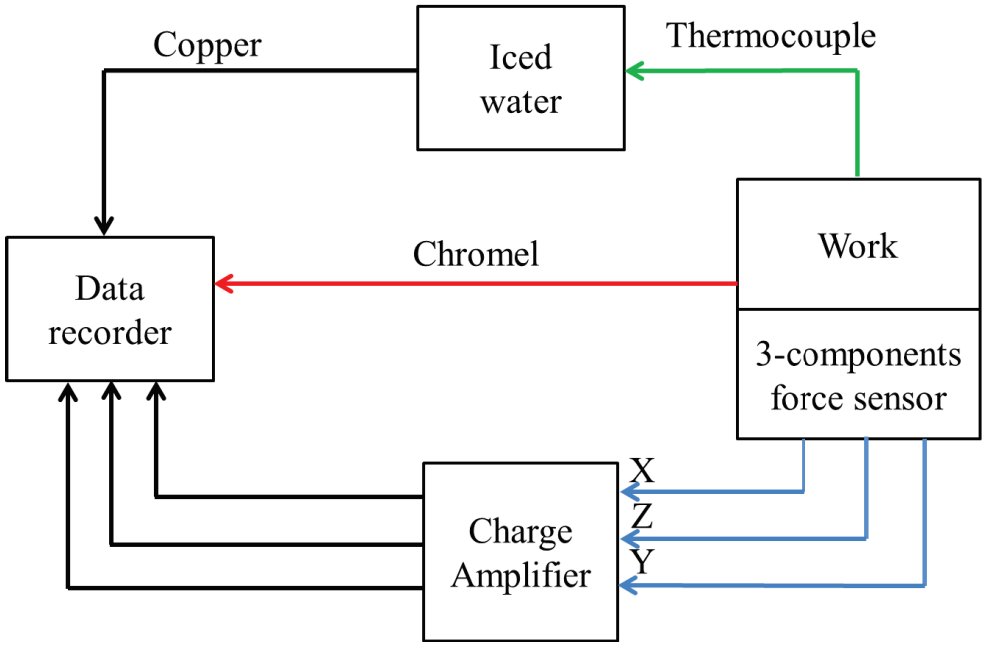

Fig.4.3. Concept of measurement method.

Table 4.1. Cutting conditions.

		Tilt taper end mill	Ball end mill	Square end mill
Work material		SUS403 (HRC45)		
Tool	Material	TiAlN coated cemented carbide		
	Diameter [mm]	32	6	6
	Number of teeth	1	2	2
Pick feed p_f [mm]		4.5	0.11	4
Cutting speed V [m/min]		161	34	113
Feed per tooth f_z [mm/min]		0.38	0.1	0..03
Axial depth of cut a_a [mm]		0.1	0.1	0.1

The experimental setup as shown in **Fig.4.1**. It has the trend to drift when 3-component force gauge using a piezoelectric effect of the crystal measuring the low frequency band. For this, the sample mounting jig, tightened at a uniform tightening stress distribution as much as possible, the squareness of female screw with respect to mounting surface of the three-component force sensor, and the parallelism of end face of the tightening cap bolt head with respect to the mounting surface and flat counter bore part are enhanced. In order to measure the cutting temperature and cutting force of the same point, the thermocouples are embedded in the workpiece. We used two ways to measure the temperature change. The sectional view as shown in **Fig.4.2**. The thermocouple is selected K type by 0.2mm chromel and alumel, and compensation lead wire are copper, The other one in composed by 0.2mm chromel and the workpiece. All the wire were

not machined with the workpiece, and the compensation lead wire are Nickel-Chromium alloy and Nickel alloy. In order to avoid the influence of the noise, the head of chromels are put in the PFA fluorocarbon polymers tubes which the external diameter are 0.4mm. Concept of the measurement method as shown in **Fig.4.3.** For the cutting force and temperature, we select three parts of the sampling, and average data of each part are seen as the maximum value of cutting force or cutting temperature. The temperature will evaluated by the sum of the two thermocouples. The experiments of ball end mill and square end mill were carried out on 5 –axis machine tool (MAKINO D500), and the experiments of taper end mill were performed on 3-axis machine tool (OSAKAKIKO Rakuraku Mill 3V).

4.3 Experimental results and discussion

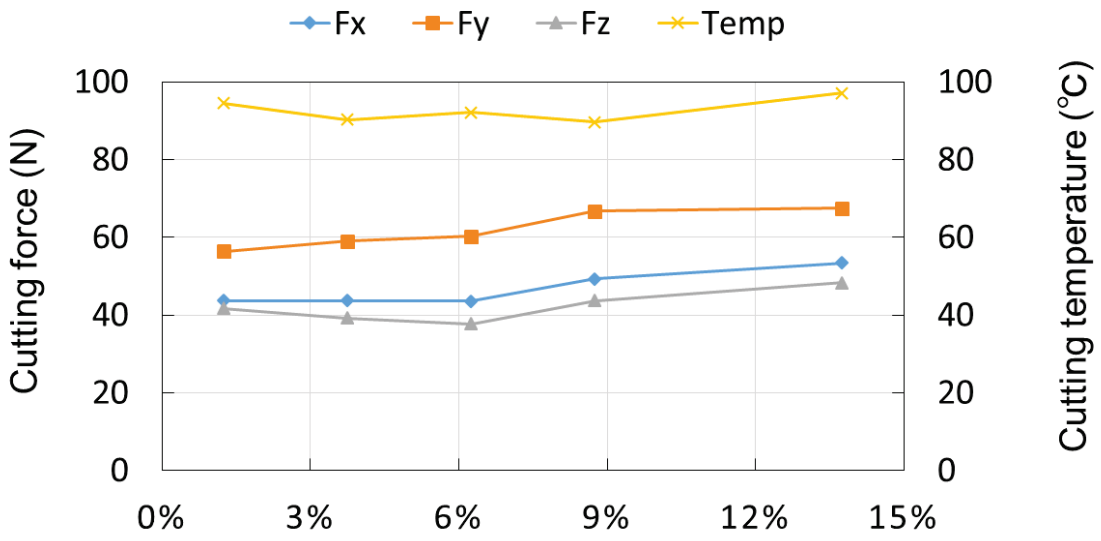

Fig.4.4. Cutting force and cutting temperature using ball end mill.

The cutting force and cutting temperature using ball end mill as shown in **Fig.4.4.** With the tool wear, the cutting force in X, Y, and Z direction keep the nearly the same trend, the value in Y direction is larger than that in the other two direction, about 1.3 times and 1.4 times that of in X, Z direction, respectively. The pick feed value is larger than that of feed per tooth and axial depth of cut, thus, the force in Y direction appears greater. The values of feed per tooth and axial depth of cut

are same, the force in these directions keep nearly the same. Cutting temperature using ball end mill keeps similar trend with cutting force until removal degree 8.75%, especially with the cutting force in Z direction, and then the value decreases, it may be caused by tool worn, and real axial depth of cut becomes small. The heat generated by friction between flank face and machined surface is reduced.

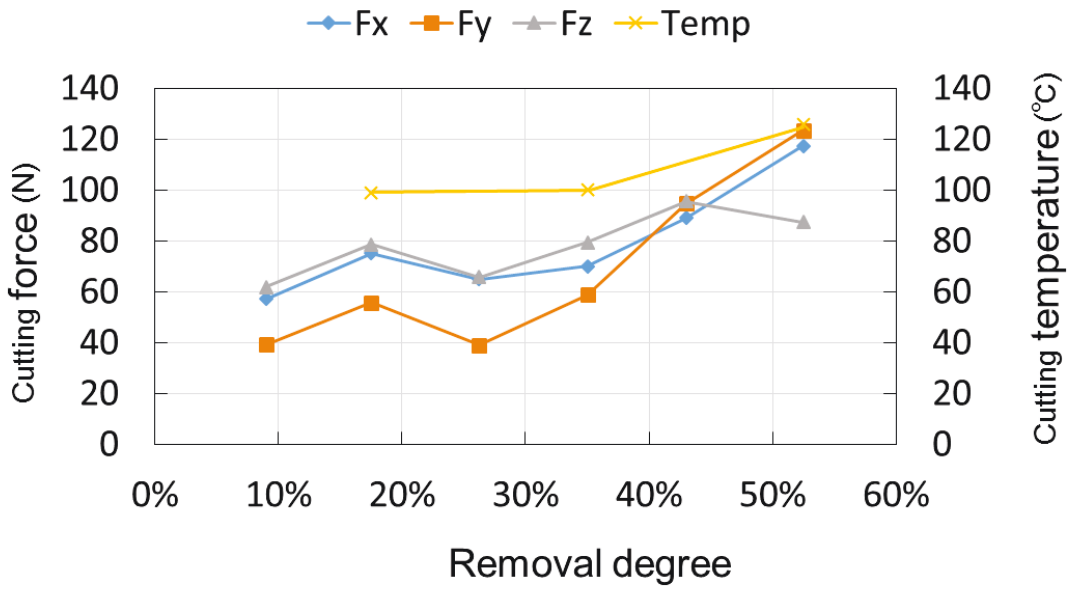

Fig.4.5. Cutting force and cutting temperature using square end mill.

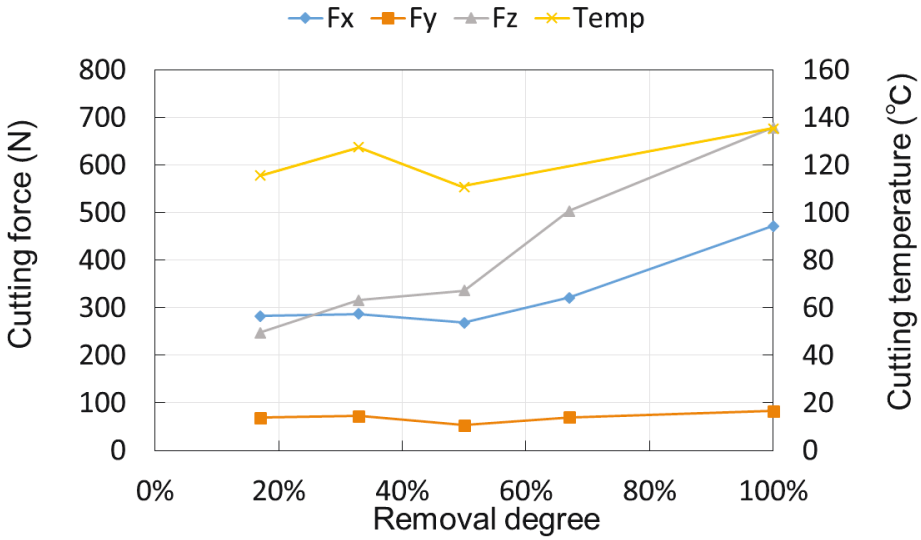

Fig.4.6. Cutting force using tilt taper end mill.

The relationship between flank wear and cutting force and temperature are given in **Fig.4.7.** Flank wear is positively correlated with cutting force in each direction, and nearly negative correlation with cutting temperature, the reason is that the tool wear both in rake face and flank face are not seriously, it cannot complete the total removal amount just because the surface roughness value over required value.

The cutting force and cutting temperature using square end mill as shown in **Fig.4.5.** The cutting force and cutting temperature are smaller than that of using ball end mill, although the pick feed value of square end mill is larger, the cutting speed is over 100m/min, the higher speed lower the cutting force, so that the cutting temperature is also smaller than that of using ball end mill. The reason that the cutting force decreases due to increasing velocity is that the material strength decreases with increasing temperature at high cutting velocity. From **Fig.3.38** and **Fig.3.39**, tool wear and surface roughness keep steady until removal degree 35%, and there are no apparent abrasion can be seen, therefore, the cutting force in each direction keeps increase steadily with tool wear as a whole. There is no obvious correlation between flank wear and cutting force or cutting temperature in this stage (see **Fig.4.8**).

The cutting force using taper end mill as shown in **Fig.4.6**. The value is more than that of using ball end mill and square end mill. The reason is that the removal amount is greater, and the maximum diameter is larger. The force in Y direction is smaller than that in X or Z direction, the reason is that the workpiece is rotated 10 degree relative to Y axis in order to keep the cutting edge parallel to machined surface, a part of force is distribute in Z direction. For taper end mill method, the cutting force keeps steady increase with the progress, cutting force in Z direction changes with the flank wear can be seen (see **Fig.4.9**). Another, the surface roughness Rz changes nearly the same as the cutting force in Y direction, the reason probably is that part of the cutting edge close to the corner retreats more than area because the cutting speed is high, and until complete the total removal amount, tool wear is still occur in the film layer, friction occurs at the surface between the minor cutting edge and the workpiece is slight.

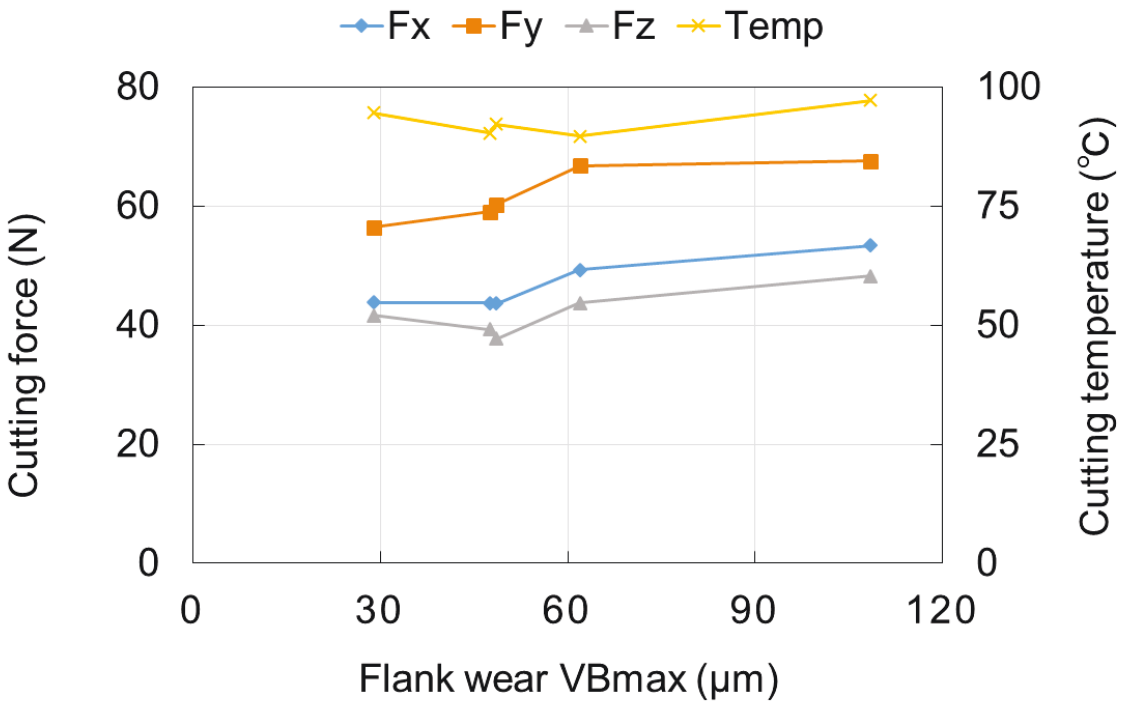

Fig.4.7. Relationships between flank wear and cutting force and cutting temperature using ball end mill.

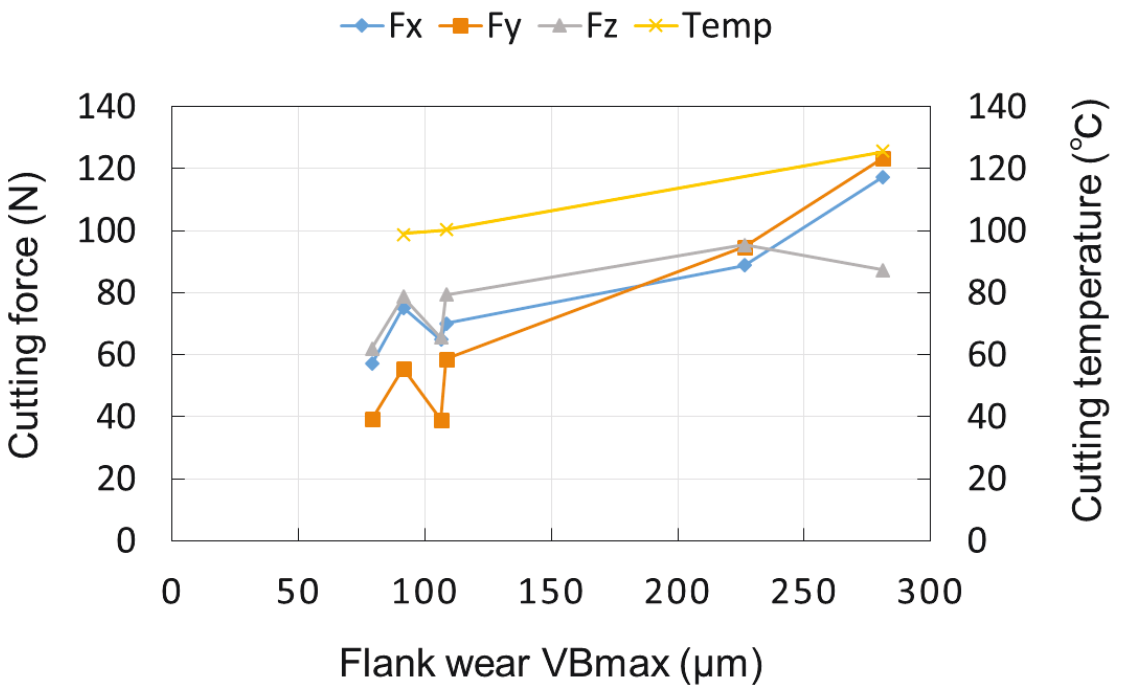

Fig.4.8. Relationships between flank wear and cutting force and cutting temperature using square end mill.

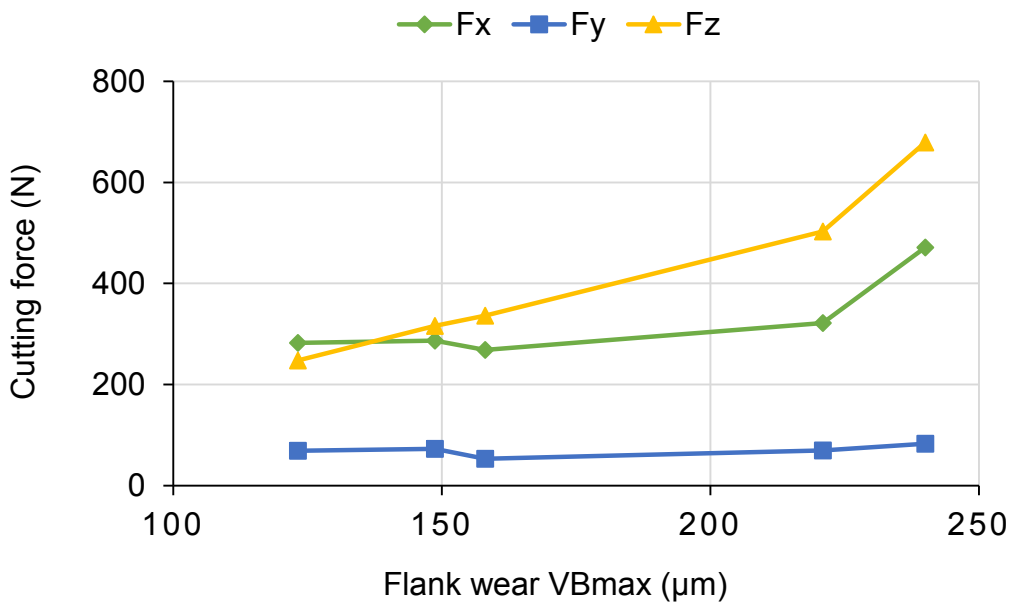

Fig.4.9. Relationships between flank wear and cutting force using taper end mill.

The cutting force at different removal degree are given as **Fig.4.10 -12**. For the ball end mill, in the three directions, the peak value of cutting force in each period is changing irregular, the reason is that there is whirling of spindle, the shape errors of two cutting edges, and attachment error of tool holder and so on. The maximum cutting speed of ball end mill is 34 m/min, it is smaller than the high speed milling, which caused the cutting force to be higher and tool chatter seriously. Therefore, the tool wear is easily and surface roughness value increase quickly. Cutting force values are almost positive, it reflects that the tool acts in direction of pressing the workpiece.

For the square end mill, the cutting force in three direction keeps regular, until removal degree is 52.5% the waviness of cutting force appears no obvious fluctuation of peak value. Due to this, the milling process is steady so that the tool wear is retarded, and as a result of good surface integrity.

For taper end mill, it can be seen that the cutting process is discontinuous, and the real cutting time in a period is quite short, thus, the cutting heat will not be accumulated at the cutting area, it can overcome the shortage that using ball end mill for milling stainless, and it can retard the tool abrasion of cutting edge so that extending the tool life. Although the value of cutting force is larger, the peak value still keeps steady until complete the total removal amount. With of tool wear on both rake face and flank face are enlarged with progress, the coated film layer

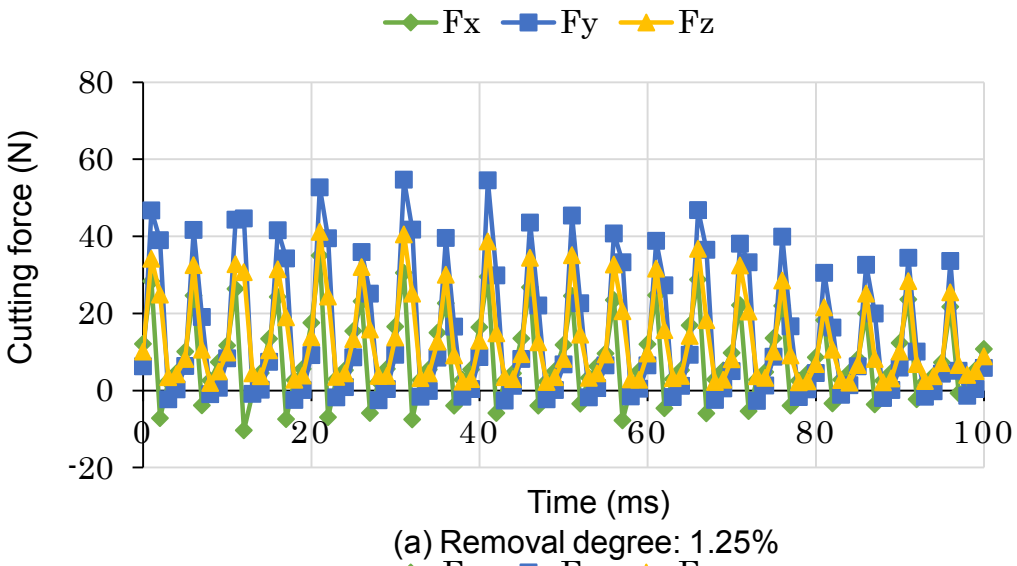

(a) Removal degree: 1.25%

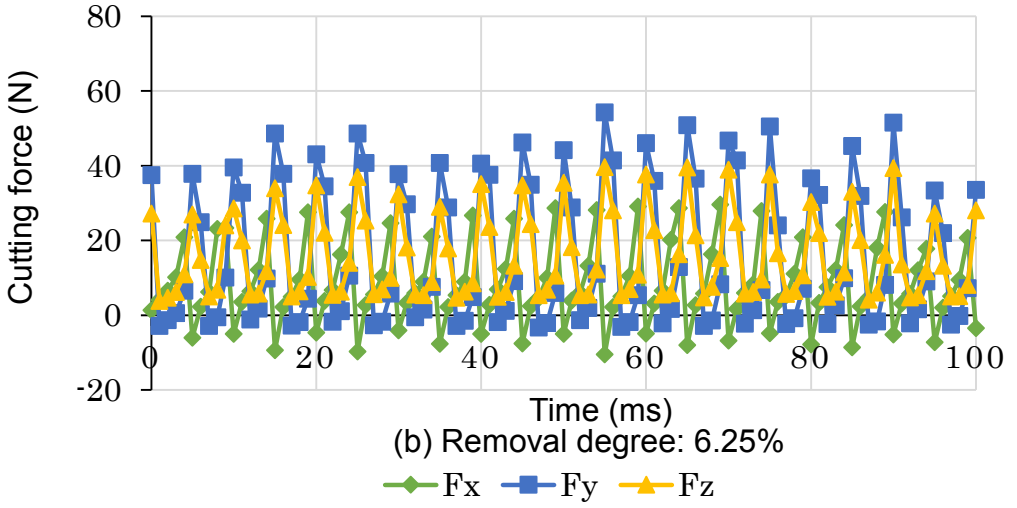

(b) Removal degree: 6.25%

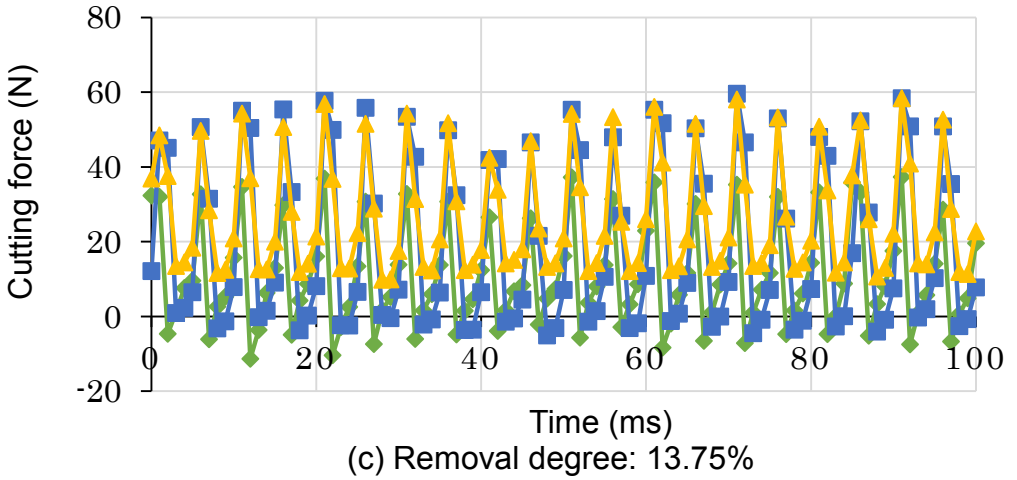

(c) Removal degree: 13.75%

Fig.4.10. Cutting force using ball end mill at different removal degree.

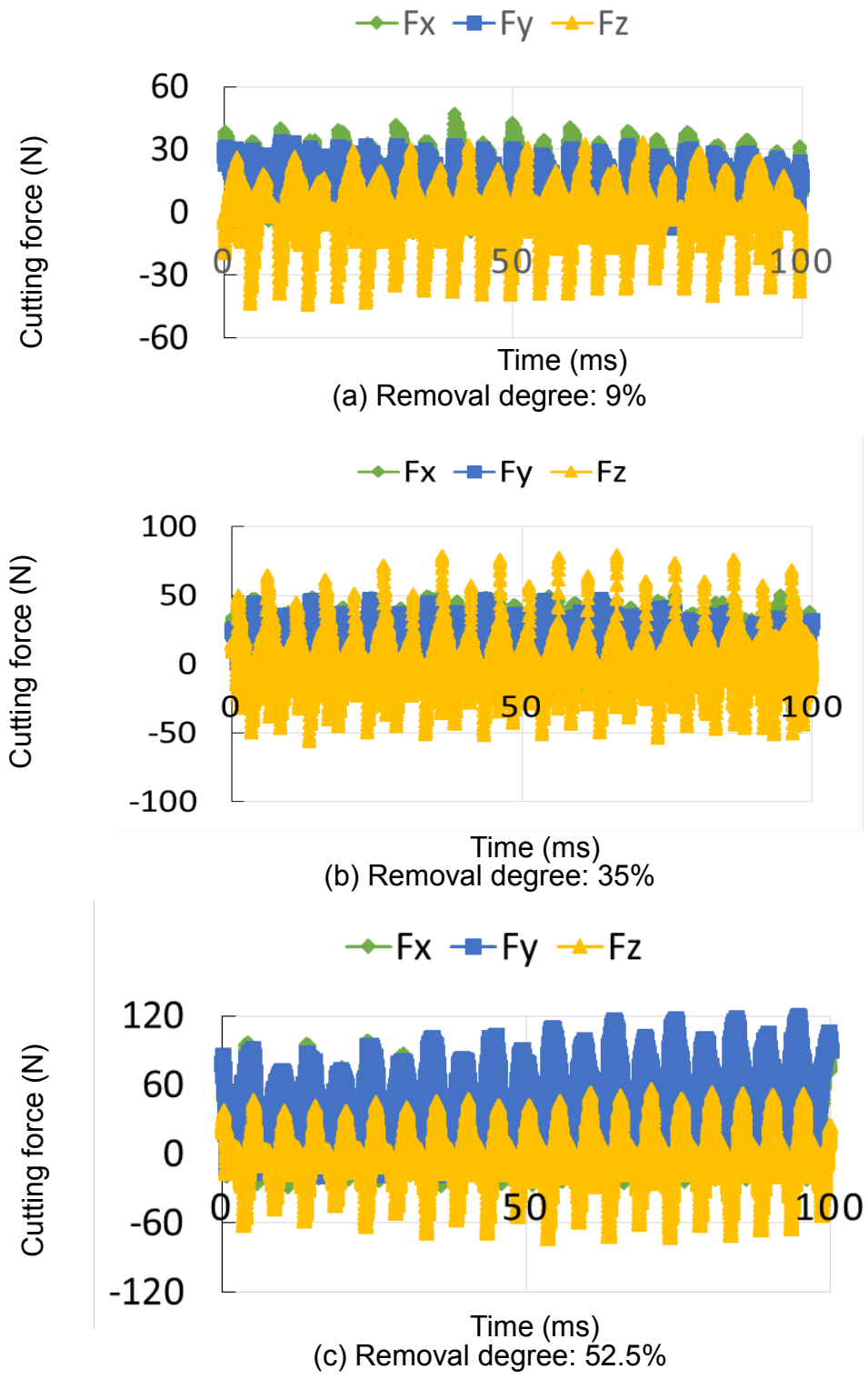

Fig.4.11. Cutting force using square end mill at different removal degree.

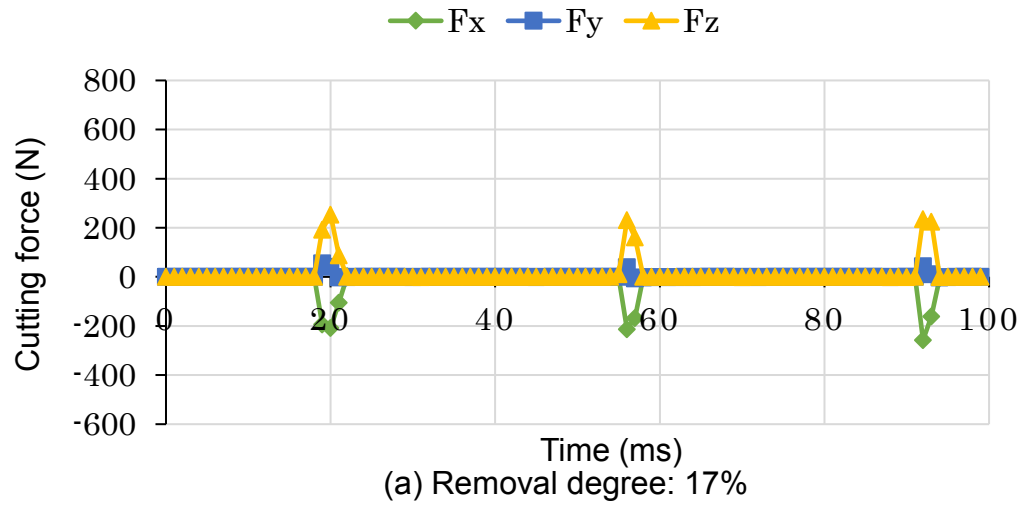

(a) Removal degree: 17%

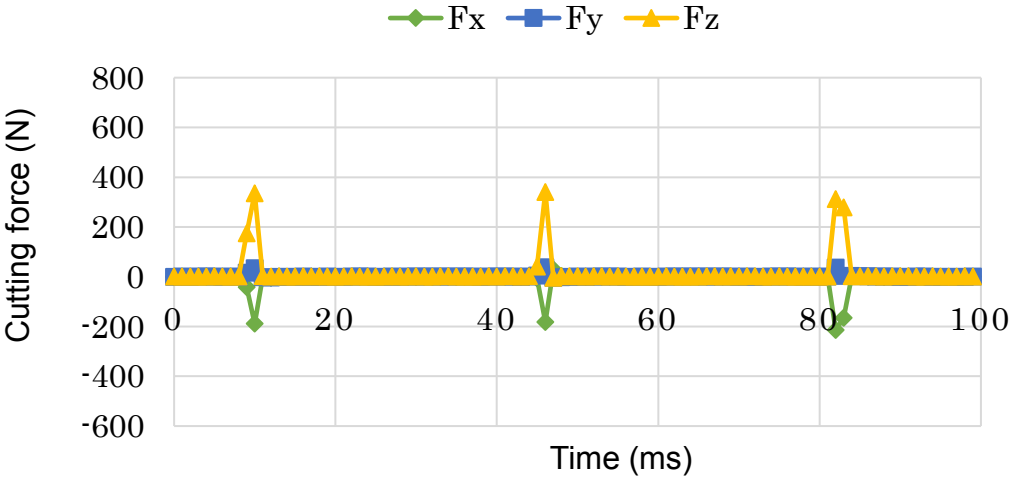

(b) Removal degree: 50%

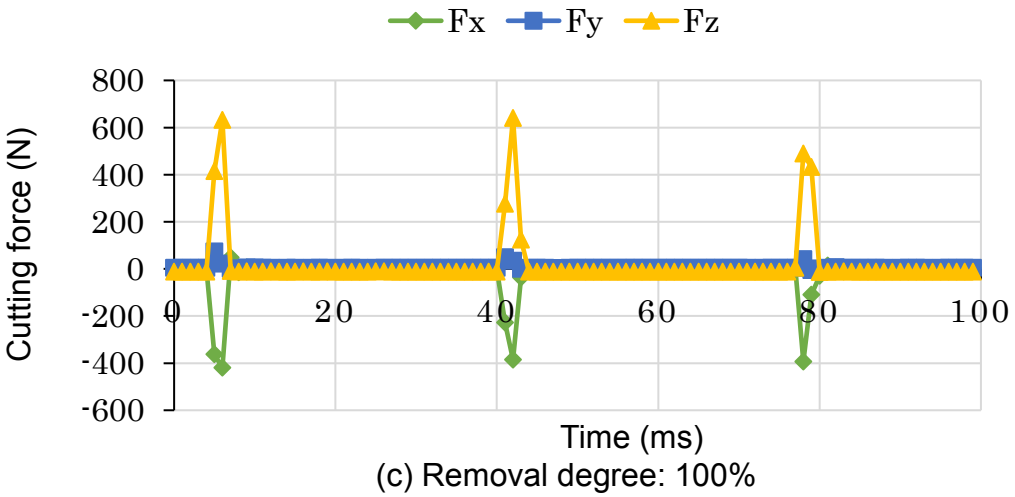

(c) Removal degree: 100%

Fig.4.12. Cutting force using taper end mill at different removal degree.

is degressive, which caused the friction coefficient to be larger, and then the friction force becomes greater. Owing to the wear only occurs at the film layer, it affects the surface integrity slightly.

4.4 Conclusions

In this chapter, in order to explain the mechanism using taper end mill, the cutting force and cutting temperature were measured, some conclusions can be drawn as following:

1. In order to measure the cutting force and cutting temperature of each milling method, a measurement device was designed.
2. On the whole, the results shows that cutting force and cutting temperature increase with process. Cutting force using ball end mill and taper end mill shown a positive correlation with flank wear.
3. For the selected cutting conditions, peak values of cutting force using ball end mill change irregularly, oppositely, the waviness of cutting force using square end mill and taper end mill can keep steady, but only using taper end mill can keep steady until complete the total work.
4. The cutting process using taper end mil is discontinuous so that the heat can be removed, real cutting time only takes approximately 10% of a period. Owing to this, the tool life is extended and surface integrity keeps good.

References

[1] E.O. Ezugwu. Key improvements in the machining of difficult-to-cut aerospace superalloys. International Journal of Machine Tools and Manufacture 2005; vol45:1353-1367.

[2] D. Ulutan, T. Ozel. Machining induced surface integrity in titanium and nickel alloys: A review. International Journal of Machine Tools & Manufacture 2011; vol51:31.

[3] E.O. Ezugwu, Z.M. Wang, A.R. Machodo. The machinability of nickel-based alloys: A review. Journal of Materials Processing Technology 1999; vol86:1-16.

[4] M. San-Juan, Ó. Martín, M. del P. de Tiedra, F. J. Santos, R. López, J. A. Cebrián. Study of cutting forces and temperatures in milling of AISI 316L. Procedia Engineering 2015; vol132:500-506.

[5] Chen Ming, Sun Fanghong, Wang Haili, Yuan Renwei, Qu Zhenghong, Zhang Shuqiao. Experimental research on the dynamic characteristics of the cutting temperature in the process of high-speed milling. Journal of Materials Processing Technology 2003; vol138:468-471.

[6] N. Michailidis. Variations in the cutting performance of PVD-coated tools in milling Ti6Al4V, explained through temperature-dependent coating properties. Surface & Coatings Technology 2016; vol304: 325-329

[7] David K. Aspinwall, Andrew L. Mantle, Wai Kok Chan, Richard Hood, Sein Leung Soo. Cutting temperatures when ball nose end milling γ-TiAl intermetallic alloys.

[8] Lincoln Cardoso Brandão, Reginaldo Teixeira Coelho, Alessandro Roger Rodrigues. Experimental and theoretical study of workpiece temperature when end milling hardened steels using (TiAl) N-coated and PcBN-tipped tools. Journal of Materials Processing Technology 2008; vol199-234-244.

[9] Sijie Yan, Dahu Zhu, Kejia Zhuang, Xiaoming Zhang, Han Ding. Modeling and anslysis of coated tool temperature variation in dry milling of Inconel 718 turbine blade considering flank wear effect. Journal of Materials Processing Technology 2014; vol214:2985-3001.

[10] Takeshi Yashiro, Takayuki Ogawa, Hiroyuki Sasahara. Temperature measurement of cutting tool and machined surface layer in milling of CFRP. International Journal of Machine Tools & Manufacture 2013; vol70:63-69.

[11] Ali Mamedov, Ismail Lazoglu. Thermal analysis of micro milling titanium alloy Ti-6Al-4V. Journal of Materials Processing Technology 2016; vol229:659-667.

[12] N. Fang, Q. Wu. A comparative study of the cutting forces in high speed machining of Ti–6Al–4V and Inconel 718 with a round cutting edge tool. Journal of Materials Processing Technology 2009, vol209:4385-4389.
[13] Wang, J., Huang, C.Z., Song, W.G. The effects of tool flank wear on the orthogonal cutting process and its practical implications. Journal of Materials Processing Technology2003, vol142:338–346.
[14] M. Ben Said, K. saï, W. Bouzid Saï. An investigation of cutting forces in machining with worn ball-end mill. Journal of Materials Processing Technology 2009; vol 209:3198-3217.
[15] Oguzhan Tuysuz, Yusuf Altintas, His-Yung Feng. Prediction of cutting forces in three and five-axis ball-end milling with tool indentation effect. International Journal of Machine Tools & Manufacture 2013; vol66:66-81.
[16] H. Aknouche, A. Outahyon, C. Nouveau, R. Marchal, A. Zerizer,J.C.Butaud. Tool wear effect on cutting forces: In routing process of Aleppo pine wood. Journal of materials processing technology 2009; vol209:2918–2922.
[17] H.Z. Li, H. Zeng, X.Q. Chen. An experimental study of tool wear and cutting force variation in the end milling of Inconel 718 with coated carbide inserts. Journal of Materials Processing Technology2006; vol180: 296–304.

Chapter 5 Tool path generation

5.1 Introduction

The former chapters have discussed the validity of taper end mill method when milling plane model, and examined the cutting force and cutting force for explaining it. The surface of steam turbine blade is freeform surface, tool path is needed when milling it. Computer-aided manufacturing (CAM) systems as well as computer numerical control (CNC) machine tools are widely used in today's manufacturing industries [1, 2]. For the complex surfaces, the traditional machine tool can no longer satisfy the requirement of such complex task. Only by the help of CAD/CAM can fulfill the requirement. Free-form surface design and manufacturing are important steps in product developments for free-form surface, many research have done the work to generate tool paths using different approaches [3-9]. Machining industry is presented with a growing demand to produce increasingly more complex shapes in difficult-to-cut material grades [10]. The machining of mechanical parts, such as turbine blades, is challenged with both geometrical complexity and the material's properties. The shape must be modeled as a free-form. Since the blades are exposed to severe conditions, they must be made from special grades of difficult-to-cut material, which causes the cutting forces to vary widely. The risk of a poor surface finish is high because cutting forces strongly influence the surface finish in multi-axis milling of complex geometries [11]. To achieve high efficient and gauging-free cutter path planning, many algorithms for the cutter-path generation and the cutter-gauging avoidance have been developed [12-19]. These researches mainly focus on the ball end mill or square end mill, there is no research on generating the tool path for tilt taper end mill. Current commercial CAM is difficult to generate the tool path for the proposed method. Due to this, the objective of this chapter is to solve it and obtain a high accuracy surface, it will present an implementing work in automatic generation of 5-axis tool paths and NC code for the special taper end mill, and then verify the validity through modeling experiments of sphere.

5.2 Conceptual approach

Because the work is the primary stage of special CAM development, it will take no account of tool path optimization. This section will introduce the definitions of the special tool and the parametric surface, and the NC data generation by

software MATHEMATICA 9.0.

5.3 Tool path generation

Tool orientation control plays a key role in the efficiency and quality of 5-axis machining operations. The main objective it to specify the parameters (tilt and inclination angles) that define the tool orientation at each cutter contact (CC) point, so that the machining time is minimized and the machined surface is gouge-free, within tolerance, and of uniform quality across the surface [20]. Tool orientations of ball end mill and taper end mill as shown in **Fig.5.1**. As the cutting edge is parallel to the tangential line, commercial CAD/CAM cannot define the tool orientations and cutting point directly. Therefore, tool definition is needed.

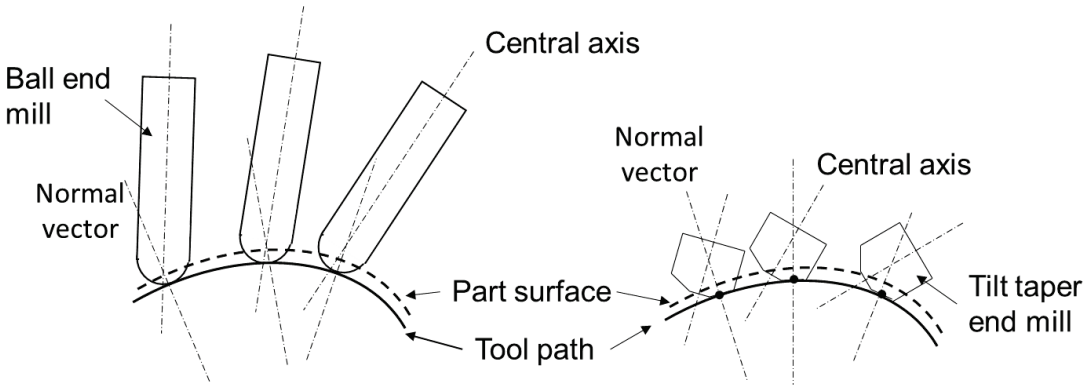

Fig.5.1. Tool orientation.

Instead of the ball end mill, the propose method uses a tilt taper end mill to machine the steam turbine blade. Local coordinate system as shown in **Fig.5.2**. In order to satisfy the concept of proposed tilt taper end mill, the coordinate conversion is needed. At first, cutting point on the cutting edge was defined. Tool sectional view in XZ plane as shown in **Fig.5.3**, t_r is the edge point of top end, t_θ is angle of the taper edge, t_p is the point at the cutting edge, v is the length from t_r to t_p, it is decided according to the defined point. ω is the angle in rotating direction relative to z axis. **Eq. (1)** represents the coordinate of arbitrary point on the cutting edge for a given tool, t_r and t_θ are known quantities. Defined taper end mill as shown in **Fig.5.4**.

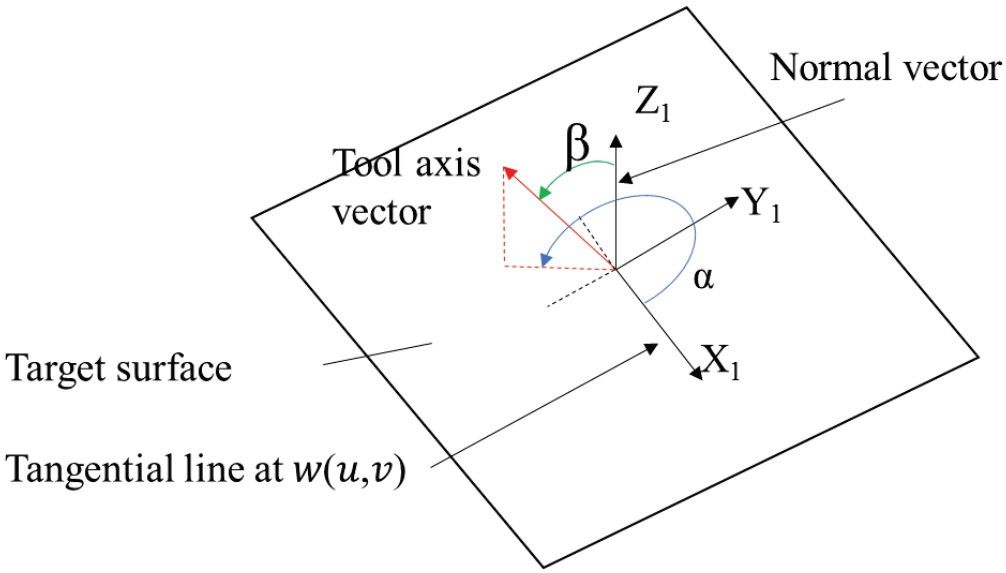

Fig.5.2. Local coordinate system.

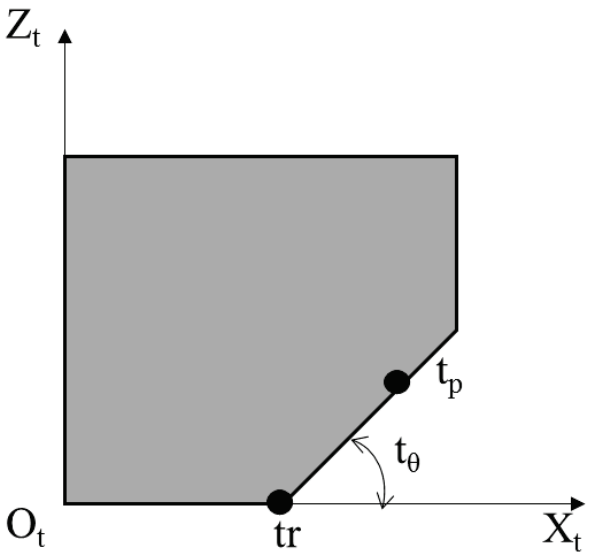

Fig.5.3. Sectional of taper end mill.

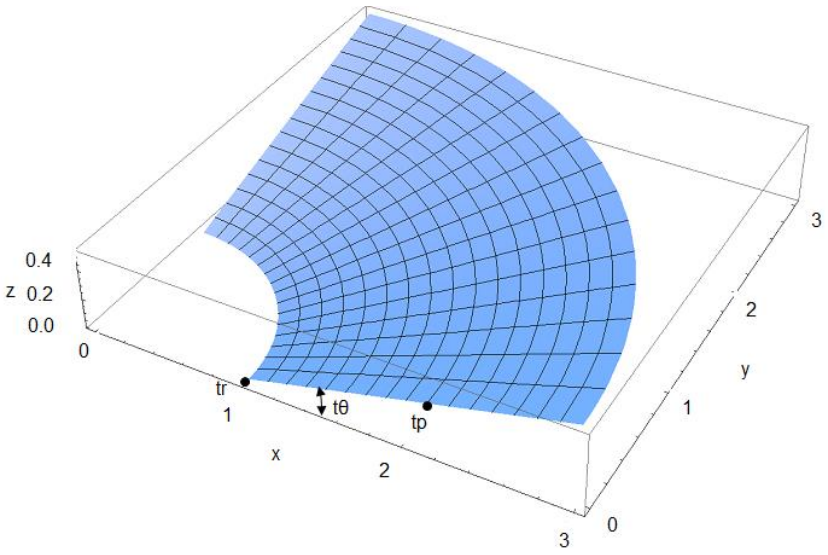

Unit: mm

Fig.5.4. Schematic of the defined taper end mill.

$$\mathbf{tp}(v,\omega) = \begin{bmatrix} tx \\ ty \\ tz \end{bmatrix} = \begin{bmatrix} (tr + vcos(t\theta))\cos(\omega) \\ (tr + vcos(t\theta))\sin(\omega) \\ vsin(t\theta) \end{bmatrix} \quad (1)$$

Before generating the tool path, it has to define the target shape. In order to facilitate the validity evaluation of the developed CAM, here, spherical surface is selected. Its formula is given in **Eq. (2).** Each point on the surface should own directionality, u_s and u_e represent the start angle and end angle in rotating direction respectively, and v_s and v_e represent the start angle and end angle in height direction respectively. Both the start angle is 0 degree, end angle in two direction are -360 degree and 45 degree. The *u* and *v* are the parametric variables of sphere, thus, $u \in [\, us, ue \,]$ and $v \in$ [vs, ve]. When setting the curvature radius r 40mm, the target shape as shown in **Fig.5.5.**

$$\mathbf{w}(u,v) = \begin{bmatrix} wx \\ wy \\ wz \end{bmatrix} = \begin{bmatrix} rcos(v)\cos(u) \\ rcos(v)\sin(u) \\ rsin(v) - rsin(ve) \end{bmatrix} \quad (2)$$

Partial derivatives in *u* and *v* are calculated respectively. Thus, normal vector **n** (*u*, *v*) is the outer product of two tangent vector (see **Eq. (3)**).

$$\mathbf{n}(u,v) = \frac{\frac{\partial \boldsymbol{w}(\boldsymbol{u},\boldsymbol{v})}{\partial u} \times \frac{\partial \mathbf{w}(u,v)}{\partial v}}{\left|\frac{\partial \boldsymbol{w}(\boldsymbol{u},\boldsymbol{v})}{\partial u} \times \frac{\partial \mathbf{w}(u,v)}{\partial v}\right|} \tag{3}$$

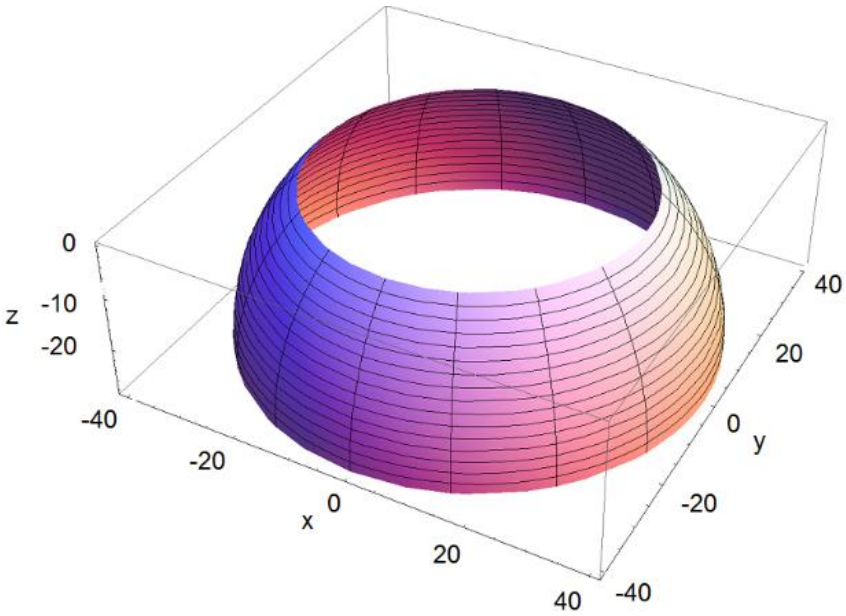

Unit: mm

Fig.5.5. Target surface.

This experiment adopt the Contour machining. ***Pn*** is the number of tool path, ***i*** is the ordinal number of the tool path. ***Ps*** is the start tool path angle in height direction, so it is equal to *ve*, ***Pd*** is the angle of two adjacent tool paths relative to the center of sphere, therefore, spatial parameter **b**(*u*) of the tool path can be derived. Each tool path formula is denoted as **cp(***u, i***)**, as shown in **Fig.5.6**. Thus, its tangent vector *D***cp** can be calculated (see **Eq. (7)**).

$$\mathrm{Pd} = (\mathrm{ve} - \mathrm{vs}) / (Pn - 1) \tag{4}$$

$$\mathbf{b}(\mathrm{u}) = \left[{}^{u}_{Ps - Pd * i}\right] \ (i \in [0, \mathrm{Pn} - 1]) \tag{5}$$

$$\mathbf{cp}(u,i) = \begin{bmatrix} rcos(Ps - Pd * i)\cos(u) \\ rcos(Ps - Pd * i)\sin(u) \\ rsin(Ps - Pd * i) - rsin(ve) \end{bmatrix} \quad (6)$$

$$\mathrm{D}\mathbf{cp} = \frac{\partial \mathbf{cp}(u,i)}{\partial u} \quad (7)$$

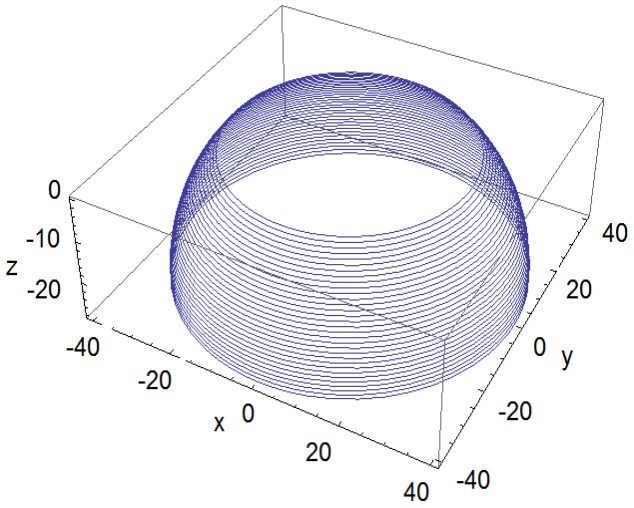

Unit: mm

Fig.5.6. Generated tool path.

When generating the NC code, it has to take into the structure of the machine tool, here, we adopt the desktop 5-axis machine tool (TAKUMI UNC-100-M5) (see **Fig.5.7**), arrangement of each axis as shown in **Fig.5.8**. The l is the distance from pivot point of B axis to the bottom surface of tool, therefore, it includes the tool length, in the experiment, its length subtracts the tool length is 54.939mm. Depth of cut *dd* can be set according to the machining allowance. All the tool paths start at *u* is zero. The **cf** is the unit tangent vector of the cutter contact (CC) points in feed direction, **cn** is surface normal at the point, **cb** is their cross product, **ccp** (i) is the local coordinate of the starting point (see **Fig.5.9**).

$$\mathbf{cf} = \frac{\frac{\partial \mathbf{cp}(u,i)}{\partial u}}{\left|\frac{\partial \mathbf{cp}(u,i)}{\partial u}\right|} \quad (8)$$

$$\mathbf{ccp(i)} = \begin{bmatrix} \boldsymbol{ccpx} \\ \boldsymbol{ccpy} \\ \boldsymbol{ccpz} \end{bmatrix} = \mathbf{cp}(0, i) \tag{9}$$

Fig. 5.7. Images of 5-axis machine tool (UNC-100-M5).

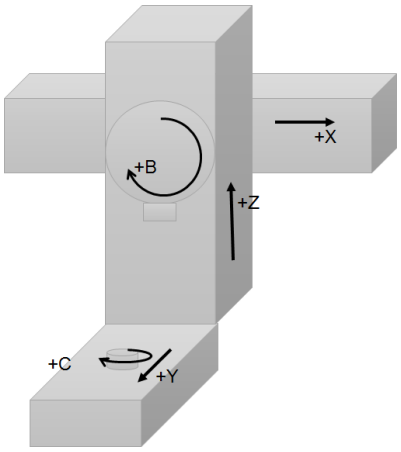

Fig.5.8. Structure of machine tool.

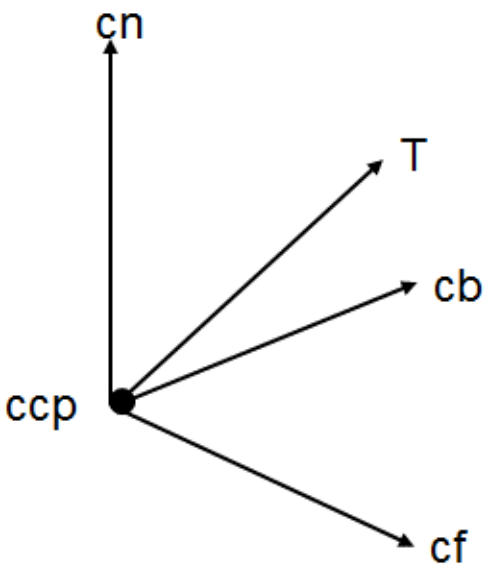

Fig.5.9. Local coordinate system.

Using the calculated *cc* data, machine coordinate can be deduced to generate the corresponding NC data. At present, coordinate transformations of 5-axis machine tool all adopt 4×4 matrix. **Eq. (10)** includes all the coordinate information of CC points, **Eq. (11)** represents the translation in Z direction, **Eq. (12)** represents the rotation relative to C axis, and **Eq. (13)** is the rotation relative to B axis. When the tool is rotated relative to B axis, it has to compensate the rotation translation of cutting edge, that because when the tool rotated, the cutting edge cannot contact the target cutting point, so it cannot remove the material enough, as a result, the machining accuracy becomes low. Therefore, the inverse transform of the rotation is compensated. Additionally, **tp** in **Eq. (13)** is the midpoint of the cutting edge to satisfy the proposed method, in a word, the theoretical machining is the midpoint of the cutting edge is exactly at the cutting point.

$$\mathbf{M}0=\begin{bmatrix} cfx & cbx & cnx & ccpx \\ cfy & cby & cny & ccpy \\ cfz & cbz & cnz & ccpz \\ 0 & 0 & 0 & 1 \end{bmatrix} \tag{10}$$

$$\mathbf{M}1 = \begin{bmatrix} 1 & 0 & 0 & 0 \\ 0 & 1 & 0 & 0 \\ 0 & 0 & 1 & dep \\ 0 & 0 & 0 & 1 \end{bmatrix} \tag{11}$$

$$\mathbf{M}2 = \begin{bmatrix} \cos(\alpha) & -\sin(\alpha) & 0 & 0 \\ \sin(\alpha) & \cos(\alpha) & 0 & 0 \\ 0 & 0 & 1 & 0 \\ 0 & 0 & 0 & 1 \end{bmatrix} \tag{12}$$

$$\mathbf{M}3 = \begin{bmatrix} \cos(\beta) & 0 & \sin(\beta) & -\cos(\beta)\mathrm{tp}x - \sin(\beta)\mathrm{tpz} \\ 0 & 1 & 0 & 0 \\ -\sin(\beta) & 0 & \cos(\beta) & \sin(\beta)\mathrm{tpx} - \cos(\beta)\mathrm{tpz} \\ 0 & 0 & 0 & 1 \end{bmatrix} \tag{13}$$

The **M**4 is the inner product of the former four matrixes, it represents the overall coordinate transform when tool moves between two cutting points. **Eq. (15)** and **Eq. (16)** mean that choose the forth row and third row as **pp** and **qq** respectively. In order to facilitate the calculation, we use px and so on to represent some value of the matrix.

$$\mathbf{M}4 = \mathbf{M}0 \times \mathbf{M}1 \times \mathbf{M}2 \times \mathbf{M}3 \tag{14}$$

$$\mathbf{pp} = \begin{bmatrix} px \\ py \\ pz \\ 1 \end{bmatrix} = \mathbf{M}4 \cdot [0 \quad 0 \quad 0 \quad 1]^T \tag{15}$$

$$\mathbf{qq} = \begin{bmatrix} qx \\ qy \\ qz \\ 1 \end{bmatrix} = \mathbf{M}4 \cdot [0 \quad 0 \quad 1 \quad 0]^T \tag{16}$$

Since CL and orientation data are defined with respect to the coordinate system of workpiece, they need converting for machine control commands in machine coordinate system [21]. Each absolute coordinate of cutting points can be calculated by **Eq. (17)**. As the target shape is symmetrical, we just consider the positive direction. Besides, the rotation center of B axis is not the tool end, when B rotating, the x and y coordinate of machine system is changed with it, thus, it

also should be taken into consideration.

$$
\begin{aligned}
bb &= \mathbf{arccos}\,(qz)\ (b \in [0, \pi/2]) \\
cc &= \mathbf{arcTan}\,(\tfrac{qx}{qy}) \\
xx &= px\,\mathbf{cos}\,(cc) + l\,\mathbf{sin}\,(bb) + py\,\mathbf{sin}\,(cc) \\
yy &= py\,\mathbf{cos}\,(cc) - px\,\mathbf{sin}\,(cc) \\
zz &= pz - l + l\,\mathbf{cos}\,(bb)
\end{aligned}
\tag{17}
$$

5.4 Application

Using the generated NC code, an experiment is carried out to examine the validity of the proposed method. Target surface as shown in **Fig.5.10**.Cutting conditions are given in **Table 5.1**.The *tr* is 1mm, *tθ* is 15°, and the radius of the tool 3mm. *ve* is set 45°, Pn is set 32, and the depth of cut is 0.4mm. The material is chemical wood, pick feed is set about 1mm. Machined surface was inspected by CMM (Mitutoyo LEGEX9106). In pick feed direction, the proposed method use short straight lines to replace curves, the geometry error cannot be avoided, however, machining error in feed direction is very little. Therefore, only line profile of section in vertical direction are discussed. **Fig.5.11** shows the line profile of the section, it appears smooth, and cannot see obvious error, **Fig.5.12** shows its curvature radius error relative to target value. It can see that the errors changes in a small range within 50μm. The theoretical curvature radius is 39mm, the experimental value is 39.04mm, which relative error can be controlled within 0.15%. In a word, the validity of the proposed method in the experiments is verified.

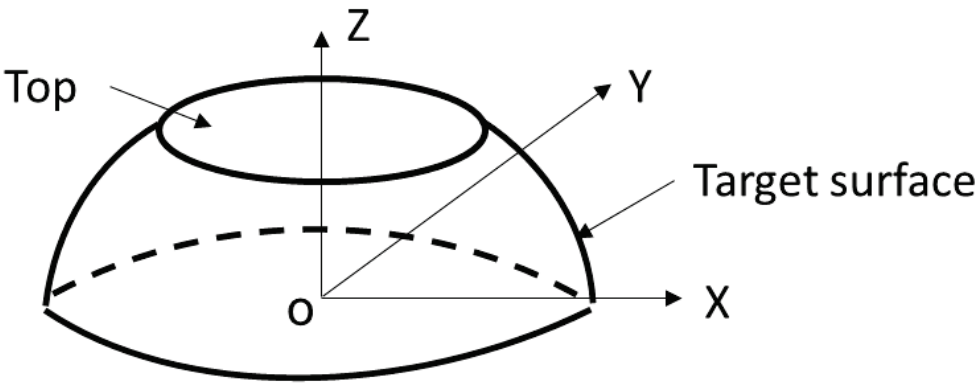

Fig.5.10. Target surface.

Table 5.1 Cutting conditions.

Machine	UNC-100-M5
Tool	Diameter Φ6mm, Tilt angle t_θ 15°, tool tip radius 1mm.
Workpiece	Chemical wood
Feed per tooth f_z [mm/tooth]	0.075
Pick feed p_f [mm]	1
Feed speed F [mm/min]	450
Coordinate measuring machine	Mitutoyo LEGEX9106

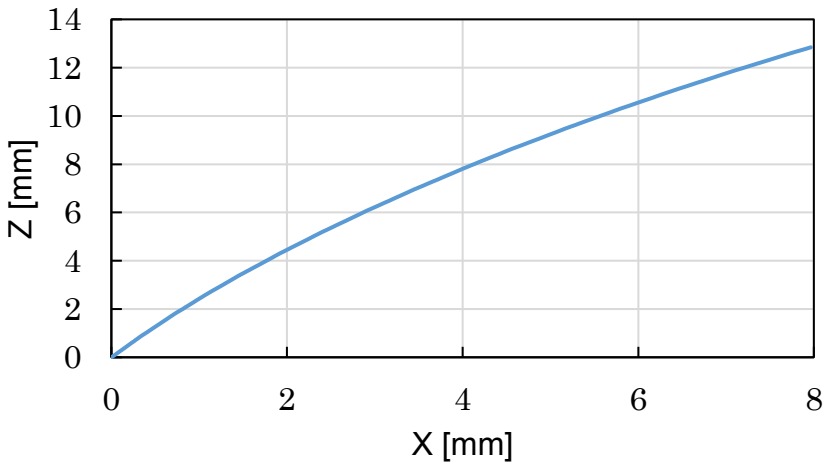

Fig.5.11. Line profile of section.

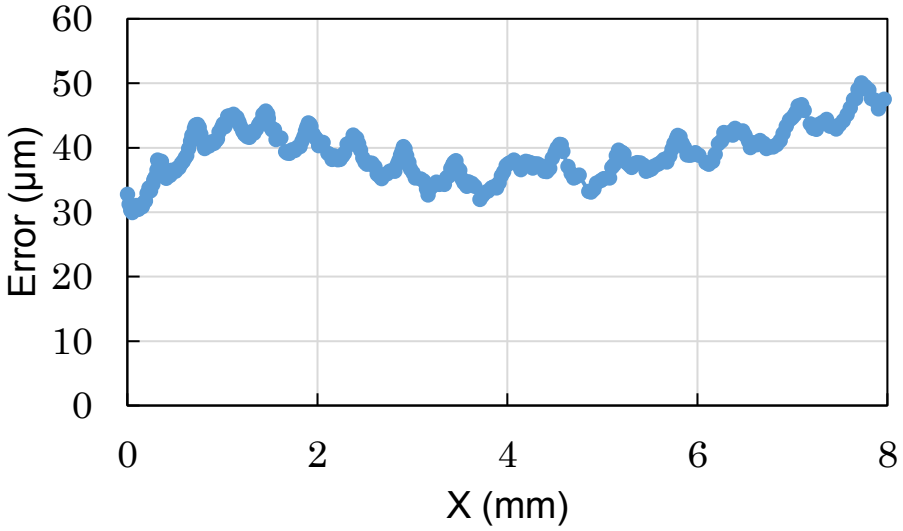

Fig.5.12. Curvature radius error of machined profile.

5.5 Conclusions

Commercial CAD/CAM cannot satisfy concept of proposed tilt taper end mill, some work was did in this chapter, and conclusions can be drawn as following:

1. A special CAM is developed to realize the proposed milling method. The special tool definition and target shape definition were carried out.
2. NC generation algorithm was given. Tool coordinate can be computed

automatically.

3. From the application example, it knew that the generated NC code could be successfully implemented in machining spherical surface, and relative error can be controlled within 0.15%.

References

[1] D. Dimitrov, M. Saxer. Productivity Improvement in Tooling Manufacture through High Speed 5 Axis Machining. Procedia CIRP 2012; vol1: 277 – 282.
[2] Chin-Ching Lo. A new approach to CNC tool path generation. Computer-Aided Design1998; vol30: 649-655.
[3] Young-Keun Choi, A.Banerjee. Tool path generation and tolerance analysis for free-form surfaces. International Journal of Machine Tools & Manufacture2007; vol47:689-696.
[4] Nan Wang, Kai Tang. Five-axis tool path generation for a flat-end tool based on iso-conic partitioning. Computer-Aided Design2008; vol40:1067-1079.
[5] Sergej N.Grigoriev, A.A. Kutin, V.V.Pirogov. Advanced method of NC programming for 5-axis machining. Procedia CIRP 2012; 1:102-107.
[6] Young-Keun Choi, A. Banerjee, Jae-Woo Lee. Tool path generation for free form surfaces using Bézier curves/surfaces. Computers & Industrial Engineering 2007; vol52:486–501.
[7] En-tao Yuan, Bing Shao. Tool-path Generation of Multi-axis Machining for Subdivision Surface. AASRI Procedia 2012; vol3:60 – 65.
[8]Liu Huran. Computer Aided Simulation Machining Programming In 5-Axis Nc Milling Of Impeller Leaf. Physics Procedia2012; vol25:1457 – 1462.
[9] B.S. So, Y.H. Jung, J.W. Park, D.W. Lee. Five-axis machining time estimation algorithm based on machine characteristics. Journal of Materials Processing Technology 2007; vol187-188: 37-40.
[10] B. Gopalakrishnan, T. Yoshii, S.M. Dappili. Decision support system for machining center selection. Journal of Manufacturing Technology Management2004; vol15:144-154.
[11] Wojciech Zębala, Malgorzata Plaza. Comparative study of 3- and 5-axis CNC centers for free-form machining of difficult-to-cut material. Int. J. Production Economics 2014; vol158: 345-358.
[12] C.H. Chu, W.N. Huang, Y.Y. Hsu. Machining accuracy improvement in five-axis flank milling of ruled surfaces. International Journal of Machine Tools & Manufacture 2008; vol48: 914-921.
[13] C-C. Lo. Efficient cutter-path planning for five-axis surface machining with a flat-end cutter. Computer-Aided Design1999; vol31:557–566.

[14] Xu Liu, Yingguang Li, Sibo Ma, Chen-han Lee. A tool path generation method for freeform surface machining by introducing the tensor property of machining strip width. Computer-Aided Design 2015; vol66: 1-13.
[15] Pengcheng Hu, Kai Tang. Improving the dynamics of five-axis machining through optimization of workpiece setup and tool orientations. Computer-Aided Design 2011; vol43:1693-1706.
[16] Tao Ye, Cai-hua Xiong. Geometric parameter optimization in multi-axis machining. Computer-Aided Design 2008; vol40:879-890.
[17] Mohsen Soori, Behrooz Arezoo, Mohsen Habibi. Dimensional and geometrical errors of three-axis CNC milling machines in a virtual machining system. Computer-Aided Design 2013; vol45:1306-1313.
[18] Chuang-Jang Chiou, Yuan-Shin Lee. A machining potential field approach to tool path generation for multi-axis sculptured surface machining. Computer-Aided Design 2002; vol34:357-371.
[19] Rida T. Farouki, Shiqiao Li. Optimal tool orientation control for 5-axis CNC milling with ball-end cutters. Computer Aided Geometric Design 2013; vol30:226-239.
[20] Lasemi, A. Xue, D. Gu. P. Recent development in CNC machining of freeform surfaces: A state-of-art review. Computer-Aided Design2010; vol42:641-654.
[21] Y.H. Jung, D.W. Lee, J.S .Kim, H.S. Mok. NC post-processor for 5-axis milling machine of table-rotating/tilting type. Journal of Materials Processing Technology. 2002; 130-131: 641-646.

Chapter 6 Summary and future work

In order to shorten the cutting time of steam turbine blade, instead of ball end mill, this research proposed a method using tilt taper end mill. Its validity was examined through simulations and experiments. Moreover, the validity was elucidated by cutting force and cutting temperature. A special CAD/CAM was developed for tilt taper end mill. From the results, it can see that using tilt taper end mill can satisfy the surface roughness and shape requirement, and can shorten the cutting time remarkably.

The following will summary from chapter 2 to chapter 5.

6.1 Conclusions of each chapter

Chapter 2 Tilt taper end mill

Considering the problems of conventional method using ball end mill, a new method using tilt taper end mill was proposed, conclusions can be drawn as following:

3. In pick feed direction, waviness error occurs, in case of curvature radius over 400mm, it is under 6μm when pick feed less than 4mm.
4. In the feed direction, cusps occurs, the height increases with the feed per tooth and decreases with curvature radius grows, the value is less than 6μm when curvature radius over 100mm. When milling concave, the value is larger than milling convex.

Owing to the little surface roughness value, hand finish is not needed. Cutting speed on the cutting edge of tilt taper end mill changes in a small range, it is not like with ball end mill that the cutting speed changes from zero, this is benefit to keep the machined surface uniform. Moreover, pick feed can be selected a larger value than that of ball end mill, it will shorten the cutting length, therefore, results of shortening cutting time and retarding tool wear are expected.

Chapter 3 Validity examination

This chapter examined the validity of tilt taper end mill through tool wear experiments based on the selected conditions. The following conclusions can be drawn from this chapter:

4. For taper end mill, when pick feed was selected 4mm, the influence on

surface roughness R_z of each parameter was examined, the optimum values were selected. And then when milling efficiency and a selected cutting parameter are constant, the influence on surface roughness of two parameters were examined, and the cutting conditions at the maximum point are selected. And then cutting conditions of ball end mill and square end mill were selected according to this conditions. Comparing with ball end mill and square end mill method, using tilt taper end mill can reduce the cutting time approximately 94% and 25 % respectively in theoretically.

5. Axial depth of cut is set 0.1mm, the influence on surface roughness R_z of pick feed, feed per tooth and revolution speed were examined respectively. Optimum parameters of each milling method were selected for tool wear experiments. Comparing with ball end mill and square end mill method, using tilt taper end mill can reduce the cutting time approximately 94% and 47 % respectively in theoretically.
6. Tool wear experiments were carried out according to the selected two cutting conditions. The results show that only taper end mill can complete the total removal amount under required surface roughness, and until completing the work, machined surface keeps regular with tool wear. Surface integrity of the other two methods were effected by tool wear easily, surface roughness value over the required value before completed the total work.

For tilt taper end mill and square end mill, it is easy to affected by feed per tooth, and for ball end mill, pick feed influences surface roughness R_z greatly. When using the first cutting conditions, ball end mill only completed about 23%, square end mill can reach the removal degree about 78%. Flank wear of ball end mill increases quicker than those of the other two methods. The reason is because chipping occurs at the top. For the square end mill, scratch occurs from the start, it influences the surface roughness, and with the removal degree scratch becomes serious, even this, the profile of machined surface keeps steady. Tool wear of tilt taper end mill with removal degree nearly the same as that of square end mill, the reason is that they owns the similar milling efficiency. From the relationship between flank wear and surface roughness, it can see that surface roughness R_z of ball end mill and tilt taper end mill positively correlated with the flank wear, and for square end mill, R_z appears positively correlated with flank wear before flank wear approximately 90μm. Although the slope of tilt taper end mill is larger, due to the small constant value, surface roughness R_z can be less

than 6μm before completing the total work.

When using the second cutting conditions, ball end mill and square end mill can finish the total removal amount approximately 12% and 38% respectively, their surface roughness deteriorated rapidly before reaching 6μm. For tilt taper end mill, the surface roughness R_z increases gradually until removal degree 100%. For ball end mill and square end mill, chipping is an important factor influences on surface roughness. Especially square end mill, apparent chipping can be seen from removal degree 35%. Some adhesion on cutting edge of tilt taper end mill can be seen, it causes the material cannot be removed totally. There are good linear relation between flank wear and surface roughness when using ball end mill and tilt taper end mill. The influence of flank wear on surface roughness when using tilt taper end mill is weaker those of the other two methods.

Chapter 4 Cutting force and cutting temperature

In this chapter, in order to explain the mechanism using taper end mill, the cutting force and cutting temperature were measured, some conclusions can be drawn as following:

5. In order to measure the cutting force and cutting temperature of each milling method, a measurement device was designed.
6. On the whole, the results shows that cutting force and cutting temperature increase with process. Cutting force using ball end mill and taper end mill shown a positive correlation with flank wear.
7. For the selected cutting conditions, peak values of cutting force using ball end mill change irregularly, oppositely, the waviness of cutting force using square end mill and taper end mill can keep steady, but only using taper end mill can keep steady until complete the total work.
8. The cutting process using taper end mil is discontinuous so that the heat can be removed. Owing to this, the tool life is extended and surface integrity keeps good.

The cutting force increases with flank wear in three directions in general. For square end mill, it changes irregularly because chipping occurred. Cutting temperatures when using ball end mill and square end mill not present some regular with tool wear, it is probably caused by noise. Only using ball end mill and tilt taper end mill, the cutting force in three direction keep a good linear with flank wear. Among the three methods, tilt taper end method appears Fz easily affected

by flank wear. From the comparisons of wave shape of cutting force, it can see that when using ball end mill, the force in three direction changes irregular. The cutting speed is lower, chatter is serious at this cutting speed area. It is also a reason that cutting force of ball end mill is larger that of square end mill. Cutting speed of tilt taper end mill is high, the machined surface can keep uniform until removal degree 100%. The cutting process of tilt taper end mill is discontinuous, the real cutting time in a period only about 10%, it has enough time to cool off the heat generated by cutting, and can retard the tool wear. This probable can explain the mechanism of its validity.

Chapter 5 Tool path generation

Commercial CAD/CAM cannot satisfy concept of proposed tilt taper end mill, some work was did in this chapter, and conclusions can be drawn as following:

4. A special CAM is developed to realize the proposed milling method. The special tool definition and target shape definition were carried out.
5. NC generation algorithm was given. Tool coordinate can be computed automatically.
6. From the application example, it knew that the generated NC code could be successfully implemented in machining spherical surface, and relative error can be controlled within 0.15%.

From the model experiments of a 45 degree spherical surface, it can see that proposed method can satisfy the shape error requirement, the profile error change between 30μm and 50μm, it is far less than 200μm. The results shows that the validity of processing curved surface when using tilt taper end mill.

6.2 Future work

Before realizing the machining of steam turbine blade, there is still much work need to do. At first, is has to examine the validity when milling freeform surface. In chapter 5, convex of constant curvature has been discussed, but curvature of concaves have not been examined. Therefore, the freeform surface contained by concave and convex. A process plan based on the CAD geometric model is created, that defines how the part geometry will be generated through the use of certain machining processes and tools. Tool paths are created for each cutting process — sequences of cutter contact (CC) points on the part surface are

defined, and cutter location (CL) data are then generated according to the desired tool shape and orientation at each point. This time a post-processor creates numerical control (NC) code based on the CL data and properties of the particular CNC machine. After verification of the part program by simulation or trial cut, it can be employed in running the CNC milling machine for mass production in future. At last, it will perform a steam turbine trial process experiment.

The tools of former experiments were commercial, they are cannot exhibits the merits of the proposed method. Thus, a special tool is needed to be developed for improving the machining accuracy and efficiency as much as possible. Influences of approach angle, relief angle, coated film and corner of insert on surface roughness will be examined. Changes of cutting force and cutting temperature will be verified to explain the influence of each cutting parameter. Tool life experiments of the developed tool also will be carried out.

Application range of tilt taper end mill will be examined. The merits when milling low thermal conductivity material such as titanium alloy, nickel alloy and so on will be verified. Moreover, building a tool wear and tool life predict equation at different cutting conditions.

Acknowledgements

This thesis is a summary of the research conducted at Nagasaki University Graduate School of Engineering Doctoral Degree from 2011 to 2016.

During this research, I deeply appreciated Dr. Takanori Yazawa Professor of Nagasaki University Graduate School of Engineering who gave me valuable guidance and advices from the beginning.

In preparing this thesis, I am full of gratitude to Dr. Yukio Maeda Professor of Toyama Prefectural University Intelligent Stems Design Engineering, Dr. Akihide Saimoto Professor and Dr. Atsuhiro Koyama associate Professor of the Graduate School of Engineering for your useful advices and criticisms.

Thanks Nobutoshi Baba (Now in NIPPON SHARYO, LTD.) very much for his previous research. Thanks assistant technical officer Hideki Hisada, Fuminori Katsugawa and Yuto Onizuka at machine shop of Nagasaki University School of Engineering, and senior researcher Shinichi Kogusu and Yohei Fukuda of Industrial Technology Center of Nagasaki for their help on experiments.

Thanks Dr. Yasuhiko Ougiya associate Professor, Tatsuhiro Kojima and Reiko Yamada Technical staff of Nagasaki University Graduate School of Engineering, and Dr. Tatsuki Otsubo assistant Professor of Salesian Polytechnic for their useful advices on experiments. Giving thanks to Hideo Ito and other members of Precision Production Technology Laboratory for their cooperation and encouragement.

Finally, I would like to express my gratitude and thanks to my wife for her care, company and inspiration all the time, and to my daughter for giving me momentum everyday.